
Doctoral Dissertations


Student Theses and Dissertations

Spring 2016

Single particle-inductively coupled plasma-mass spectrometry technology development for metallic nanoparticle characterization in complex matrices

Yongbo Dan

Follow this and additional works at: https://scholarsmine.mst.edu/doctoral_dissertations

 Part of the [Analytical Chemistry Commons](#), [Environmental Chemistry Commons](#), [Environmental Sciences Commons](#), and the [Nanoscience and Nanotechnology Commons](#)

Department: Chemistry

Recommended Citation

Dan, Yongbo, "Single particle-inductively coupled plasma-mass spectrometry technology development for metallic nanoparticle characterization in complex matrices" (2016). *Doctoral Dissertations*. 2741.
https://scholarsmine.mst.edu/doctoral_dissertations/2741

This thesis is brought to you by Scholars' Mine, a service of the Missouri S&T Library and Learning Resources. This work is protected by U. S. Copyright Law. Unauthorized use including reproduction for redistribution requires the permission of the copyright holder. For more information, please contact scholarsmine@mst.edu.

SINGLE PARTICLE-INDUCTIVELY COUPLED PLASMA-MASS
SPECTROMETRY TECHNOLOGY DEVELOPMENT FOR METALLIC
NANOPARTICLE CHARACTERIZATION IN COMPLEX MATRICES

by

YONGBO DAN

A DISSERTATION

Presented to the Faculty of the Graduate School of the
MISSOURI UNIVERSITY OF SCIENCE AND TECHNOLOGY

In Partial Fulfillment of the Requirements for the Degree

DOCTOR OF PHILOSOPHY

in

CHEMISTRY

2016

Approved

Honglan Shi, Advisor
Yinfa Ma
Jeffrey Winiarz
Paul Nam
Xinhua Liang

© 2016

Yongbo Dan

All Rights Reserved

PUBLICATION DISSERTATION OPTION

This dissertation has been prepared in the style utilized by several scientific journals: *Environmental Science and Technology*, *Microchemical Journal*, *Clinica Chimica Acta*, and *Analytical and Bioanalytical Chemistry*.

Paper I (Page 7-33) has been published: Dan Y., Shi H., Stephan C., Liang X., Rapid analysis of titanium dioxide nanoparticles in sunscreens using single particle inductively coupled plasma-mass spectrometry. *Microchem. J.*, 2015, 122: 119-126.

Paper II (Page 34-57) has been published: Dan Y., Zhang W., Xue R., Ma X., Stephan C., Shi H., Characterization of Gold Nanoparticle Uptake by Tomato Plants Using Enzymatic Extraction Followed by Single-Particle Inductively Coupled Plasma-Mass Spectrometry Analysis. *Environ. Sci. Technol.*, 2015, 49 (5): 3007-3014.

Paper III (Page 58-85) has been submitted to *Analytical and Bioanalytical Chemistry* and is under revision: Dan Y., Ma X., Zhang W., Liu K., Stephan C., Shi H., Application of Single Particle ICP-MS for the Determination of Plant Uptake and Accumulation of CeO₂ Nanoparticles. *Anal. Bioanal. Chem.*, under revision.

Paper IV (Page 86-110) is a collaboration with Casey Burton et al. Yongbo Dan (me, second author) developed and validated the ICP-MS method and analyzed the urine samples, and Casey Burton (first author) analyzed the data. It has been published: Burton C., Dan Y., Donovan A., Liu K., Shi H., Ma Y., Bosnak C., Urinary Metallomics as a Novel Biomarker Discovery Platform: Breast Cancer as a Case Study. *Clin. Chim. Acta.* 2016, 452: 142-148.

ABSTRACT

As the rapid growing of nanotechnology, the release of engineered nanoparticles (ENPs) into the environment is inevitable. After entering the real environment, ENPs tend to react with different components of the ecosystem (e.g. water, soil, air, plants) and make their characterization difficult. Analyzing ENPs in these complex matrices still remains as a grand challenge. ENPs characterization is normally the first step of risk assessment. Current analytical techniques have shown some limitations in revealing the unique characteristics of ENPs in complex matrices and reliable analytical techniques are in urgent need. Single particle inductively coupled plasma mass spectrometry (SP-ICP-MS) is an emerging technique capable of determining the ENPs particle size, particle concentration and dissolved analyte concentration and has the potential to fill the analytical gap. In the presented dissertation, several SP-ICP-MS methods were developed and validated to determine the ENPs particle size, size distribution, particle concentration, and dissolved analyte concentration in complex matrices, such as sunscreens and plant tissues. An enzymatic digestion method was also developed to extract ENPs within plant tissues without causing particle dissolution for subsequent SP-ICP-MS quantification. Utilizing enzymatic digestion-SP-ICP-MS, the presence of dissolved cerium in plant shoots exposed to CeO₂ NPs hydroponically was confirmed for the first time. Our results also suggest that CeO₂ NPs might be taken up by plant roots as ionic cerium. Collectively, SP-ICP-MS has shown great advantages over other techniques, such as high sensitivity, tolerance of complex matrices, high throughput, and informative results (particle size, size distribution, particle concentration, and dissolved analyte concentration).

ACKNOWLEDGMENTS

I have to thank numerous people who have helped me in the past several years. First, I want to express my sincere gratitude to my advisor Dr. Honglan Shi for her constant support and valuable suggestions, which make this work possible. She always encourages me to attend conferences and workshops to improve English and presentation skills which has benefited me a lot. I also want to thank my other committee members, Dr. Yinfa Ma, Dr. Jeffrey Winiarz, Dr. Paul Nam and Dr. Xinhua Liang, for their valuable advices. Special thanks to Dr. Yinfa Ma for his suggestions and encouragement.

My Ph.D work was mainly SP-ICP-MS related, which won't be possible without the fantastic collaboration with PerkinElmer. I like to thank Dr. Chady Stephan, Heidi Grecsek, Cynthia Bosnak and Jack Quade from PerkinElmer for their time and effort. I also want to thank Dr. Xingmao Ma and Weilan Zhang for their tremendous help and valuable discussions when we collaborated to study the interactions between plants and nanoparticles. Special thanks to Kun Liu for her help in taking care of the plants. I want to thank my former and current group members and secretaries of Chemistry Department and Environmental Research Center for their help.

I want to thank my family members and friends for their support and understanding. My wife, Yan Li, travelled thousands of miles to Missouri S&T and accompanied me along this endeavor. She has sacrificed so much for me and our family during my Ph.D study here. She took care of our baby son Vincent at daytime and had to go to class for her MBA at night. While some people cannot even get one of them done smoothly, she did so well on both of them at the same time. I am just so proud of her and want to thank her for everything she did for me and our family.

TABLE OF CONTENTS

	Page
PUBLICATION DISSERTATION OPTION	iii
ABSTRACT.....	iv
ACKNOWLEDGMENTS	v
LIST OF ILLUSTRATIONS.....	x
LIST OF TABLES	xiii
SECTION	
1. INTRODUCTION.....	1
1.1. ENGINEERED NANOPARTICLES	1
1.2. IMPORTANT PROPERTIES OF ENGINEERED NANOPARTICLES AND THEIR SIZE/COMPOSITION CHARACTERIZATION.....	1
1.3. SINGLE PARTICLE-INDUCTIVELY COUPLED PLASMA-MASS SPECTROMETRY	3
1.4. FUTURE PERSPECTIVES OF SP-ICP-MS	5
1.5. INTERACTIONS BETWEEN NANOMATERIALS AND PLANTS	6
PAPER	
I. RAPID ANALYSIS OF TITANIUM DIOXIDE NANOPARTICLES IN SUNSCREENS USING SINGLE PARTICLE INDUCTIVELY COUPLED PLASMA-MASS SPECTROMETRY	7
ABSTRACT.....	8
1. Introduction.....	9
2. Experiments	11
2.1 Chemicals and Instrumentation	11
2.2 SP-ICP-MS Method	12
2.3 Sample Preparation for SP-ICP-MS Analysis.....	14
2.4 Standard Addition-SP-ICP-MS Method to Measure TiO ₂ Mass Content in Sunscreens	15
2.5 Hot Block Acid Digestion and ICP-MS Determination of TiO ₂ Mass Content in Sunscreens.....	16

3. Results and Discussions.....	17
3.1 Particle Size Detection Limit of the Developed SP-ICP-MS Method.	17
3.2 Sunscreen Containing no TiO ₂ NPs as Quality Control.....	18
3.3 Size distribution for different sunscreens.....	19
3.4 Particle Concentration	23
3.5 Standard Addition method for TiO ₂ mass content determination.	25
4. Conclusions.....	28
Acknowledgement	29
References.....	30
II. CHARACTERIZATION OF GOLD NANOPARTICLES UPTAKE BY TOMATO PLANTS USING ENZYMATIC EXTRACTION FOLLOWED BY SINGLE PARTICLE INDUCTIVELY COUPLED PLASMA-MASS SPECTROMETRY ANALYSIS	34
ABSTRACT.....	35
INTRODUCTION	37
EXPERIMENTS	40
Materials and Instrumentation.....	40
SP-ICP-MS Method Parameters.....	41
The Detection Limit of Particle Size and Particle Concentration.	42
Plant Growth and Treatment.	42
Effect of Macerozyme R-10 Enzyme on AuNPs.	43
Enzymatic Digestion Method.....	44
Reproducibility Study of the Enzymatic Digestion Method.	44
RESULTS AND DISSCUSSION.....	45
The Detection Limit of Particle Size and Particle Concentration of the Developed SP-ICP-MS Method.....	45
Effect of the Enzyme on AuNPs.	47
Reproducibility of Enzymatic Digestion Method.	48
Enzymatic Digestion of AuNPs in Plants and SP-ICP-MS Analysis.....	49
ACKNOWLEDGEMENT	54

REFERENCES	55
III. APPLICATION OF SINGLE PARTICLE ICP-MS FOR THE DETERMINATION OF PLANT UPTAKE AND ACCUMULATION OF CeO ₂ NANOPARTICLES.....	58
Abstract	59
1. Introduction	60
2. Materials and Methods	63
2.1 Chemicals and Instrumentation	63
2.2 CeO ₂ NPs SP-ICP-MS method development and validation	64
2.2.1 SP-ICP-MS method description.....	64
2.2.2 Size measurement accuracy of the SP-ICP-MS method for CeO ₂ NPs	65
2.2.3 Effect of enzyme solution on CeO ₂ NPs.....	66
2.3 Plant growth and CeO ₂ NPs exposure.....	66
2.4 Enzymatic digestion and SP-ICP-MS analysis	67
2.5 Acid digestion of the enzymatic digestate.....	68
2.6 TEM imaging of cucumber shoot.....	69
3. Results and Discussion.....	69
3.1 SP-ICP-MS Method Performance	69
3.1.1 Particle size detection limit.....	69
3.1.2 Sizing accuracy of the developed SP-ICP-MS method	70
3.1.3 Effect of enzymatic digestion on CeO ₂ NPs.....	72
3.2 CeO ₂ NPs Uptake and Biotransformation	73
4. Conclusions	80
Acknowledgement	81
Conflict of Interest.....	81
References.....	82
IV. URINARY METALLOMICS AS A NOVEL BIOMARKER DISCOVERY PLATFORM: BREAST CANCER AS A CASE STUDY	86
ABSTRACT.....	87
1. Introduction.....	88

2. Materials and Methods.....	90
2.1 Patients and specimens.....	90
2.2 ICP-MS Urinary Metal Assay	91
2.3 Urine specific gravity assay	93
2.4 Statistical analyses.....	94
3. Results.....	95
3.1 Patient Population.....	95
3.2 Association of Urinary Metals with Breast Cancer	96
3.3 Correlations among urinary metals and clinicopathological factors	99
4. Discussion.....	102
5. Conclusions.....	105
Acknowledgements.....	105
References.....	107
SECTION	
2. CONCLUSIONS	111
BIBLIOGRAPHY	113
VITA	117

LIST OF ILLUSTRATIONS

	Page
PAPER I	
Figure 1. (a) Raw data for diluted sunscreen 3; (b) Raw data of spiking 6.65 $\mu\text{g/L}$ 40 nm TiO_2 into diluted sunscreen 3; (c) Processed data of spiking 6.65 $\mu\text{g/L}$ 40 nm TiO_2 into sunscreen 3 based on Figure 1(b).....	19
Figure 2. (a) The overview of raw data (1,000,000 data points in total) for 2×10^4 times-diluted sunscreen 1. Inset: the first 5000 data points out of 1,000,000 data points; (b) Size distribution for 2×10^4 times-diluted sunscreen 1. (c) Size distribution for 10^5 times-diluted sunscreen 1. (d) Size distribution for diluted sunscreen 1 measured at Day 1, Day 5 and Day 12.	21
Figure 3. (a) Size distribution for 2×10^4 times-diluted Sunscreen 2; (b) Size distribution for 10^5 times-diluted Sunscreen 2; (c) Size distribution for 2×10^4 times-diluted Sunscreen 4; (d) Size distribution for 10^5 times-diluted Sunscreen 4.....	22
Figure 4. SEM image for TiO_2 NPs extracted from Sunscreen 2.	23
Figure 5. Standard addition method for four sunscreens to detect TiO_2 mass content. (a), (b), (c), (d) stands for 10000 times-diluted sunscreen 1, sunscreen 2, sunscreen 3 and sunscreen 4, respectively.	27
Figure 6. Comparison of TiO_2 mass content determined by standard addition-SP-ICP-MS method, acid digestion-ICP-MS method and manufacturer-claimed.	28
PAPER II	
Figure 1. Particle size distribution histogram of enzyme-treated 50 nm AuNP (without plant tissue).....	48
Figure 2. AuNPs size distribution for three replicates of tomato plant dosed with 5 mg/L of 40 nm AuNPs for enzymatic extraction reproducibility study.....	48
Figure 3. (a) Raw data for reagent blank (reagent blank: enzyme in 2 mM citrate solution, without plant tissues and AuNPs); (b) Raw data for control plant without exposure to AuNPs; (c) Raw data for spiking 4.7×10^4 NPs/mL of 100 nm AuNPs into control plant sample; (d) Size distribution histogram for spiking 4.7×10^4 /mL of 100 nm AuNPs into control plant sample.	49
Figure 4. (a)&(b) Raw data of duplicated tomato plants exposed to 5 mg/L of 40 nm AuNPs for 4 days; (c) Size distributions histograms of duplicated tomato plants exposed to 5 mg/L of 40 nm AuNPs from Figure 4(a) and 4(b); (d) Size distribution histogram of spiking 4.7×10^4 particles/mL of 100 nm AuNPs into tomato plants exposed to 5 mg/L of 40 nm AuNPs.....	52

- Figure 5. (a) Raw data of tomato plant dosed with 0.2 mg/L of 40 nm AuNPs for 4 days; (b) Size distribution histogram from Figure 5(a); (c) Size distribution histogram of spiking 4.7×10^4 NPs/mL of 100 nm AuNPs into tomato plants dosed with 0.2 mg/L of 40 nm AuNPs..... 53

PAPER III

- Figure 1. (a) Histogram of 30-50 nm CeO₂NPs measured by developed SP-ICP-MS method (b) TEM images of purchased 30-50 nm CeO₂NPs, (c) Histogram of 50-100 nm CeO₂NPs measured by developed SP-ICP-MS method (d) TEM images of purchased 50-100 nm CeO₂NPs. (scale bar on both TEM images is 50 nm)..... 71
- Figure 2. Size distribution of spiked 50-100 nm CeO₂NPs in different plant digestate matrix measured by developed SP-ICP-MS method after 100-fold dilution in 20 mM MES buffer (pH 5): (a) tomato, (b) soybean, (c) cucumber, (d) pumpkin..... 72
- Figure 3. Comparison of the size distribution of 50-100 nm CeO₂NPs after 24 hours digestion in enzyme solution at 37 °C to the size distribution of freshly prepared 50-100 nm CeO₂NPs in enzyme solution..... 73
- Figure 4. SP-ICP-MS raw data of plant shoots digestates: (a) tomato control without dosing CeO₂NPs, (b) tomato dosed with 7 mg/L 30-50 nm CeO₂NPs for 19 days, (c) cucumber control without dosing CeO₂NPs, (d) cucumber dosed with 7 mg/L 30-50 nm CeO₂NPs for 19 days, (e) pumpkin control without dosing CeO₂NPs, (f) pumpkin dosed with 7 mg/L 30-50 nm CeO₂NPs for 19 days, (h) soybean control without dosing CeO₂NPs, (i) soybean dosed with 7 mg/L 30-50 nm CeO₂NPs for 19 days. The inset shows the data points in the first one second..... 74
- Figure 5. SP-ICP-MS raw data of enzymatic digestate filtered by Millipore 5 kDa Ultrafree[®]-MC centrifugal filter. The inset shows the data points in the first one second. 75
- Figure 6. Size distribution of CeO₂NPs in plant shoots dosed with 7 mg/L 30-50 nm CeO₂NPs for 19 days, (a) histogram of tomato shoot, (b) histogram of cucumber shoot, (c) histogram of pumpkin shoot, (d) histogram of soybean shoot 77
- Figure 7. (a) freshly prepared 7 mg/L of CeO₂NPs dosing solution filtered by Millipore 5kDa Ultrafree[®]-MC centrifugal filter, (b) 20 mM MES buffer (Dilution factor:10 for a) 79

PAPER IV

- Figure 1. Patient enrollment flowchart including excluded specimens. 96

Figure 2 ROC data comparing incremental increases in diagnostic performance for the univariate models of Cu and Pb and the multivariate model comprising Cu, Pb, and patient age in women newly diagnosed with breast cancer (n=47) and benign conditions (n=84).....	99
---	----

LIST OF TABLES

	Page
PAPER I	
Table 1. ICP-MS operation conditions and SP-ICP-MS method parameters.....	13
Table 2. Particle concentration information for 2×10^4 times-diluted sunscreen samples.	25
PAPER II	
Table 1. ICP-MS conditions after optimization for ^{197}Au	46
Table 2. Comparison of the measured and prepared particle concentration of 40 nm AuNP.....	47
PAPER III	
Table 1. ICP-MS conditions for the developed SP-ICP-MS method	65
Table 2. Results of fresh shoots obtained by SP-ICP-MS analysis and acid digestion followed by conventional ICP-MS analysis.....	79
PAPER IV	
Table 1. Method performance parameters for the detection of 22 urinary metals using ICP-MS operating in KED mode.	93
Table 2 Comparison of USG-adjusted urinary metal levels in women with benign conditions (n=84) and breast cancer (n=47). All data are expressed as median (IQR).....	97
Table 3 Significant correlations among USG-adjusted urinary metals.	101

SECTION

1. INTRODUCTION

1.1. ENGINEERED NANOPARTICLES

Engineered nanoparticles (ENPs) are broadly defined as man-made nano-object with all their external dimensions in the nanoscale (1 nm -100 nm).¹ As particle size decreases into the nanometer range, the specific surface area increases exponentially and a higher portion of atoms are exposed on the particle surface, resulting in more reactive groups on the surface and subsequently making nanoparticles totally different from their bulk counterparts.² Due to their unique properties, ENPs have been widely incorporated into many commercial products. TiO₂ NPs and ZnO NPs have been widely used as effective inorganic UV filter in many sunscreens and other cosmetics.³⁻⁶ CeO₂ NPs are popular fuel additives.⁷ SiO₂, CeO₂ and Al₂O₃ NPs are widely used as catalysts.⁸ Due to the increasing use of engineered nanomaterials in consumer products and toxicity studies of engineered nanomaterials, regulatory agencies and other research organizations have determined that the development of robust, reliable, and accurate methodologies to characterize ENPs in complex matrices is a top priority and are in urgent need.⁹

1.2. IMPORTANT PROPERTIES OF ENGINEERED NANOPARTICLES AND THEIR SIZE/COMPOSITION CHARACTERIZATION

The main properties of ENPs include particle size, size distribution, chemical composition, particle concentration, aggregation state, shape, crystallinity, surface charge, specific area, surface speciation and functionality, and so on.¹ Different techniques and instrumentations are required to characterize different properties of ENPs.

There is no single technique can fully characterize all of the main properties of ENPs aforementioned. For ENPs, the size, size distribution, chemical composition are of primary interest for many purposes. Electron microscopy, field flow fractionation (FFF) and light scattering are the most widely used methodologies for ENP size characterization, even though some other techniques are also available. Characterizing ENPs in complex matrices (e.g. in real water, soil, biological matrices) is far more complicated than characterizing pure synthesized ENPs.

Electron microscopy is a powerful technique for ENPs size characterization and chemical composition analysis coupled with energy dispersive spectroscopy detector. However, its application is usually limited by its sensitivity for environmental and biological samples. Characterizing ENPs in biological matrices also requires extensive sample preparation which usually involves fixation, dehydration, sectioning, and staining. Electron microscopy only examines a tiny fraction of the whole specimen and therefore sometimes it is not representative.

FFF is a particle separation technique. The particle size can be calculated either by FFF theory or by establishing a particle size-retention time calibration curve.^{10, 11} In FFF, a physical field is perpendicularly applied to a solution pumped through a long and narrow channel, to separate the particles/macromolecules in the solution, depending on their differing "mobility" under the force exerted by the field.¹² Based on the different fields applied, FFF can be classified into symmetrical flow FFF, asymmetrical flow FFF, centrifugal/sedimentation FFF, thermal FFF, electrical FFF etc. After FFF separation, UV/Vis detector, light scattering detector and elemental based detectors (ICP-OES/ICP-MS) are usually used to detect the analyte, either alone or online coupled together. FFF-

UV/MALS-ICP-MS has shown great potential for particle characterization, especially to study the interactions between particles/colloids and other chemicals. For example, FFF-ICP-MS recently has been successfully used to study the interactions between toxic elements and environmental colloids/NPs or humic acid, such as U(VI) sorption to nano-hematite,¹³ interaction of bentonite colloids with Cs, Eu, Th and U in presence of humic acid,¹⁴ NOM-metal complexes in water.¹⁵ Even though FFF coupling with multi detectors holds quite some analytical merits, some challenges still remains. For example, each analysis usually takes 1 hour or even longer if the size range of particles are wide, which makes FFF not a high throughput technique. Another challenge in FFF is the non-specific interactions between analyte particles and FFF membranes, which can cause the retention time shift and sample loss.^{9, 16, 17}

1.3. SINGLE PARTICLE-INDUCTIVELY COUPLED PLASMA-MASS SPECTROMETRY

Single particle inductively coupled plasma-mass spectrometry (SP-ICP-MS) is an emerging technique for NP characterization and quantification, especially at low NP concentrations and in complex matrices. Degueldre and his colleagues pioneered in this field in the early 21th Century and laid the foundation for SP-ICP-MS.¹⁸⁻²² Briefly, in SP-ICP-MS analysis, NPs suspensions enter the plasma and get ionized individually, and then are detected as pulse (non-continuous) signals by the mass spectrometer, making SP-ICP-MS a powerful technique to detect the masses of metal elements in each NP.²³⁻²⁷ Meanwhile, the corresponding dissolved analyte is detected as a continuous signal, meaning that SP-ICP-MS is capable of simultaneously detecting both the particle analyte and the dissolved analyte.²⁶ In SP-ICP-MS analysis, the signal intensity of a NP depends

on the particle size, and the signal frequency is proportional to the particle concentration in samples.²²⁻²⁷ At the early stage, SP-ICP-MS was a more qualitative technique due to the absence of well-characterized NP standards, and highly sensitive and rapid mass scanning ICP-MS instrument. Recently, quantitative results have been achieved by SP-ICP-MS after some well-defined NP standards, such as AuNPs and silver NPs (AgNPs), and fast scanning ICP-MS, such as NexION 350 ICP-MS, become commercially available.^{23, 24, 28-31}

There have been some successful applications of SP-ICP-MS for analysis of the size and concentration of NPs in environmental and biological matrices. For instance, Tuoriniemi et al. analyzed titanium (Ti), cerium (Ce) and Ag associated particles in wastewater effluent samples and the measured particle concentration was in the order of magnitude of the predicted concentrations.³² Mitrano et al. used SP-ICP-MS to quantitatively track the dissolution of 60 and 100 nm silver NPs in laboratory, natural and processed water matrices, and found that the water chemistry significantly affected the NP dissolution.³³ For NP analysis in biological tissues, the major challenge is the extraction of NPs from these tissues without compromising their properties. Concentrated acids are commonly used for metal extraction from tissues. However, they are not applicable for NP analysis because the concentrated acids can dissolve the NPs. Gary et al. extracted Ag and Au NPs from ground beef, *Daphnia magna*, and *Lumbriculus variegatus* using tetramethylammonium hydroxide (TMAH) and quantified the NP sizes and NP particle concentrations using SP-ICP-MS method.³⁴ Loeschner et al. and Peters et al. digested chicken meat with Proteinase K to extract Ag NPs.^{35, 36} Loeschner et al. also used alkaline and enzymatic treatment on rat spleens for AuNP extraction prior to SP-

ICP-MS quantification, and obtained similar size distributions of AuNPs with both treatments.³⁷ Marshall et al. used enzymatic digestion (1- β -endoglucanase) to extract AuNPs in Brassica Juncea followed by X-ray absorption near edge spectroscopy (XANES) quantification.³⁸ These progresses on SP-ICP-MS and tissue digestion provide an excellent opportunity to simultaneously obtain particle size, particle concentration, and dissolved analyte concentration information in biological and environmental samples.

1.4. FUTURE PERSPECTIVES OF SP-ICP-MS

So far, SP-ICP-MS is still limited to one isotope due to the scanning nature of most commercial ICP-MS systems as well as the extremely short signal duration of one single nanoparticle (typically 0.3-0.5 ms), even though there is one publication on two-isotope SP-ICP-MS.²⁹ One feasible approach is to use extremely fast scanning quadrupole ICP-MS with dwell time much shorter than the signal duration of one single nanoparticle (e.g. 10 μ s), such as PerkinElmer's NexION 350 ICP-MS. Another promising approach is to use dispersive mass analyzer (e.g. sector field) instead of scanning mass analyzer (e.g. quadrupole). All of the isotopes/elements from one single particle will be dispersed onto a focal plane for simultaneous detection. Unfortunately, sector field ICP-MS systems with dwell time/integration time close to or shorter than 0.3-0.5 ms are not commercially available. The multi-element capability of SP-ICP-MS will significantly broaden its applications and provide researchers with more information of the samples.

Another issue in SP-ICP-MS is its size detection limit. To date, it is difficult to accurately size particles less than 10 nm. Most ions do not get into the mass spectrometer after being ionized in the plasma. The ion transmission from the plasma to the detector

needs to be improved. The improvement of detector efficiency can also significantly decrease the size detection limit.

1.5. INTERACTIONS BETWEEN NANOMATERIALS AND PLANTS

The rapid development and mass production of ENPs will result in potential release of ENPs into the environment. After being released into the environment, ENPs tend to react with different components in the ecosystem. Plant is a critical component of the ecosystem and its interaction with ENPs has attracted researchers' attention in the last decade. Plant uptake and accumulation of ENPs represent an important pathway for potential human exposure to ENPs. Different kinds of ENPs have been studied extensively in recently years. Uptake of ENPs was found, however, the uptake mechanism is still not clear and is under debate.

Among ENPs, CeO₂ NPs have attracted significant attention on their fate and transport. Due to the low solubility of CeO₂ NPs, the detection of Ce in plant tissues is usually interpreted as evidence of Ce uptake as intact CeO₂ NPs.³⁹ The interpretation is also supported by the detection of Ce⁴⁺ oxidation state by near edge X-ray absorption fine structure (XANES).⁴⁰ However, the detection of biotransformed products (e.g. CePO₄, cerium carboxylate) in plant tissues and elevated Ce³⁺ around root surface spurred a new theory that CeO₂ NPs may release Ce³⁺ on root surface, which are then taken up by plant roots and immediately oxidized to CeO₂ NPs.³⁹ No definitive evidence is available to confirm the existence or significance of this pathway. Another unsettled issue associated with the plant and CeO₂ NPs interaction is that even though biotransformed product was detected in plant tissues, it is unclear whether the Ce³⁺ in plant tissues are dissolved from CeO₂ NPs following their uptake or are directly taken up from the growth media.

PAPER**I. RAPID ANALYSIS OF TITANIUM DIOXIDE NANOPARTICLES IN SUNSCREENS USING SINGLE PARTICLE INDUCTIVELY COUPLED PLASMA-MASS SPECTROMETRY**

Yongbo Dan^{1,2}, Honglan Shi^{1,2,§}, Chady Stephan³, Xinhua Liang^{2,4}

¹*Department of Chemistry, Missouri University of Science and Technology, Rolla, MO, 65409, United States*

²*Center for Single Nanoparticle, Single Cell, and Single Molecule Monitoring (CS³M), Missouri University of Science and Technology, Rolla, MO, 65409, United States*

³*PerkinElmer, Inc., 501 Rowntree Dairy Rd, Woodbridge, On, Canada, L4L 8H1*

⁴*Department of Chemical and Biochemical Engineering, Missouri University of Science and Technology, Rolla, MO, 65409, United States*

§Corresponding author

Address: Department of Chemistry
Missouri University of Science and Technology
400 West 11th Street
Rolla, MO 65409, United States
Phone: (+1) 573-341-4433
Fax: (+1) 573-341-6033
E-mail: honglan@mst.edu

ABSTRACT

Titanium dioxide (TiO₂) particles in the nanometer (nm) size range are widely used in commercial sunscreens. Single particle inductively coupled plasma-mass spectrometry (SP-ICP-MS) is an emerging methodology for nanoparticle (NP) characterization and quantification. In this study, a rapid SP-ICP-MS method was developed to simultaneously determine the primary particle size, size distribution, particle concentration (particles/mL), and mass content (weight percent) of TiO₂ NPs in commercial sunscreens. Quality control data indicated that the developed method was capable of accurately measuring TiO₂ particle size in sunscreen matrix. Four types of commercial sunscreens containing different amounts of TiO₂ were analyzed, and the primary particle sizes detected varied from 32 nm to 40 nm in the different sunscreens tested. TiO₂ existed as TiO₂ particles in the tested sunscreens. The TiO₂ mass contents in these sunscreens were also determined by a novel standard addition-SP-ICP-MS method, using a 40 nm TiO₂ NP as the NP standard. Although the measured TiO₂ mass content was close to that determined by acid digestion and the manufacturer-claimed content, improvement in accuracy is needed and can be achieved if better-matched NP standards available. The standard addition-SP-ICP-MS method offers a promising alternative for determining the TiO₂ NP mass content in sunscreen, in lieu of using the laborious, time-consuming, and costly acid digestion-ICP-MS method. The major advantages of SP-ICP-MS analysis are easy sample preparation, high throughput, and informative results (particle size information and total TiO₂ mass content).

Key words: single particle inductively coupled plasma-mass spectrometry (SP-ICP-MS), TiO₂ nanoparticle, sunscreen, standard addition method

1. Introduction

TiO₂ nanoparticles (NPs) have been widely used as an effective inorganic UV filter in many sunscreens and other cosmetics. However, their safety has been questioned due to potential skin penetration and bio-accumulation.[1] The smaller the particle, the greater the potential adverse health effects, since smaller particles more easily enter the human body and cross biological membranes where larger particles normally cannot.[2] Research has shown that most of the TiO₂-containing sunscreens catalyze the photo-oxidation of phenol and sunlight-illuminated TiO₂ even caused DNA damage in human cells.[3] TiO₂ NPs can react with natural entities such as natural organic matter, colloids and microorganisms after entering the ecosystem.[4] It has also been demonstrated that various plants can uptake NPs and thereby penetrate the food chain.[5] Recent research shows that TiO₂ NP is toxic to many organisms, such as marine abalone,[6] Japanese medusa,[7] *Mytilus galloprovincialis*,[8] fish,[9] *Daphnia magna* and *Oryzias latipes*,[10] rats,[11] zebrafish embryos.[12, 13] Sunscreens are usually applied to human skin to block ultraviolet rays from sun light. However, visible light or ultraviolet light play a critical role in enhancing TiO₂ toxicity.[8-10, 12] Therefore, there is a need to characterize TiO₂ in sunscreens so as to assess its impact on human health and the environment.

However, to date, there is no official method for TiO₂ characterization that includes particle size, size distribution, existing form (solid TiO₂ or dissolved Ti), and mass content (weight percent) in commercial sunscreens.[2] The primary particle size of TiO₂ NP used for sunscreen formulation is usually less than 50 nm.[14] Since small particles can cross biological membranes, but larger particles normally cannot,[2] it is necessary and important to have a method that has the ability to detect the

primary/smallest (non-aggregated) TiO₂ NP in commercial sunscreens. For TiO₂ particle size determination in cosmetic products, the technique used is mainly field flow fractionation (FFF) orientated, such as FFF-UV,[2] and FFF-ICP-MS.[15-17] The major disadvantages of the FFF method are more complicated sample preparation and the long analysis time, usually 1 hour for each run. For TiO₂ mass content determination, the dominant method is time consuming acid digestion followed by inductively coupled plasma-atomic emission spectroscopy (ICP-AES) or ICP-MS quantification.[18-20] X-ray fluorescence has also been used to measure TiO₂ mass content.[21, 22] However, none of the above-mentioned techniques is able to simultaneously measure particle size distribution, particle concentration (particles/mL), and mass content of TiO₂ rapidly in a single method.

Single particle-ICP-MS (SP-ICP-MS) is an emerging technique for NP characterization, especially in environmental matrices where NP concentrations are relatively low. The principles of SP-ICP-MS were well explained by Degueldre and his colleagues.[23-27] In SP-ICP-MS analysis, NPs enter the plasma and get ionized individually and then are detected as pulse (non-continuous) signals, which means SP-ICP-MS is capable of detecting the masses of metal elements in each NP.[28-30] Meanwhile, the signal of corresponding dissolved analyte is detected as a continuous signal. Therefore, SP-ICP-MS is capable of simultaneously detecting particle analyte and dissolved analyte.[28] The signal intensity of a NP is proportional to the particle size, and the signal frequency is proportional to the particle concentration.[26, 27] SP-ICP-MS has been used for NP size and NP concentration analysis in environmental and biological matrices, such as detecting NPs in wastewater[31, 32] and in chicken meat,[33, 34]

studying the uptake of silver and gold NPs (AuNPs) by *Daphnia magna* and *Lumbriculus variegatus*,[35] detecting AuNPs in rat spleen,[36] characterizing AuNPs uptake by tomato,[37] and tracking the dissolution of silver NPs in several water matrices.[38] These research mainly focused on the determination of NP size and NP concentration in different matrices using the SP-ICP-MS method. To the best of our knowledge, quantitative determination of the NP mass content in complex matrices by the SP-ICP-MS method has not been reported. In this study, a novel and rapid standard addition-SP-ICP-MS method was also developed to determine the TiO₂ mass content in commercial sunscreens, in addition to rapid analysis of TiO₂ NP size, size distribution, and particle concentration.

2. Experiments

2.1 Chemicals and Instrumentation

Four commercial sunscreens containing different amounts of TiO₂ were purchased from local stores. Triton X-100 used to disperse sunscreens, was purchased from Alfa Aesar (Ward Hill, MA). Ultrapure water, with a resistivity of 18.2 MΩ·cm, was produced by a Simplicity185 water system from Millipore. Concentrated trace metal grade sulfuric acid, nitric acid, and hydrochloric acid for hot block acid digestion of sunscreens were purchased from Fisher Scientific (Pittsburgh, PA). A hand-held tissue homogenizer was used to homogenize sunscreens. A dissolved Ti calibration stock solution was obtained from PerkinElmer (Shelton, CT). Three AuNP standards, with particle sizes of 50, 80, and 100 nm, purchased from NanoComposix (San Diego, CA) were used to measure the transport efficiency of the sample introduction system of ICP-MS. These AuNP standards, with a narrow size distribution (TEM data from the vendor),

were citrate-stabilized to prevent aggregation/agglomeration and to achieve an accurate particle concentration. A 40 nm TiO₂ NP, purchased from US-NANO (Houston, TX), was used for the standard addition-SP-ICP-MS method to measure the TiO₂ mass content in these commercial sunscreens. NexION 300/350D ICP-MS (PerkinElmer, Shelton, CT) with Syngistix Nano Application module was used for SP-ICP-MS analysis. Acid digestion was performed using a MOD hot block digester (CPI International-USA, Santa Rosa, CA) to verify the TiO₂ NPs mass content in sunscreen. Hexane purchased from Fisher Scientific (Pittsburgh, PA) was used for TiO₂ particle extraction from sunscreen for scanning electron microscope-energy dispersive spectroscopy (SEM-EDS) analysis (FEI, Hillsboro, Oregon) according to “Method A” in published methods with slight modifications (repeat the extraction three times and centrifuge the aqueous phase).[16]

2.2 SP-ICP-MS Method

The ICP-MS operating conditions and SP-ICP-MS method parameters are listed in **Table 1**. ⁴⁸Ti, with a natural abundance of 73.8%, was measured with SP-ICP-MS. The Syngistix Nano Application module was used for data collection and processing. In SP-ICP-MS analysis, the Ti mass was measured first, and then a mass fraction of 60% was used to convert the Ti mass to TiO₂ mass since the ratio of Ti/TiO₂ is 60% by weight. The TiO₂ mass (*m*) was then converted into TiO₂ particle size (*d*) with the knowledge of TiO₂ density (*ρ*) and by assuming the spherical TiO₂ particle according to **Equation (1)**.

$$m = \rho \times V = \rho \times (4/3) \times \pi \times (d/2)^3 \text{-----}(1)$$

m-mass of a spherical TiO₂ particle; *ρ* -density of TiO₂; *V*-volume of a spherical TiO₂ particle with a diameter of *d*; *d* -diameter of a spherical TiO₂ particle.

Solid TiO₂ has several different forms which have different densities, the most common being rutile and anatase TiO₂. According to Lewicka's study,[39] TiO₂ pigments are usually rutile nanocrystals with a near spherical shape. Therefore, the density of rutile TiO₂, 4.23 g/cm³, was used in the SP-ICP-MS method.

Table 1. ICP-MS operation conditions and SP-ICP-MS method parameters

ICP-MS Operating Condition	
RF Power, W	1600
Gas Flow, L/min	1.06-1.08
Sample Introduction System	Cyclonic Spray chamber with Meinhard nebulizer
Sampler Cone	Nickel
Skimmer Cone	Nickel
SP-ICP-MS Method Parameters	
Analyte	Ti
Mass (amu)	48
Dwell Time, μ s	100
Settling Time, μ s	0
Density, g/cm ³	4.23
Mass Fraction, %	60
Ionization Efficiency, %	100
RPq	0.5

The dwell time was set to 100 μ s for ⁴⁸Ti measurement and the sampling time was 100 seconds. Therefore, one million data points were generated for each sample. Dwell time is a critical parameter and significantly affects the data quality of SP-ICP-MS.[40] A 100 μ s dwell time is much shorter than the typical signal duration of a single NP in ICP-MS, which is 300-500 μ s [40, 41] and, thus, makes peak profiling of a single NP possible. With such short dwell time, particle signal overlapping was minimized as long

as the particle concentration was not too high and, thus, the accuracy of the size measurement was satisfactory. After each run, the software automatically integrated the peak area of each single particle and generated information about particle size distribution, particle concentration, and dissolved concentration.

2.3 Sample Preparation for SP-ICP-MS Analysis

Our preliminary experimental results showed that commercial sunscreens are usually not homogenous (data not shown), which will deteriorate the reproducibility of the developed method. Therefore, the first step was homogenization of these commercial sunscreens using a hand-held homogenizer. After homogenization, 0.2 g or more of the sunscreen sample was dispersed in 1% Triton X-100 aqueous solution to make a 0.1% (w/v) suspension. The mixture was sonicated and vortexed until no aggregates could be seen visually and a milky well-dispersed sample was formed. The mixture was appropriately diluted using ultrapure water for SP-ICP-MS analysis. To measure transport efficiency, stock solutions of 50, 80, and 100 nm AuNP standards were diluted using a diluted sunscreen sample (to match the matrix) to a particle concentration of approximately 10^5 particles/mL, with the exact NP concentration recorded. After dilution, the sunscreen samples contained 0.00005% and 0.00001% Triton X-100 for 2×10^4 and 10^5 times dilution, respectively. Therefore, dissolved Ti calibration standards were prepared in 0.00005% Triton X-100, 0.00001% Triton X-100, and ultrapure water to calculate the TiO_2 particle size and to measure the dissolved Ti concentrations in the samples if present, according to established SP-ICP-MS theory.[30]

2.4 Standard Addition-SP-ICP-MS Method to Measure TiO₂ Mass Content in Sunscreens

From SP-ICP-MS analysis, the TiO₂ particle size and the number of particles at each size were available. With the knowledge of particle density, the mass of each particle could be calculated, assuming a spherical particle. Therefore, by summing the mass of each particle size, the TiO₂ mass content could be calculated theoretically. However, due to partial aggregation of TiO₂ and the complex matrix of sunscreen, the TiO₂ mass content calculated using this method was much lower (data not shown here) than hot block digestion and the manufacturer-claimed value. The standard addition method could correct the matrix effect/aggregation effect by the addition of different known amounts of the analyte standard (provided the size is well-matched) into the samples to measure the mass concentration. Therefore, the standard addition method was developed to measure the TiO₂ mass content in sunscreens.

First, a 0.1% (w/v) sunscreen suspension in 1% Triton X-100 was prepared, as described above, then further diluted 100 times using 1% Triton X-100 first, followed by another 100 times dilution, using ultrapure water. A 40 nm TiO₂ (purity of 99.5%) NP standard stock suspension was prepared by dispersing the TiO₂ NP in a 1% Triton X-100 aqueous solution. Four spike concentrations, 0, 1.33, 3.33, and 6.65 µg/L of 40 nm TiO₂ NP, were achieved by adding different volumes of the NP stock suspension into the diluted sunscreen samples. These spike concentrations were chosen because they were at the same order of magnitude of the endogenous TiO₂ NP mass concentration in the sunscreen, according to the manufacturer-claimed TiO₂ mass content. The samples were analyzed using the SP-ICP-MS method.

After SP-ICP-MS analysis, a plot of total ion counts *versus* spiked concentration was established. The absolute value of the intersection of the extrapolated curve and X-axis was the endogenous TiO₂ mass concentration in sunscreen samples diluted 10,000 times. The TiO₂ mass content in the original sunscreen cream was then calculated based on the dilution factor. All sunscreen samples were analyzed in triplicate.

2.5 Hot Block Acid Digestion and ICP-MS Determination of TiO₂ Mass Content in Sunscreens

Hot block acid digestion, followed by conventional ICP-MS detection, was performed to verify the TiO₂ mass content in chosen sunscreens. The same 40 nm TiO₂ NP used in the standard addition method was used as an indicator to evaluate hot block digestion performance. The 40 nm TiO₂ NP was digested both alone and by spiking into the commercial sunscreen samples. The spike recovery was calculated to evaluate the digestion performance. An aliquot of 0.2 g homogenized sunscreen sample was weighed into a 70-mL digestion vessel. After weighing, it was heated at 95 °C for approximately 5 minutes to evaporate any possible volatile organics in the sunscreens. After organics being evaporated, 4 mL each of trace metal grade concentrated sulfuric acid, nitric acid, and hydrochloric acid were added sequentially for sample digestion. (Caution: A lot of heat was generated when adding concentrated nitric acid and hydrochloric acid into concentrated sulfuric acid. Drop by drop addition and personal protective equipment were required.) The digestion temperature was set at 95 °C and the digestion was continued until the 40 nm TiO₂ particles were completely dissolved and a clear solution was obtained. After digestion, the solution was brought to 50 mL with ultrapure water. The sample was filtered by a 0.45 micron Nylon membrane filter, and then was further diluted

with 1% trace metal grade nitric acid for conventional ICP-MS analysis. Due to the potential interference of S-O from the sulfuric acid used in digestion, ^{47}Ti isotope with a natural abundance of 7.3% was monitored instead of ^{48}Ti with a natural abundance of 73.8%.

3. Results and Discussions

3.1 Particle Size Detection Limit of the Developed SP-ICP-MS Method.

In SP-ICP-MS analysis, a particle can only be detected if the pulse signal generated by the particle can be distinguished from the background signal.[42, 43] Most reported size detection limit was determined by finding the value of three times of the standard deviations above the average background intensity (usually ultrapure water) and calculating the corresponding particle size.[42, 43] The size detection limit calculated using this method is largely affected by dwell time, and a shorter dwell time can enhance the signal-to-noise ratio.[44] In this study, a dwell time of 0.1 ms was used, which is significantly shorter than that in most publications (usually several milliseconds). Therefore, the calculated size detection limit was unpractically small (~20 nm for TiO_2 , Supplementary Information, Sheet “Ti48 for ultrapure water” and “Ti48 for 0.00005% Triton”). However, there was a peak with an intensity of 3 counts for the blanks (ultrapure water and diluted Triton X-100). The Nano Application module converted the instrument response (counts) into TiO_2 particle size (nm) using the dissolved Ti calibration curve, according to the SP-ICP-MS theory.[30] Based on the dissolved Ti calibration curve, 3 counts were equal to 27-29 nm TiO_2 (due to day-to-day instrument sensitivity variation, the value fluctuated slightly). In the blanks, there was no TiO_2 NP

present theoretically. However, a 27-29 nm TiO₂ peak was always obtained for them, which indicated that the practical particle size detection limit for the developed method was approximately 27-29 nm for TiO₂ NP, if ⁴⁸Ti was measured. ⁴⁸Ca is a major interference for ⁴⁸Ti measurement in quadrupole ICP-MS, especially for environmental sample matrices.[45] However, ICP-MS results showed that the calcium content was extremely low (Supplementary Information, Sheet “Calcium content in sunscreens”) in sunscreens compared to TiO₂ mass content, which enables us to measure ⁴⁸Ti (natural abundance, 73.8%) instead of ⁴⁷Ti (7.3%) or ⁴⁹Ti (5.5%).

3.2 Sunscreen Containing no TiO₂ NPs as Quality Control

One sunscreen (sunscreen 3) that did not contain any TiO₂ NP (manufacturer claimed) served as a negative control in this study. **Figure 1(a)** shows the raw data of SP-ICP-MS detection for the 10⁵ times-diluted sunscreen 3 sample. **Figure 1(b)** shows the raw data for diluted sunscreen 3 with spiking at 6.65 µg/L of 40 nm TiO₂ NPs. From these two plots, it is evident that no TiO₂ NPs were detected in the unspiked sunscreen, while many TiO₂ NPs were detected in the spiked sample. The processed data for diluted sunscreen 3, with spiking at 6.65 µg/L of 40 nm TiO₂, depicted in **Figure 1(c)**, shows that the measured size was approximately 40 nm, which matched the spiked TiO₂ NPs size. A tailing peak in the size distribution plot was observed, due to either particle aggregation (40 nm TiO₂ NPs do not contain any surface stabilizing agent to prevent aggregation) or the nature of the TiO₂ NPs standard used. These data were quality control for this method and indicated that the developed method was able to accurately determine the size of TiO₂ NPs in the sunscreen matrix.

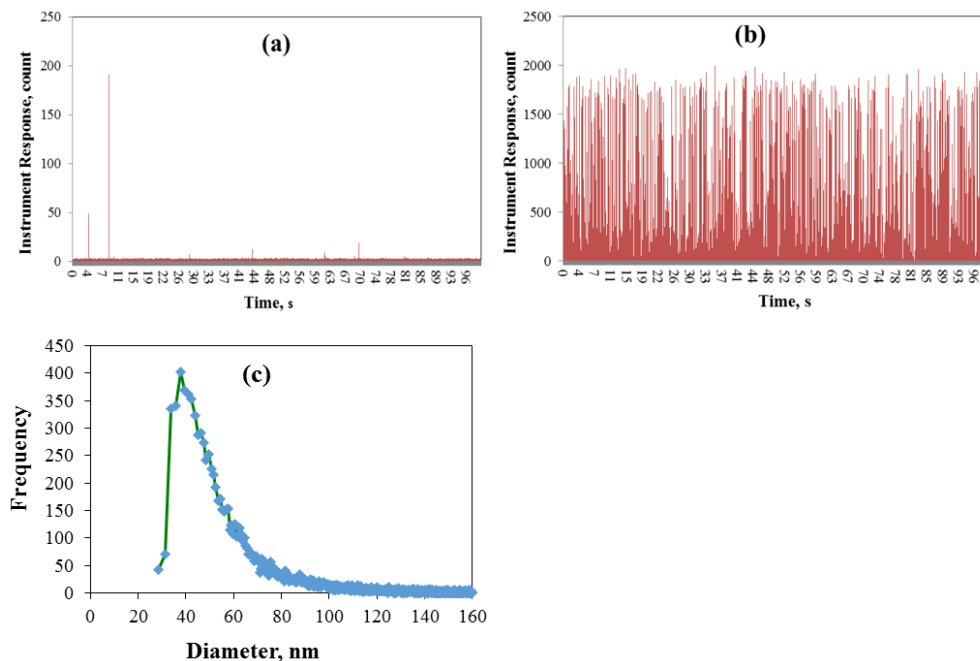


Figure 1. (a) Raw data for diluted sunscreen 3; (b) Raw data of spiking 6.65 $\mu\text{g/L}$ 40 nm TiO_2 into diluted sunscreen 3; (c) Processed data of spiking 6.65 $\mu\text{g/L}$ 40 nm TiO_2 into sunscreen 3 based on Figure 1(b).

3.3 Size distribution for different sunscreens

For determination of particle size by SP-ICP-MS, two methods are currently reported in the literature. The first method, which is also the most straightforward one, is to use well-characterized NPs of different sizes with accurate particle size and narrow size distribution as calibration standards.[28, 29, 31, 38] The instrument response is proportional to the third power of the particle diameter. However, due to the absence of commercially available well characterized, surface-stabilized TiO_2 NP standards with narrow size distributions, the above described correlation could not be routinely used. Alternatively, we used the corresponding dissolved metal standard intensity to determine particle size, the method described by Pace *et al.*[30] In this method, the dissolved Ti

mass concentration ($\mu\text{g/L}$) was converted to Ti mass (μg) per event/dwell time using sample flow rate, dwell time, and transport efficiency. In this way, the relationship between the instrument response (counts) and Ti mass could be established. The Ti mass was then converted to TiO_2 particle size. The assumption for this method was that NP suspension and the dissolved analyte solution had similar transport efficiency and sensitivity in the sample introduction system. Both methods have been incorporated in the software of the Syngistix Nano Application module. In this study, well-defined AuNP standards were used to measure the transport efficiency, and dissolved Ti standards were used to calculate the TiO_2 particle size and dissolved Ti concentration if present.

Figure 2(a) shows typical raw data for a diluted TiO_2 NP-containing sunscreen sample. The large pulses with intensities of several hundred or several thousand counts represent aggregates of primary TiO_2 NPs or the nature of the TiO_2 NPs used in the sunscreen manufacturing. For a better view of the raw data, the inset of **Figure 2(a)** is the first 5,000 data points and shows a lot of small pulses with intensities of several counts, which represent the primary TiO_2 NPs in the sunscreen. Nano-sized TiO_2 can form TiO_2 aggregates of a much larger size during sunscreen formulation.[14] Only pulse signals were observed (**Figure 2(a)**), which indicated TiO_2 existed as TiO_2 particles instead of dissolved Ti in the sunscreens because, if dissolved Ti is present, a continuous Ti signal would be observed. The result agrees with the fact that TiO_2 is very difficult to dissolve under common conditions. **Figure 2(b)** shows the size distribution for 2×10^4 times-diluted sunscreen 1. Considering that the size detection limit was 27-29 nm, the major peak of 2×10^4 times-diluted sunscreen 1 appeared at approximately 32-35 nm. Three replicates also indicated very good reproducibility. This indicated that the 32-35

nm peak represented the primary TiO₂ NP size in the sunscreen. To further verify this, a sample with a higher dilution factor was analyzed. **Figure 2(c)** shows the size distribution for 10⁵ times-diluted sunscreen 1 sample. With further dilution, the major peak was still at 32-35 nm with a decreased frequency/particle concentration, which was caused by further dilution. This confirmed that the major peak at 32-35 nm represented the smallest/primary TiO₂ NPs in sunscreen 1. These primary NPs represent the smallest TiO₂ particles that the human body can potentially be exposed to when sunscreen is applied to human skin. **Figure 2(d)** shows the size distribution of diluted sunscreen 1 measured on different days, which demonstrated good day-to-day reproducibility of the method.

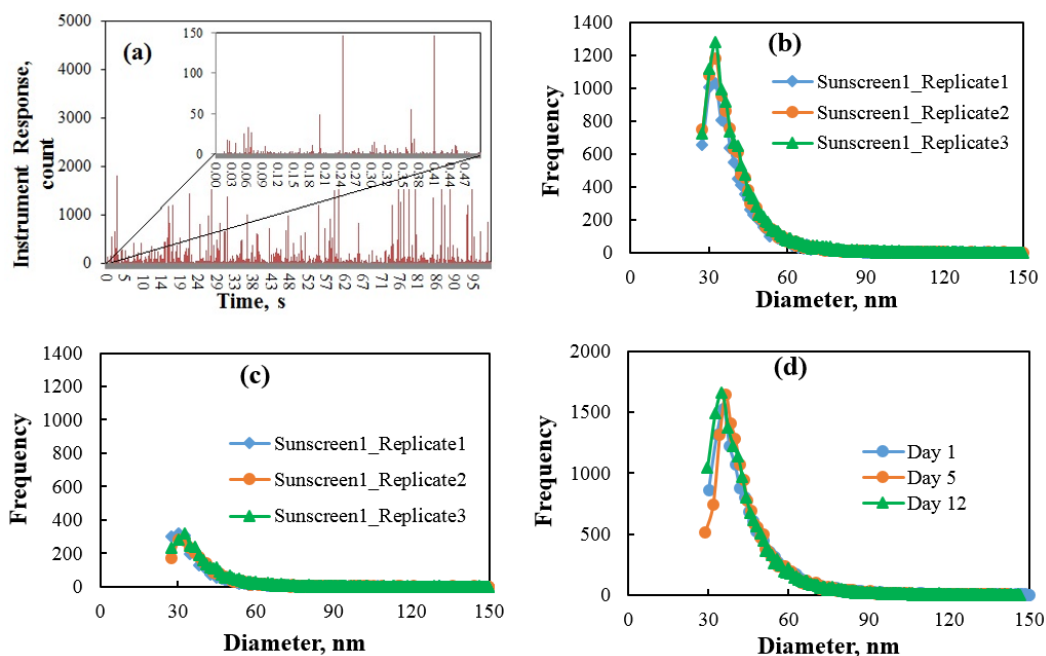


Figure 2. (a) The overview of raw data (1,000,000 data points in total) for 2×10^4 times-diluted sunscreen 1. Inset: the first 5000 data points out of 1,000,000 data points; (b) Size distribution for 2×10^4 times-diluted sunscreen 1. (c) Size distribution for 10^5 times-diluted sunscreen 1. (d) Size distribution for diluted sunscreen 1 measured at Day 1, Day 5 and Day 12.

Figures 3(a) and 3(b) show the size distributions for 2×10^4 times-diluted and 10^5 times-diluted sunscreen 2, respectively. With different dilution factors, the size distribution remained the same. The measured primary particle size for this sunscreen was 35-40 nm, slightly larger than that for sunscreen 1. Three replicates also showed good reproducibility, especially for 2×10^4 times-diluted samples. The TiO_2 particle size in sunscreen 2 was confirmed by SEM shown in **Figure 4**. The chemical identity of particles shown in **Figure 4** was confirmed by SEM-EDS to be Ti-containing particles and it should be TiO_2 in this case. The particle size measured by SP-ICP-MS and SEM agreed well with each other. **Figure 3(c)** shows the size distribution for 2×10^4 times-diluted sunscreen 4 and **Figure 3(d)** shows the size distribution for 10^5 times-diluted sunscreen 4. The measured particle size was approximately 32-35 nm, which is similar to that in sunscreen 1.

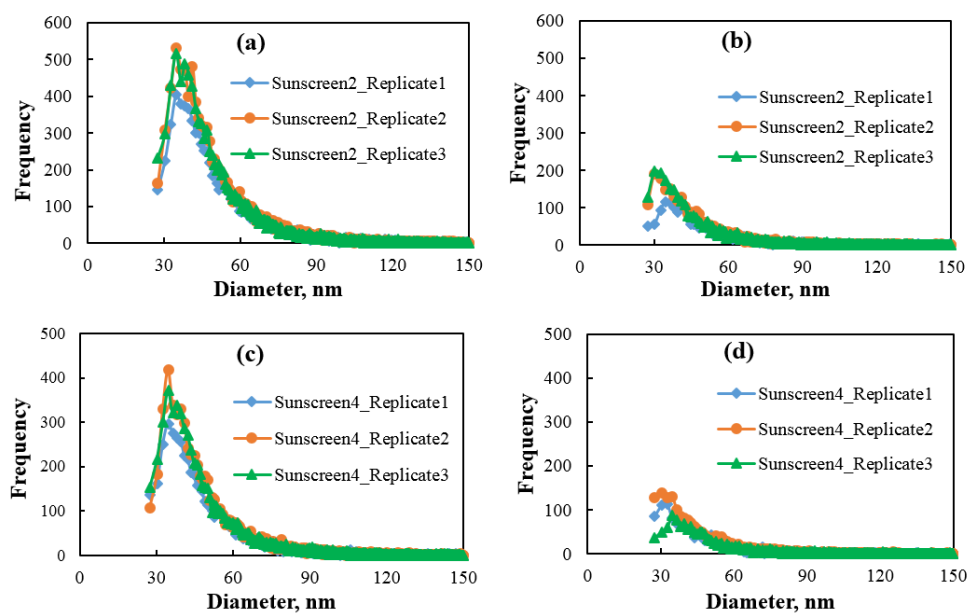


Figure 3. (a) Size distribution for 2×10^4 times-diluted Sunscreen 2; (b) Size distribution for 10^5 times-diluted Sunscreen 2; (c) Size distribution for 2×10^4 times-diluted Sunscreen 4; (d) Size distribution for 10^5 times-diluted Sunscreen 4.

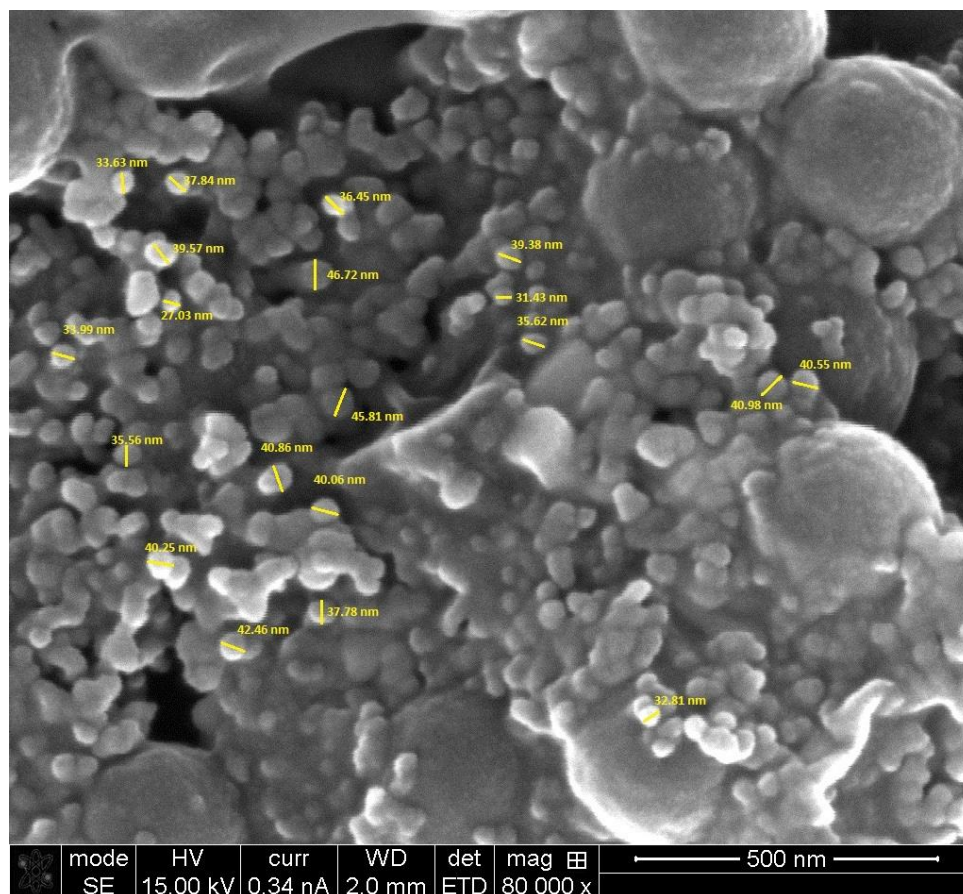


Figure 4. SEM image for TiO₂ NPs extracted from Sunscreen 2.

3.4 Particle Concentration

For particle concentration determination in SP-ICP-MS, the transport efficiency of the sample introduction system is a critical parameter. Transport efficiency is the efficiency of the sample introduction system transporting NPs into plasma. The transport efficiency measured with gold reference nanoparticles can be extended to the characterization of other metallic nanoparticles.[30] Transport efficiency (η) was measured using 50, 80, and 100 nm AuNPs, according to Method 3 in Pace's paper.[30] The TiO₂ NP concentration (C_p) was calculated using the knowledge of transport

efficiency (η), aspiration rate (f), sampling time (t), and number of TiO₂ particle signals (N_i), based on **Equation (2)**.

$$C_p = \frac{N_i}{f \cdot t \cdot \eta} \text{-----(2)}$$

N_i -number of particle signals; f -aspiration rate, mL/min; t -sampling time, min; C_p -particle concentration, particles/mL.

Table 2 shows the particle concentration for the 2×10^4 times-diluted sunscreen samples. The sampling time (t) was 100 seconds for the developed method and the flow/aspiration rate (f) was 0.268 mL/min. The transport efficiency (η) was measured using 50, 80, and 100 nm (similar η for 50, 80, and 100 nm AuNPs) AuNPs and was averaged to be 6.87% (a small variation every time) The number of particle signals seen by the instrument (N_i) was given by the software as shown in the No. of Peaks column of **Table 2**. With all of this information, the particle concentration (C_p) was calculated using **Equation (2)**. The relative standard deviations (RSDs) of the triplicated detection were less than 12% for 29-100 nm range, which indicates good reproducibility, especially for NP analysis. It should be noted that the particle concentration of particles larger than 100 nm was also calculated using the same transport efficiency as the particles 29-100 nm, which was measured using 50, 80, 100 nm AuNPs. The actual transport efficiency of these larger particles is expected to be lower than that of particles less than 100 nm. Since this research was mainly focused on NPs (< 100 nm) analysis, the particle concentrations of larger than 100 nm particles were not further studied and only semi-qualitative data were provided.

Table 2. Particle concentration information for 2×10^4 times-diluted sunscreen samples

Sample Name		No. of Peaks		Particle Concentration (particles/mL)		RSD, %	
		29-100 nm	>100 nm	29-100 nm	>100 nm	29-100 nm	>100 nm
Sunscreen 1	Replicate 1	10402	415	338982	13524	11.63	17.19
	Replicate 2	12012	508	391449	16555		
	Replicate 3	13145	588	428371	19162		
Sunscreen 2	Replicate 1	9524	1514	310370	49338	9.47	4.79
	Replicate 2	11479	1530	374079	49860		
	Replicate 3	10926	1400	356058	45623		
Sunscreen 4	Replicate 1	6080	1025	198136	33403	10.02	2.75
	Replicate 2	7351	1083	239555	35293		
	Replicate 3	7172	1054	233722	34348		

3.5 Standard Addition method for TiO₂ mass content determination.

Sunscreens usually contain high level of inorganic and organic ingredients, which makes the matrix complex. Microwave-assisted or hot block acid digestion can be used for TiO₂ mass content determination. However, acid digestion is time-consuming, labor intensive, and costly. The standard addition method can correct the matrix effect/aggregation effect by adding different known amounts of analyte standard (provided the size is well-matched) in the samples for concentration measurement. In SP-ICP-MS analysis, the total ion count is available by simply summing all ion counts. The total ion count is proportional to the TiO₂ mass content in a sunscreen sample. The correlation of total ion counts and TiO₂ mass content was obtained by adding known amounts of the TiO₂ NP standard into the sunscreen sample.

In this study, since the measured TiO₂ size in these sunscreens was 32-40 nm, a 40 nm TiO₂ NP was chosen as the standard for the standard addition method to quantify the TiO₂ mass content, considering the fact that similar sizes of NPs are supposed to have

similar behaviors in the same matrix. For each sunscreen, one aliquot of a sample, without adding any 40 nm TiO₂ NPs, and three more aliquots were spiked with different amounts of 40 nm TiO₂ NPs standard to make spiked concentrations of 1.33, 3.33, and 6.65 µg/L. All samples were prepared and analyzed in triplicate by the SP-ICP-MS method to determine reproducibility of the method. A plot of total ion counts *versus* spiked concentration (0, 1.33, 3.33, 6.65 µg/L) was established from the SP-ICP-MS data. The curve was extrapolated to X-axis and the absolute value of the intersection of the extrapolated curve and the X-axis was the endogenous TiO₂ mass concentration in the diluted sunscreen sample.

Figures 5(a)-5(d) show the results of the standard addition-SP-ICP-MS method for sunscreen 1, sunscreen 2, sunscreen 3, and sunscreen 4, respectively. The concentration calculated from **Figure 5** was TiO₂ mass concentration in sunscreen samples diluted 10,000 times. The TiO₂ mass content in the original sunscreen was calculated back into a percentage based on the sample preparation procedures. **Figure 6** shows the comparison of TiO₂ mass content determined by the standard addition-SP-ICP-MS method, with the hot block digestion-ICP-MS method, and with the manufacturer-claimed mass content. The TiO₂ mass contents, measured by the standard addition-SP-ICP-MS method for sunscreen 2 and sunscreen 3, were very close to those determined by the acid digestion-ICP-MS method and what the manufacturer-claimed. However, for sunscreen 1 and sunscreen 4, the TiO₂ mass content determined by the standard addition-SP-ICP-MS method was lower than that determined by the conventional acid digestion-ICP-MS method. Three possible reasons may have caused this. (1) The size of the TiO₂ in sunscreen 2 had a primary particle size of 35-40 nm, as shown in **Figure 3(a)**. This

was closer to the size of the 40 nm TiO₂ NP standard than those of sunscreen 1 and sunscreen 4, which were approximately 32-35 nm. (2) The 40 nm TiO₂ NP used for the standard addition was anatase TiO₂. It is possible that the TiO₂ used in these commercial sunscreens was rutile TiO₂ or the mixture of rutile and anatase TiO₂. [39] (3) The shape of the 40 nm TiO₂ NP standard was spherical, while, the shape of the TiO₂ in sunscreen 1 and sunscreen 4 may not be perfectly spherical. In the standard addition method, choosing the right standard was important to achieve good accuracy. Nevertheless, the standard addition-SP-ICP-MS method still offered a promising rapid and simple alternative for determining the TiO₂ NP mass content in sunscreen. The 40 nm TiO₂ NP standard used in this study was the best match we have been able to find so far. The accuracy could be improved if better matched NP standards were available.

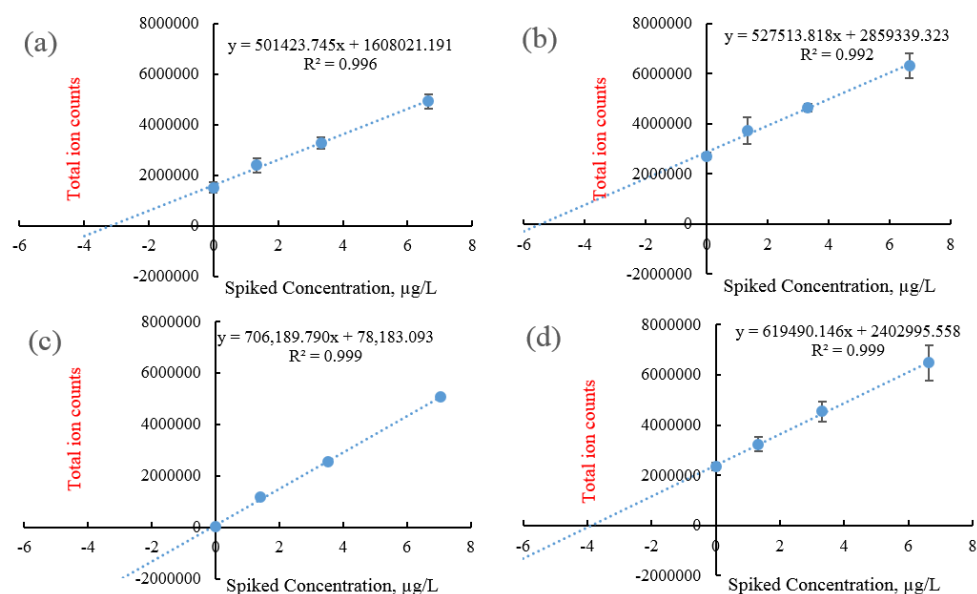


Figure 5. Standard addition method for four sunscreens to detect TiO₂ mass content. (a), (b), (c), (d) stands for 10000 times-diluted sunscreen 1, sunscreen 2, sunscreen 3 and sunscreen 4, respectively.

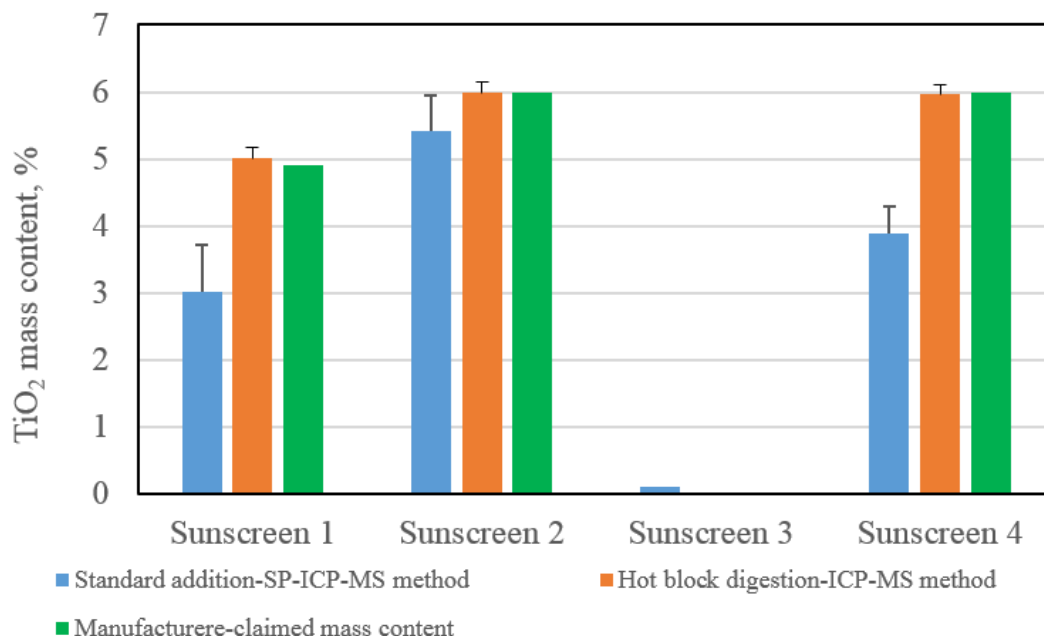


Figure 6. Comparison of TiO_2 mass content determined by standard addition-SP-ICP-MS method, acid digestion-ICP-MS method and manufacturer-claimed.

4. Conclusions

A novel SP-ICP-MS method was developed to determine the TiO_2 NP size, size distribution, and particle concentration in commercial sunscreens. The developed method is high throughput, reproducible, and sensitive. The primary particle size determined by the SP-ICP-MS in commercial sunscreens was in the range of 32-40 nm. TiO_2 NP mass content was also determined by a standard addition-SP-ICP-MS method which takes much less time than the conventional acid digestion-ICP-MS method. The TiO_2 mass content in sunscreens that was determined by the standard addition-SP-ICP-MS method was close to that determined by the conventional acid digestion-ICP-MS method, and the TiO_2 content claimed by the manufacturer. Further improvement in accuracy can be achieved if better-matched NP standards are available. This SP-ICP-MS method provides

unique advantages over other currently available methods, such as high throughput, informative (simultaneous detection of particle size, size distribution, aggregation, dissolved concentration), and economical. The developed method should also be applicable for other samples containing TiO₂ NPs and other metallic NPs with appropriate modifications.

Acknowledgement

The NexION 300/350D ICP-MS was provided by PerkinElmer, Inc. The authors appreciate the support provided by University of Missouri Research Board, the Chemistry Department and the Center for Single Nanoparticle, Single Cell, and Single Molecule Monitoring (CS³M) at the Missouri University of Science and Technology, Rolla, Missouri. The authors also thank Qian Yao Li for assistance with SEM imaging and EDS analysis.

References

- [1] H. Shi, R. Magaye, V. Castranova, J. Zhao, Titanium dioxide nanoparticles: a review of current toxicological data, *Part. Fibre Toxicol.* 10 (2013) 15.
- [2] C. Contado, A. Pagnoni, TiO₂ in Commercial Sunscreen Lotion: Flow Field-Flow Fractionation and ICP-AES Together for Size Analysis, *Anal. Chem.* 80 (2008) 7594-7608.
- [3] R. Dunford, A. Salinaro, L. Cai, N. Serpone, S. Horikoshi, H. Hidaka, J. Knowland, Chemical oxidation and DNA damage catalysed by inorganic sunscreen ingredients, *FEBS Lett.* 418 (1997) 87-90.
- [4] F. Loosli, P. Le Coustumer, S. Stoll, Effect of natural organic matter on the disagglomeration of manufactured TiO₂ nanoparticles, *Environ. Sci.: Nano* 1 (2014) 154-160.
- [5] X. Ma, J. Geisler-Lee, J. Geiser-Lee, Y. Deng, A. Kolmakov, Interactions between engineered nanoparticles (ENPs) and plants: phytotoxicity, uptake and accumulation, *Sci. Total Environ.* 408 (2010) 3053-3061.
- [6] X. Zhu, Z. Jin, Z. Cai, The toxicity and oxidative stress of TiO₂ nanoparticles in marine abalone (*Haliotis diversicolor supertexta*), *Mar. Pollut. Bull.* 63 (2011) 334-338.
- [7] G. Paterson, J.M. Ataria, M.E. Hoque, D.C. Burns, C.D. Metcalfe, The toxicity of titanium dioxide nanopowder to early life stages of the Japanese medaka (*Oryzias latipes*), *Chemosphere* 82 (2011) 1002-1009.
- [8] G. Libralato, D. Minetto, S. Totaro, I. Micetic, A. Pigozzo, E. Sabbioni, A. Marcomini, A. Volpi Ghirardini, Embryotoxicity of TiO₂ nanoparticles to *Mytilus galloprovincialis* (Lmk), *Mar. Environ. Res.* 92 (2013) 71-78.
- [9] Z. Clemente, V.L. Castro, L.O. Feitosa, R. Lima, C.M. Jonsson, A.H.N. Maia, L.F. Fraceto, Fish exposure to nano-TiO₂ under different experimental conditions: Methodological aspects for nanoecotoxicology investigations, *Sci. Total Environ.* 463-464 (2013) 647-656.
- [10] S. Li, X. Pan, L.K. Wallis, Z. Fan, Z. Chen, S.A. Diamond, Comparison of TiO₂ nanoparticle and graphene-TiO₂ nanoparticle composite phototoxicity to *Daphnia magna* and *Oryzias latipes*, *Chemosphere* 112 (2014) 62-69.
- [11] M.M. Dobrzynska, A. Gajowik, J. Radzikowska, A. Lankoff, M. Dusinska, M. Kruszewski, Genotoxicity of silver and titanium dioxide nanoparticles in bone marrow cells of rats in vivo, *Toxicology* 315 (2014) 86-91.
- [12] Z. Clemente, V.L.S.S. Castro, M.A.M. Moura, C.M. Jonsson, L.F. Fraceto, Toxicity assessment of TiO₂ nanoparticles in zebrafish embryos under different exposure conditions, *Aquat. Toxicol.* 147 (2014) 129-139.

- [13] S. Pavagadhi, M. Sathishkumar, R. Balasubramanian, Uptake of Ag and TiO₂ nanoparticles by zebrafish embryos in the presence of other contaminants in the aquatic environment, *Water Res.* 55 (2014) 280-291.
- [14] S. Wiechers, P. Biehl, C. Luven, M. Maier, J. Meyer, J. Muenzenberg, C. Schulze-Isfort, P. Albers, Titanium dioxide particle size vs. sun protection performance, *Cosmet. Toiletries* 128 (2013) 332, 334, 336, 338-339.
- [15] I. Lopez-Heras, Y. Madrid, C. Camara, Prospects and difficulties in TiO₂ nanoparticles analysis in cosmetic and food products using asymmetrical flow field-flow fractionation hyphenated to inductively coupled plasma mass spectrometry, *Talanta* 124 (2014) 71-78.
- [16] V. Nischwitz, H. Goenaga-Infante, Improved sample preparation and quality control for the characterization of titanium dioxide nanoparticles in sunscreens using flow field flow fractionation on-line with inductively coupled plasma mass spectrometry, *J. Anal. At. Spectrom.* 27 (2012) 1084-1092.
- [17] A. Samontha, J. Shiowatana, A. Siripinyanond, Particle size characterization of titanium dioxide in sunscreen products using sedimentation field-flow fractionation-inductively coupled plasma-mass spectrometry, *Anal. Bioanal. Chem.* 399 (2011) 973-978.
- [18] T. Bunhu, A. Kindness, B.S. Martincigh, Determination of titanium dioxide in commercial sunscreens by inductively coupled plasma-optical emission spectrometry, *S. Afr. J. Chem.* 64 (2011) 139-143.
- [19] M.C.E. Lomer, R.P.H. Thompson, J. Commisso, C.L. Keen, J.J. Powell, Determination of titanium dioxide in foods using inductively coupled plasma optical emission spectrometry, *Analyst* 125 (2000) 2339-2343.
- [20] A. Salvador, M.C. Pascual-Marti, J.R. Adell, A. Requeni, J.G. March, Analytical methodologies for atomic spectrometric determination of metallic oxides in UV sunscreen creams, *J. Pharm. Biomed. Anal.* 22 (2000) 301-306.
- [21] A. Kawauchi, M. Ishida, I. Saitoh, Measurement of titanium dioxide in cosmetic products with X-ray fluorescence spectrometry, *Spectrosc. Lett.* 29 (1996) 345-366.
- [22] F.L. Melquiades, D.D. Ferreira, C.R. Appoloni, F. Lopes, A.G. Lonni, F.M. Oliveira, J.C. Duarte, Titanium dioxide determination in sunscreen by energy dispersive X-ray fluorescence methodology, *Anal. Chim. Acta* 613 (2008) 135-143.
- [23] C. Degueldre, P.Y. Favarger, Colloid analysis by single particle inductively coupled plasma-mass spectroscopy: a feasibility study, *Colloids Surf. A* 217 (2003) 137-142.
- [24] C. Degueldre, P.Y. Favarger, Thorium colloid analysis by single particle inductively coupled plasma-mass spectrometry, *Talanta* 62 (2004) 1051-1054.

- [25] C. Degueldre, P.Y. Favarger, C. Bitea, Zirconia colloid analysis by single particle inductively coupled plasma-mass spectrometry, *Anal. Chim. Acta* 518 (2004) 137-142.
- [26] C. Degueldre, P.Y. Favarger, R. Rosse, S. Wold, Uranium colloid analysis by single particle inductively coupled plasma-mass spectrometry, *Talanta* 68 (2006) 623-628.
- [27] C. Degueldre, P.Y. Favarger, S. Wold, Gold colloid analysis by inductively coupled plasma-mass spectrometry in a single particle mode, *Anal. Chim. Acta* 555 (2006) 263-268.
- [28] F. Laborda, J. Jimenez-Lamana, E. Bolea, J.R. Castillo, Selective identification, characterization and determination of dissolved silver(I) and silver nanoparticles based on single particle detection by inductively coupled plasma mass spectrometry, *J. Anal. At. Spectrom.* 26 (2011) 1362-1371.
- [29] D.M. Mitrano, E.K. Leshner, A. Bednar, J. Monserud, C.P. Higgins, J.F. Ranville, Detecting nanoparticulate silver using single-particle inductively coupled plasma-mass spectrometry, *Environ. Toxicol. Chem.* 31 (2012) 115-121.
- [30] H.E. Pace, N.J. Rogers, C. Jarolimek, V.A. Coleman, C.P. Higgins, J.F. Ranville, Determining Transport Efficiency for the Purpose of Counting and Sizing Nanoparticles via Single Particle Inductively Coupled Plasma Mass Spectrometry, *Anal. Chem.* 83 (2011) 9361-9369.
- [31] J. Tuoriniemi, G. Cornelis, M. Hasseløev, Size Discrimination and Detection Capabilities of Single-Particle ICPMS for Environmental Analysis of Silver Nanoparticles, *Anal. Chem.* 84 (2012) 3965-3972.
- [32] R. Peters, Z. Herrera-Rivera, A. Undas, M. van der Lee, H. Marvin, H. Bouwmeester, S. Weigel, Single particle ICP-MS combined with a data evaluation tool as a routine technique for the analysis of nanoparticles in complex matrices, *J. Anal. At. Spectrom.* (2015) in press.
- [33] K. Loeschner, J. Navratilova, C. Kobler, K. Molhave, S. Wagner, K.F. von der, E.H. Larsen, Detection and characterization of silver nanoparticles in chicken meat by asymmetric flow field flow fractionation with detection by conventional or single particle ICP-MS, *Anal. Bioanal. Chem.* 405 (2013) 8185-8195.
- [34] R.J.B. Peters, Z.H. Rivera, G. van Bommel, H.J.P. Marvin, S. Weigel, H. Bouwmeester, Development and validation of single particle ICP-MS for sizing and quantitative determination of nano-silver in chicken meat, *Anal. Bioanal. Chem.* 406 (2014) 3875-3885.
- [35] E.P. Gray, J.G. Coleman, A.J. Bednar, A.J. Kennedy, J.F. Ranville, C.P. Higgins, Extraction and Analysis of Silver and Gold Nanoparticles from Biological Tissues Using Single Particle Inductively Coupled Plasma Mass Spectrometry, *Environ. Sci. Technol.* 47 (2013) 14315-14323.

- [36] K. Loeschner, M.S.J. Brabrand, J.J. Sloth, E.H. Larsen, Use of alkaline or enzymatic sample pretreatment prior to characterization of gold nanoparticles in animal tissue by single-particle ICPMS, *Anal. Bioanal. Chem.* 406 (2014) 3845-3851.
- [37] Y. Dan, W. Zhang, R. Xue, X. Ma, C. Stephan, H. Shi, Characterization of Gold Nanoparticle Uptake by Tomato Plants Using Enzymatic Extraction Followed by Single-Particle Inductively Coupled Plasma-Mass Spectrometry Analysis, *Environ. Sci. Technol.* 49 (2015) 3007-3014.
- [38] D.M. Mitrano, J.F. Ranville, A. Bednar, K. Kazor, A.S. Hering, C.P. Higgins, Tracking dissolution of silver nanoparticles at environmentally relevant concentrations in laboratory, natural, and processed waters using single particle ICP-MS (spICP-MS), *Environ. Sci.: Nano* 1 (2014) 248-259.
- [39] Z.A. Lewicka, A.F. Benedetto, D.N. Benoit, W.W. Yu, J.D. Fortner, V.L. Colvin, The structure, composition, and dimensions of TiO₂ and ZnO nanomaterials in commercial sunscreens, *J. Nanopart. Res.* 13 (2011) 3607-3617.
- [40] A. Hineman, C. Stephan, Effect of dwell time on single particle inductively coupled plasma mass spectrometry data acquisition quality, *J. Anal. At. Spectrom.* 29 (2014) 1252-1257.
- [41] M.D. Montano, H.R. Badieli, S. Bazargan, J.F. Ranville, Improvements in the detection and characterization of engineered nanoparticles using spICP-MS with microsecond dwell times, *Environ. Sci.: Nano* 1 (2014) 338-346.
- [42] S. Lee, X. Bi, R.B. Reed, J.F. Ranville, P. Herckes, P. Westerhoff, Nanoparticle Size Detection Limits by Single Particle ICP-MS for 40 Elements, *Environ. Sci. Technol.* 48 (2014) 10291-10300.
- [43] H.E. Pace, N.J. Rogers, C. Jarolimek, V.A. Coleman, E.P. Gray, C.P. Higgins, J.F. Ranville, Single particle inductively coupled plasma-mass spectrometry: a performance evaluation and method comparison in the determination of nanoparticle size, *Environ. Sci. Technol.* 46 (2012) 12272-12280.
- [44] S.T. Kim, H.K. Kim, S.H. Han, E.C. Jung, S. Lee, Determination of size distribution of colloidal TiO₂ nanoparticles using sedimentation field-flow fractionation combined with single particle mode of inductively coupled plasma-mass spectrometry, *Microchem. J.* 110 (2013) 636-642.
- [45] A.P. Gondikas, F.v.d. Kammer, R.B. Reed, S. Wagner, J.F. Ranville, T. Hofmann, Release of TiO₂ Nanoparticles from Sunscreens into Surface Waters: A One-Year Survey at the Old Danube Recreational Lake, *Environ. Sci. Technol.* 48 (2014) 5415-5422.

II. CHARACTERIZATION OF GOLD NANOPARTICLES UPTAKE BY TOMATO PLANTS USING ENZYMATIC EXTRACTION FOLLOWED BY SINGLE PARTICLE INDUCTIVELY COUPLED PLASMA-MASS SPECTROMETRY ANALYSIS

Yongbo Dan^{1,2}, Weilan Zhang³, Runmiao Xue^{1,2}, Xingmao Ma^{2,3}, Chady Stephan⁴,
Honglan Shi^{1,2,*}

¹*Department of Chemistry, Missouri University of Science and Technology, Rolla, MO, 65409, USA*

²*Center for Single Nanoparticle, Single Cell, and Single Molecule Monitoring (CS³M), Missouri University of Science and Technology, Rolla, MO, 65409, USA*

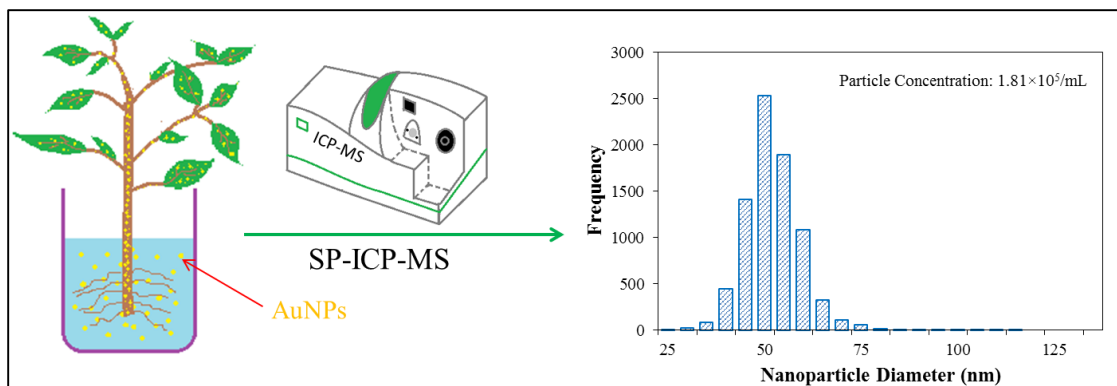
³*Zachry Department of Civil Engineering, Texas A&M University, College Station, TX, 77845, USA*

⁴*PerkinElmer, Inc., 501 Rowntree Dairy Rd, Woodbridge, ON, L4L8H1, Canada*

ABSTRACT

Plant uptake and accumulation of nanoparticles (NPs) represent an important pathway for potential human exposure to NPs. Consequently, it is imperative to understand the uptake and accumulation of NPs in plant tissues and their unique physical and chemical properties within plant tissue. Current technologies are limited in revealing the unique characteristics of NPs after they enter plant tissues. An enzymatic digestion method, followed by single particle inductively coupled plasma-mass spectrometry (SP-ICP-MS) analysis, was developed for simultaneous determination of gold NP (AuNP) size, size distribution, particle concentration, and dissolved Au concentration in tomato plant tissues. The experimental results showed that Macerozyme R-10 enzyme was capable of extracting AuNPs from tomato plants without causing dissolution or aggregation of AuNPs. The detection limit for quantification of AuNP size was 20 nm and the AuNPs particle concentration detection limit was 1000 NPs/mL. The particle concentration recoveries of spiked AuNPs were high (79%-96%) in quality control samples. The developed SP-ICP-MS method was able to accurately measure AuNP size, size distribution, and particle concentration in plant matrix. The dosing study indicated that tomato can uptake AuNPs as intact particles without altering the AuNPs properties.

Key words: single particle-ICP-MS, engineered nanoparticles, plant uptake, gold nanoparticle in tomato, Macerozyme R-10 enzyme



TOC Art/Abstract

INTRODUCTION

Rapid development of nanotechnology has reshaped the landscape of technologies in water and wastewater treatment, agriculture, medicine and manufacturing. In the agricultural industry, engineered nanoparticles (NPs), broadly defined as man-made materials with their size smaller than 100 nm in at least two dimensions,¹ have been incorporated into fertilizers, nanosensors, pathogen combating formulas,² and many other products. There are also unintentional releases of engineered NPs from the products to the environment, which may end up in agricultural land through water irrigation or biosolid disposal.^{3,4} Consequently, interactions of engineered NPs with agricultural crops are possible and their impact on crop health and food safety needs to be investigated. It is now well recognized that some engineered NPs affect crop development and yield, and many of them are accumulated in plant tissues, including the edible tissues.⁵⁻⁹ Plant uptake and accumulation of engineered NPs are of great concern because they provide a potential pathway for human exposure to engineered NPs. The determination of engineered NP characteristics, such as particle size, concentration, aggregation, chemical stability in plant tissues is, therefore, of critical importance to the understanding of the health and safety impacts of engineered NPs. Unfortunately, current technologies have many limitations in characterizing and quantifying engineered NPs in plant tissues. For example, most microscopic imaging techniques only allow qualitative investigation of a tiny fraction of plant tissues, which are often not representative of the whole plant tissues. While tissue digestion techniques, such as acid digestion followed by inductively coupled plasma-mass spectroscopy (ICP-MS) or inductively coupled plasma-optical emission spectrometry (ICP-OES) quantification, allow quantitative determination of metallic

engineered NPs, detailed information on the state and localization of engineered NPs in plant tissues is lost after acid digestion.

Single particle inductively coupled plasma-mass spectrometry (SP-ICP-MS) is an emerging technique for NP characterization and quantification, especially at low NP concentrations and in complex matrices. Degueldre and his colleagues did a lot of pioneering work in the early 21th Century and laid the foundation for SP-ICP-MS.¹⁰⁻¹⁴ Briefly, in SP-ICP-MS analysis, NPs in samples enter the plasma and get ionized individually, and then are detected as pulse (non-continuous) signals by mass spectrometer, making SP-ICP-MS a powerful technique to detect the masses of metal elements in each NP.¹⁵⁻¹⁷ Meanwhile, the corresponding dissolved analyte is detected as a continuous signal, meaning that SP-ICP-MS is capable of simultaneously detecting both the particle analyte and the dissolved analyte.¹⁵ In SP-ICP-MS analysis, the signal intensity of a NP depends on the particle size, and the signal frequency is proportional to the particle concentration in samples.¹⁰⁻¹⁴ In the early stage, SP-ICP-MS was more qualitative due to the absence of well-characterized NP standards, and highly sensitive and rapid mass scanning ICP-MS instrument. Recently, quantitative results have been achieved by SP-ICP-MS after some well-defined NP standards, such as AuNPs and silver NPs (AgNPs), and fast scanning ICP-MS, such as NexION 350 ICP-MS, have become commercially available.

There have been some successful applications of SP-ICP-MS for analysis of the size and concentration of NPs in environmental and biological matrices. For instance, Tuoriniemi *et al.*¹⁸ analyzed titanium (Ti), cerium (Ce) and Ag associated particles in wastewater effluent samples and the measured particle concentration was in the order of

magnitude of the predicted concentrations. Mitrano *et al.*¹⁹ used SP-ICP-MS to quantitatively track the dissolution of 60 and 100 nm silver NPs in laboratory, natural and processed water matrices, and found that the water chemistry significantly affected the NP dissolution. For NP analysis in biological tissues, the major challenge is the extraction of NPs from these tissues without compromising their properties. Concentrated acids are commonly used for metal extraction from tissues. However, they are not applicable for NP analysis because the concentrated acids can dissolve the NPs. Gary *et al.*²⁰ extracted Ag and Au NPs from ground beef, *Daphnia magna*, and *Lumbriculus variegatus* using tetramethylammonium hydroxide (TMAH) and quantified the NP sizes and NP particle concentrations using SP-ICP-MS method. Loeschner *et al.*²¹ and Peters *et al.*²² digested chicken meat with Proteinase K to extract Ag NPs. Loeschner *et al.*²³ also used alkaline and enzymatic treatment on rat spleens for AuNP extraction prior to SP-ICP-MS quantification, and obtained similar size distributions of AuNPs with both treatments. Marshall *et al.*²⁴ used enzymatic digestion (1- β -endoglucanase) to extract AuNPs in *Brassic Juncea* followed by X-ray absorption near edge spectroscopy (XANES) quantification. These progresses on SP-ICP-MS and tissue digestion provide an excellent opportunity to simultaneously obtain particle size, particle concentration, and dissolved analyte concentration information in biological and environmental samples. To the best of our knowledge, however, SP-ICP-MS has not been used to detect NPs in plants and to investigate NPs uptake by plants.

The objectives of this study were: (1) to develop a plant tissue digestion method for AuNPs extraction without causing dissolution or aggregation of AuNPs; (2) to develop a SP-ICP-MS method for the measurement of AuNP size, particle concentration,

and dissolved Au concentration in digested plant tissue samples; (3) to understand the uptake behavior of AuNPs by tomato plants. In this study, we chose AuNP as a representative metallic nanoparticle both because of its broad applications in the field and its relative stability in the environment. Tomato was chosen due to its popularity as a vegetable plant around the world.

EXPERIMENTS

Materials and Instrumentation.

Ultrapure water (18.2 M Ω •cm) was produced by a Simplicity185 water system from MILLIPORE. A PowerGen 125 hand-held tissue homogenizer was used to homogenize the plant tissues before enzymatic digestion. The Macerozyme R-10 enzyme (source: *Rhizopus sp.*) purchased from bioWORLD (Dublin, OH, USA) was used to digest the plant tissues for AuNPs extraction. A NexION 300/350D ICP-MS with Syngistix Nano Application module from PerkinElmer (Shelton, CT, USA) was used for SP-ICP-MS analysis. Citrate-stabilized AuNP standards with particle sizes of 10, 12, 15, 20, 30, 40, 50, 80, 100 nm were purchased from Nanocomposix (San Diego, CA, USA). These AuNP standards were citrate-stabilized to prevent aggregation/agglomeration and the size distribution of these particle standards was also relatively narrow according to the TEM results provided by Nanocomposix. Therefore, they were suitable to serve as NP calibration standards in SP-ICP-MS analysis. The polyvinylpyrrolidone (PVP)-coated 40 nm AuNPs for plant dosing were purchased from NanoComposix. Dissolved Au standard was purchased from High-Purity Standards (Charleston, SC, USA). Tomato

(*Solanum lycopersicum L.*) seeds were purchased from Johnny's Selected Seeds (Winslow, ME).

SP-ICP-MS Method Parameters.

¹⁹⁷Au with a natural abundance of 100% was measured by the developed SP-ICP-MS method. Syngistix software, with a Nano Application module from PerkinElmer, was used for data collection and processing. The dwell time was set to 0.1 millisecond (ms) and the sampling time was 100 seconds. In the Nano Application module, the settling time was totally eliminated and, therefore, one million data points were generated for each sample in 100 seconds. Dwell time is a critical parameter in SP-ICP-MS analysis and significantly affects the data quality.²⁵ With 0.1 ms of dwell time, the peak profiling of a single NP becomes possible because the typical signal duration of a single NP in ICP-MS is normally 0.3-0.5 ms.^{25, 26} With such a short dwell time, overlapping of particle signals was minimized and, thus, the particle sizing and counting accuracy were improved as compared with the dwell time of several milliseconds used by most of early published SP-ICP-MS methods. AuNP standards with sizes of 30, 50, 80 and 100 nm served as particle calibration standards to measure the particle size and particle concentration of AuNPs in the digested plant tissue samples. Dissolved Au calibration standards were also incorporated in the method to measure the dissolved Au concentration in the digested plant tissue samples, if present. After each sample analysis, the software automatically processed the raw data and generated the particle size, size distribution, particle concentration, and dissolved Au concentration information.

The Detection Limit of Particle Size and Particle Concentration.

The detection limit of particle size was determined by analyzing a series of AuNPs with different sizes. The instrument sensitivity was optimized for ^{197}Au because only ^{197}Au was analyzed in this study. The ICP-MS detector voltage is an important factor affecting the instrument sensitivity. Thus, the detector voltage was optimized to achieve the best sensitivity for ^{197}Au . Citrate-stabilized 10, 12, 15, 20, 30, 40, and 50 nm AuNP standards were analyzed under optimal conditions. The detection limit of particle concentration was determined by analyzing a series of different particle concentrations of the 40 nm AuNP standard. Particle concentrations of 10000, 5000, 2000, 1000, and 500 NPs/mL, were prepared in plant matrix (100 times diluted digested sample from the control plant, same dilution with the plant sample analysis) through series dilution from a 40 nm AuNP standard stock solution with a particle concentration of 8×10^{10} NPs/mL. The 30, 40, and 50 nm AuNP standards served as calibration standards, and transport efficiency was measured using 40 nm AuNP. In ICP-MS, transport efficiency is defined as the ratio of the amount of analyte entering the plasma to the total amount of analyte aspirated.^{17,27} In this study, the transport efficiency was measured using “method 3” described by Pace *et al.*¹⁷ All samples were prepared in triplicate and the accuracy (recovery) and precision (relative standard deviation, RSD) were calculated.

Plant Growth and Treatment.

Tomato seeds were surface sterilized with 1.25% sodium hypochlorite solution (m/v) for 10 minutes and then rinsed with deionized water three times. The sterilized seeds were germinated on DI water moistened filter paper in a Petri dish for 7 days.

Healthy young seedlings of similar size were transferred to 50 mL polypropylene centrifuge tubes containing 50 mL quarter strength Hoagland solution, purchased from PhytoTechnology Laboratories (Lenexa, KS). They were then incubated in a growth cart with a 16 hrs-light/8 hrs-dark cycle to allow the seedlings to develop further. The growth cart equipped with four T5 fluorescent tubes provided a light intensity of approximately $133 \mu\text{mol m}^{-2} \text{s}^{-1}$ at the height of plant leaves. The temperature was controlled at $27 \pm 1^\circ\text{C}$. The Hoagland solution in the tubes was replenished every other day. After about 20 days of incubation in Hoagland solution, the plants were moved to new 50 mL centrifuge tubes with only DI water for 2 days to remove the Hoagland solution from root surfaces. After that, the DI water was replaced with solutions containing different concentrations of PVP-coated 40 nm AuNPs. The treatment scenarios included: (1) control (DI water only), (2) 0.2 mg/L 40 nm AuNPs, and (3) 5 mg/L 40 nm AuNPs. Each treatment had two replicates. The plants were exposed to the solution for 4 days before they were sacrificed for enzyme extraction and SP-ICP-MS analysis.

Effect of Macerozyme R-10 Enzyme on AuNPs.

Macerozyme R-10 is a multi-component enzyme mixture containing cellulose (0.1 U/mg), hemicellulose (0.25 U/mg), and pectinase (0.5 U/mg). Considered the major component of plant tissues, Macerozyme R-10 enzyme has the capability of digesting plant tissues to release the NPs. To evaluate whether the enzyme will cause AuNPs dissolution or aggregation, a 50 nm AuNPs standard was diluted to 2.05×10^5 NPs/mL using the enzyme solution followed by an approximately 3 min homogenization with a hand-held tissue homogenizer (the same procedure used for processing plant tissue

samples). The sample was shaken in a water bath at 37 °C for 24 hours. These samples were analyzed with respect to AuNP size and particle concentration using the developed SP-ICP-MS method.

Enzymatic Digestion Method.

Since previous research^{28, 29} showed that NPs could deposit on the root surface and were difficult to wash off, only plant shoots without direct contact with the dosing solution were analyzed in this study. After cultivation, the shoots were separated from the roots. The cut point was about 1 cm above the medium and the length of the shoot was about 5-8 cm. The shoot tissues were washed three times with DI water, then cut into small pieces using scissors and homogenized by a hand-held tissue homogenizer in 8 mL of 2 mM citrate buffer. The pH was adjusted with nitric acid, to within the pH-optimum range of 3.5-7.0 for this enzyme according to the manufacturer's information. After homogenization, 2 mL of the enzyme solution (prepared by adding 1 gram of enzyme powder in 20 ml of ultrapure water) was added in. The samples were shaken at 37 °C for 24 hours. After digestion, the samples were settled down for approximately 1 hour and 0.1 mL of the supernatant was diluted 100 times using ultrapure water for SP-ICP-MS analysis. A NP concentration of 4.7×10^4 NPs/mL of 100 nm AuNPs was also spiked into an aliquot of the plant extract as quality control when running SP-ICP-MS.

Reproducibility Study of the Enzymatic Digestion Method.

The tomato plants dosed with 5 mg/L of 40 nm AuNPs were used for the reproducibility study of enzymatic digestion. The plant shoots were cut into small pieces,

combined, and then homogenized in 25 mL of 2 mM citrate buffer. After the tissue homogenization, the slurry was vortexed to ensure homogeneity. An 8 mL aliquot of the slurry was then transferred to a 50-mL centrifuge tube for enzymatic digestion and three replicates were processed in parallel. Two mL of enzyme solution (1 gram of enzyme powder in 20 ml of ultrapure water) were added to each 8 mL of slurry and the samples were incubated by shaking at 37 °C for 24 hours in a water bath shaker. After the incubation, the samples were settled down for approximately 1 hour and 0.1 mL of the supernatant was diluted 100 times using ultrapure water for SP-ICP-MS analysis.

RESULTS AND DISCUSSION

The Detection Limit of Particle Size and Particle Concentration of the Developed SP-ICP-MS Method.

Table 1 shows the optimized ICP-MS operating conditions for ^{197}Au . The size detection limit was determined by analyzing 10, 12, 15, 20, 30, 40, and 50 nm AuNPs. The intensities of 20, 30, 40, and 50 nm AuNPs were linear to the third power of AuNP diameter. However, when the AuNP size decreased to 15 nm, the calibration curve was not able to maintain good linearity and the intensities of 15, 12, and 10 nm AuNPs were similar, indicating that the quantitative particle size detection limit was 20 nm for AuNPs under optimal conditions. The upper size detection limit is limited by the upper linear limit of the ICP-MS detector. From our test, 100 nm AuNP still showed good linearity. No larger than 100 nm AuNPs were tested in this study. **Table 2** shows the accuracy and precision of five low particle concentrations of 40 nm AuNP. For 10000, 5000, 2000, and 1000 NPs/mL of 40 nm AuNP, both the accuracy (recovery, 98.00-102.67%) and precision (RSD, 4.34-6.87%) were satisfactory. However, when the particle concentration

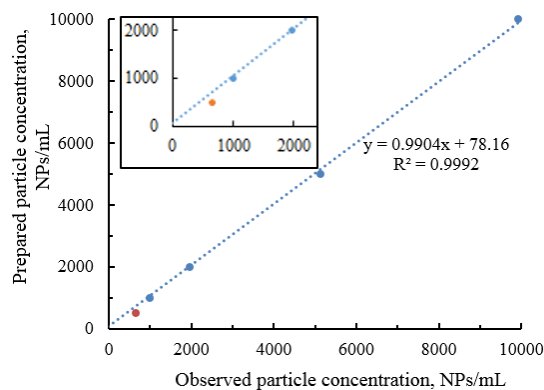
decreased to 500 NPs/mL, both the accuracy (recovery, 132.07%) and the precision (RSD, 16.12%) dropped significantly. The results suggested that the particle concentration quantitative detection limit of the developed SP-ICP-MS method was 1000 NPs/mL for AuNPs. The detection limit of particle concentration was in agreement with published result.³⁰ If converting 1000 NPs/mL of 40 nm AuNP to mass concentration, this was equal to 0.65 ng/L, with known density of Au (19.3 g/cm^3) and spherical shape of the 40 nm AuNP. The results indicated that the developed SP-ICP-MS method is extremely sensitive for AuNP and, to date, it is the only known rapid method that is capable of directly and quantitatively analyzing NPs in environmental samples with so low NP concentration.³¹

Table 1. ICP-MS conditions after optimization for ^{197}Au

Optimized ICP-MS Operating Condition	
Nebulizer Gas Flow (L/min)	1.08
Auxiliary Gas Flow (L/min)	1.2
Plasma Gas Flow (L/min)	18
ICP RF Power (W)	1600
Analog Stage Voltage (V)	-2950
Pulse Stage Voltage (V)	1625
Cell Entrance Voltage (V)	-6
Cell Exit Voltage (V)	-6
Cell Rod Offset	-15
Sampler Cones	Nickel
Skimmer Cones	Nickel
Sample Introduction System	Cyclonic Spray Chamber with Meinhard Nebulizer
SP-ICP-MS Method Parameters	
Analyte	Au
Mass (amu)	197
Dwell Time (ms)	0.1
Settling Time (ms)	0
Density (g/cm^3)	19.3

Table 2. Comparison of the measured and prepared particle concentration of 40 nm AuNP.

Prepared AuNP concentration (NPs/mL)	Observed AuNP concentration (NPs/mL)	Accuracy (%)	Precision (%RSD)	Graph
10000	Replicate 1	9456	99.23	6.87
	Replicate 2	9607		
	Replicate 3	10705		
5000	Replicate 1	5385	102.67	4.48
	Replicate 2	5083		
	Replicate 3	4933		
2000	Replicate 1	1960	98.00	6.58
	Replicate 2	2089		
	Replicate 3	1831		
1000	Replicate 1	991	99.10	4.34
	Replicate 2	948		
	Replicate 3	1034		
500	Replicate 1	711	132.07	16.12
	Replicate 2	538		
	Replicate 3	732		



Effect of the Enzyme on AuNPs.

Figure 1 shows the measured size distribution histogram and particle concentration of enzyme-treated 50 nm AuNP. The measured particle size distribution agreed well with the spiked NP size. The measured particle concentration, 1.81×10^5 NPs/mL, was also close (recovery, 88.3%) to the prepared particle concentration (2.05×10^5 NPs/mL), and no significant dissolution or aggregation of AuNPs was found. The results demonstrated that the Macerozyme R-10 enzyme is feasible for use in extracting AuNPs from plant tissues without causing dissolution or aggregation of AuNPs in plant tissues.

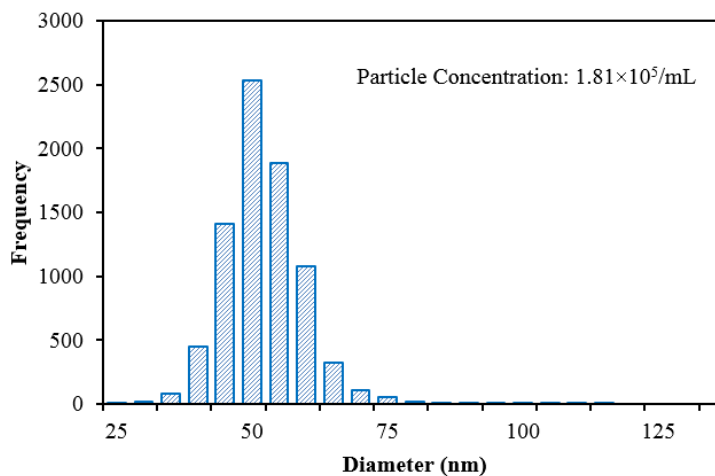


Figure 1. Particle size distribution histogram of enzyme-treated 50 nm AuNP (without plant tissue).

Reproducibility of Enzymatic Digestion Method.

Reproducibility is an important consideration for an analytical method. **Figure 2** shows good reproducibility for both particle size and particle concentration of three replicates, which indicated that the enzymatic digestion followed by SP-ICP-MS quantification method is reproducible.

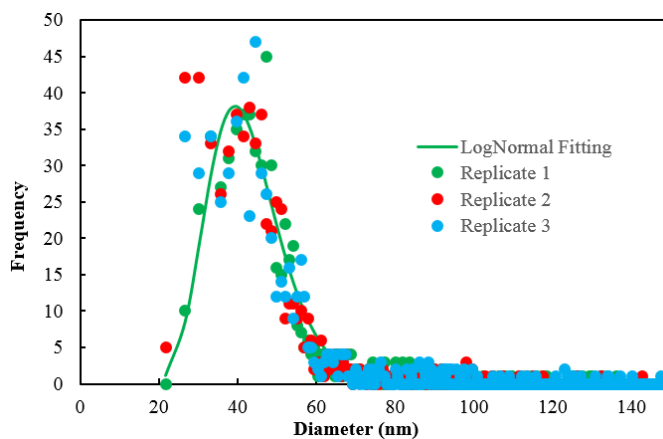


Figure 2. AuNPs size distribution for three replicates of tomato plant dosed with 5 mg/L of 40 nm AuNPs for enzymatic extraction reproducibility study.

Enzymatic Digestion of AuNPs in Plants and SP-ICP-MS Analysis.

Figure 3(b) shows the raw SP-ICP-MS data for a control plant sample without AuNPs exposure. Only a few pulse signals were observed, which was similar to the raw data for the reagent blank shown in **Figure 3(a)**. The result indicated that the control plant without exposure to AuNPs was free from AuNPs contamination. **Figure 3(c)** shows the raw data for the enzymatic digestate of control sample spiked with 4.7×10^4 NPs/mL of 100 nm AuNPs. A large number of typical NP pulse signals was observed. **Figure 3(d)** shows the size distribution histogram processed from **Figure 3(c)**. The measured particle size distribution matched well with the spiked NP size and the NP particle concentration recovery was 96% (4.5×10^4 NPs/mL detected for 4.7×10^4 NPs/mL spiked). The results suggested that the developed SP-ICP-MS method could accurately detect the particle size and particle concentration of AuNPs in plant matrix.

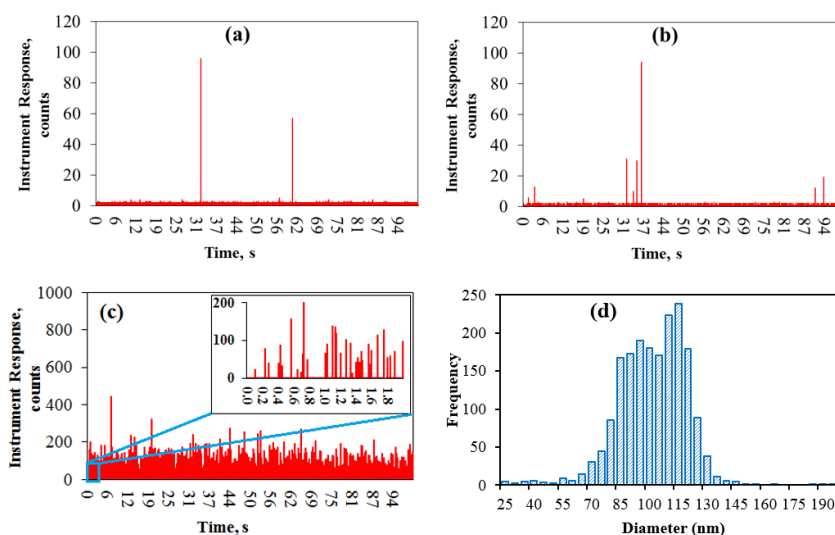


Figure 3. (a) Raw data for reagent blank (reagent blank: enzyme in 2 mM citrate solution, without plant tissues and AuNPs); (b) Raw data for control plant without exposure to AuNPs; (c) Raw data for spiking 4.7×10^4 NPs/mL of 100 nm AuNPs into control plant sample; (d) Size distribution histogram for spiking 4.7×10^4 NPs/mL of 100 nm AuNPs into control plant sample.

Figures 4(a) and **4(b)** show the raw data for two replicates of tomato plants which were dosed with 5 mg/L of 40 nm AuNPs for 4 days. A lot of typical NP pulse signals were observed and there was no continuous Au signal, suggesting that the Au in the tomato shoots existed as AuNPs rather than dissolved Au. **Figure 4(c)** shows the size distribution histograms processed from **Figures 4(a)** and **4(b)**. The major peak appeared at 40 nm, which agreed with the particle size dosed in the study. The results suggested that tomato plants could uptake the 40 nm AuNPs directly as NPs, and the AuNPs within tomato tissues existed as intact particles and were not oxidized to Au ions. This finding was in agreement with Zhai's research showing that AuNPs were not dissolved into Au ions within poplar plants.³² Two replicates yielded highly similar results. **Figure 4(d)** shows the result after spiking 4.7×10^4 NPs/mL of 100 nm AuNPs into the enzymatic digestate of tomato plant dosed with 5 mg/L of 40 nm AuNPs for 4 days. The measured size distribution agreed well with the dosed 40 nm and spiked 100 nm AuNPs. The size of 40 nm AuNPs was also resolved with spiked 100 nm AuNPs, indicating no significant interaction between the different size and surface coated AuNPs. The particle concentration spike recovery was calculated as follows: the number of particles with diameters from 70 nm to 130 nm in **Figure 4(d)** minus the background number of particles in the same diameter range in **Figure 4(c)** (Replicate 1). The calculated particle concentration was 3.7×10^4 NPs/mL, 79% of the spiked particle concentration of 4.7×10^4 NPs/mL. The results further indicated that the developed SP-ICP-MS method can accurately measure the particle size and particle concentration in plant tissue samples. Following the successful detection of AuNPs in 5 mg/L dosed tomato shoots, a lower dosing concentration (0.2 mg/L AuNPs) in tomato plants was examined using the same

extraction and SP-ICP-MS procedures. **Figure 5 (a)** shows the raw data of tomato shoot tissues treated with 0.2 mg/L of 40 nm AuNPs for 4 days. Compared to **Figures 4(a)** and **4(b)**, fewer pulse signals were observed for the 0.2 mg/L dosed samples. **Figure 5(b)** shows the size distribution histogram with the major peak still at approximately 40 nm and the particle concentration (frequency on the Figure) was much lower than that of 5 mg/L of 40 nm AuNPs dosed plants due to lower dosage. A particle concentration of 4.7×10^4 NPs/mL of 100 nm AuNPs was also spiked into the enzymatic digestate of tomato plant dosed with 0.2 mg/L of 40 nm AuNPs for 4 days, and the result is shown in **Figure 5 (c)**. The measured particle size well agreed with the spiked size. The particle concentration spike recovery was calculated in the same way as the 5 mg/L dosed samples were, as described previously. The recovery was 89% (4.2×10^4 NPs/mL detected for 4.7×10^4 NPs/mL spiked). Even at a 0.2 mg/L dosing concentration, the AuNPs in the tomato extracts were still significantly higher than the particle concentration detection limit, indicating that the developed SP-ICP-MS method was capable of detecting the uptake of NPs by plants at more environmentally relevant concentrations.³¹ The sensitivity of the SP-ICP-MS method provides a rare opportunity to investigate plant uptake and accumulation of Au and other NPs at environmentally relevant concentrations, and is a real advantage over other currently available methods. The sensitive SP-ICP-MS method offers a great opportunity to investigate the plant uptake kinetics of engineered NPs, their accumulation, localization, and possible transformation in plant tissues at environmentally relevant concentrations. Due to the varying responses of ICP-MS to different materials and elements, more detailed studies on the extraction efficiency of the enzymatic method for different NPs are under investigation to expand

the application of the enzymatic extraction-SP-ICP-MS method. It is also important to point out that the developed enzymatic digestion-SP-ICP-MS method was based on young tomato seedling. With plant matures, the cell wall becomes more rigid and there will be depositions of lignin between cells to strength plants. A study is underway to assess the method on more mature plant and on tomato fruits to broaden the application of the developed method.

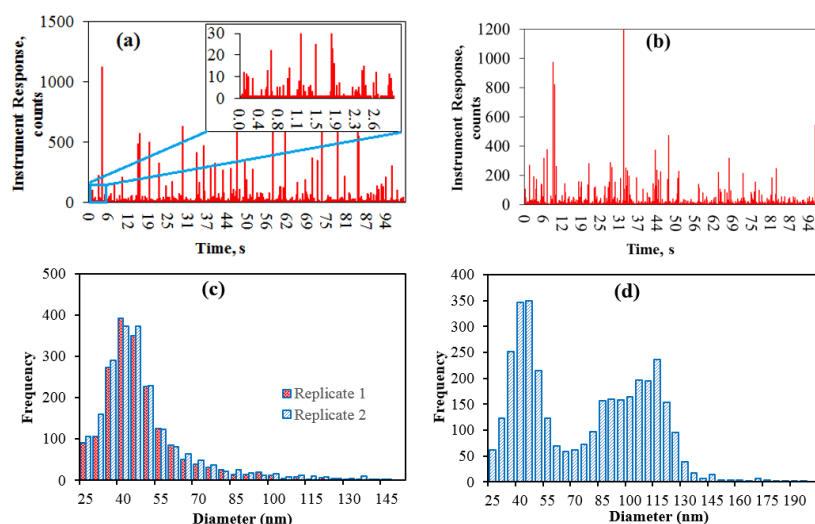


Figure 4. (a)&(b) Raw data of duplicated tomato plants exposed to 5 mg/L of 40 nm AuNPs for 4 days; (c) Size distributions histograms of duplicated tomato plants exposed to 5 mg/L of 40 nm AuNPs from Figure 4(a) and 4(b); (d) Size distribution histogram of spiking 4.7×10^4 particles/mL of 100 nm AuNPs into tomato plants exposed to 5 mg/L of 40 nm AuNPs.

The results of this study demonstrate that tomato plants can uptake intact 40 nm AuNPs and transport them up to shoots; the Macerozyme R-10 enzyme can be used to extract the AuNPs from the plant tissues as intact NPs; and the SP-ICP-MS is a sensitive and reliable method for the detection of AuNPs in plant sample matrix. The developed

SP-ICP-MS method can accurately measure particle size, particle concentration of AuNPs, and dissolved Au concentration in tomato plants. The major advantages of the developed method are: (1) the enzymatic digestion is able to extract the AuNPs from tomato plant tissues without causing dissolution or aggregation of the AuNPs; (2) AuNPs can be analyzed in a complex matrix, a major challenge for nanometrology; (3) the method is highly sensitive and applicable to environmentally relevant trace concentration as well as complex biological matrix; and (4) the developed method examines the whole or subsections of plant tissues instead of a mere fraction of plant shoots (often used in microscopic methods), and therefore, generates more accurate results. The developed method provides a promising way to systematically study the interactions between NPs and plants, including uptake kinetics, accumulation, transformation, and mechanisms of advanced impacts on plants by engineered NPs. The method overcomes the current technique challenges by revealing the concentration and unique characteristics of NPs and will contribute significantly to the risk assessment of engineered NPs in food plants.

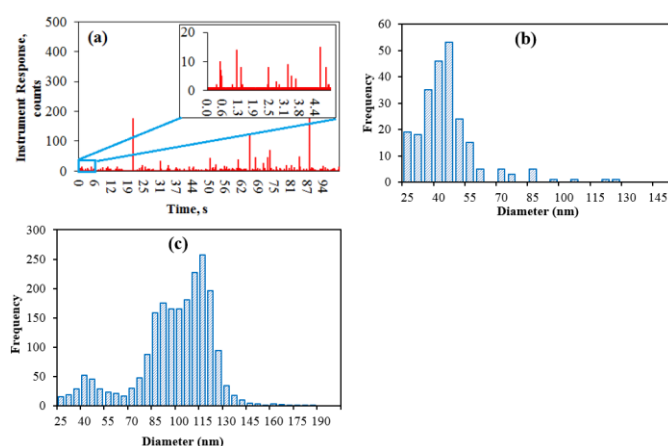


Figure 5. (a) Raw data of tomato plant dosed with 0.2 mg/L of 40 nm AuNPs for 4 days; (b) Size distribution histogram from Figure 5(a); (c) Size distribution histogram of spiking 4.7×10^4 NPs/mL of 100 nm AuNPs into tomato plants dosed with 0.2 mg/L of 40 nm AuNPs.

ACKNOWLEDGEMENT

The NexION 300/350D ICP-MS was provided by PerkinElmer, Inc. The authors appreciate the support from University of Missouri Research Board, Chemistry Department and Center for Single Nanoparticle, Single Cell, and Single Molecule Monitoring (CS³M) at Missouri University of Science and Technology. Xingmao Ma acknowledges the financial support of the US Department of Agriculture-AFRI (#2011-67006-30181).

REFERENCES

1. Klaine, S. J.; Alvarez, P. J. J.; Batley, G. E.; Fernandes, T. F.; Handy, R. D.; Lyon, D. Y.; Mahendra, S.; McLaughlin, M. J.; Lead, J. R., Nanomaterials in the environment: behavior, fate, bioavailability, and effects. *Environ. Toxicol. Chem.* **2008**, *27*, (9), 1825-1851.
2. Khot, L. R.; Sankaran, S.; Maja, J. M.; Ehsani, R.; Schuster, E. W., Applications of nanomaterials in agricultural production and crop protection: A review. *Crop Prot.* **2012**, *35*, 64-70.
3. Abbott, C. T. E.; Ajmani, G. S.; Huang, H.; Schwab, K. J., Evaluating nanoparticle breakthrough during drinking water treatment. *Environmental health perspectives* **2013**, *121*, (10), 1161-6.
4. Yang, Y.; Wang, Y.; Westerhoff, P.; Hristovski, K.; Jin, V. L.; Johnson, M.-V. V.; Arnold, J. G., Metal and nanoparticle occurrence in biosolid-amended soils. *Sci. Total Environ.* **2014**, *485-486*, 441-449.
5. Larue, C.; Veronesi, G.; Flank, A.-M.; Surble, S.; Herlin-Boime, N.; Carriere, M., Comparative uptake and impact of TiO₂ nanoparticles in wheat and rapeseed. *J. Toxicol. Environ. Health, Part A* **2012**, *75*, (13-15), 722-734.
6. Lopez-Moreno, M. L.; de la Rosa, G.; Hernandez-Viezcas, J. A.; Peralta-Videa, J. R.; Gardea-Torresdey, J. L., X-ray absorption spectroscopy (XAS) corroboration of the uptake and storage of CeO₂ nanoparticles and assessment of their differential toxicity in four edible plant species. *J. Agric. Food Chem.* **2010**, *58*, (6), 3689-3693.
7. Ma, X.; Geisler-Lee, J.; Geiser-Lee, J.; Deng, Y.; Kolmakov, A., Interactions between engineered nanoparticles (ENPs) and plants: phytotoxicity, uptake and accumulation. *The Science of the total environment* **2010**, *408*, (16), 3053-61.
8. Wang, Q.; Ma, X.; Zhang, W.; Pei, H.; Chen, Y., The impact of cerium oxide nanoparticles on tomato (*Solanum lycopersicum* L.) and its implications for food safety. *Metallomics : integrated biometal science* **2012**, *4*, (10), 1105-1112.
9. Zhao, L.; Sun, Y.; Hernandez-Viezcas, J. A.; Servin, A. D.; Hong, J.; Niu, G.; Peralta-Videa, J. R.; Duarte-Gardea, M.; Gardea-Torresdey, J. L., Influence of CeO₂ and ZnO nanoparticles on cucumber physiological markers and bioaccumulation of Ce and Zn: a life cycle study. *J. Agric. Food Chem.* **2013**, *61*, (49), 11945-11951.
10. Degueldre, C.; Favarger, P. Y., Colloid analysis by single particle inductively coupled plasma-mass spectroscopy: a feasibility study. *Colloids Surf., A* **2003**, *217*, (1-3), 137-142.
11. Degueldre, C.; Favarger, P. Y., Thorium colloid analysis by single particle inductively coupled plasma-mass spectrometry. *Talanta* **2004**, *62*, (5), 1051-1054.

12. Degueldre, C.; Favarger, P. Y.; Bitea, C., Zirconia colloid analysis by single particle inductively coupled plasma-mass spectrometry. *Anal. Chim. Acta* **2004**, *518*, (1-2), 137-142.
13. Degueldre, C.; Favarger, P. Y.; Rosse, R.; Wold, S., Uranium colloid analysis by single particle inductively coupled plasma-mass spectrometry. *Talanta* **2006**, *68*, (3), 623-628.
14. Degueldre, C.; Favarger, P. Y.; Wold, S., Gold colloid analysis by inductively coupled plasma-mass spectrometry in a single particle mode. *Anal. Chim. Acta* **2006**, *555*, (2), 263-268.
15. Laborda, F.; Jimenez-Lamana, J.; Bolea, E.; Castillo, J. R., Selective identification, characterization and determination of dissolved silver(I) and silver nanoparticles based on single particle detection by inductively coupled plasma mass spectrometry. *J. Anal. At. Spectrom.* **2011**, *26*, (7), 1362-1371.
16. Mitrano, D. M.; Leshner, E. K.; Bednar, A.; Monserud, J.; Higgins, C. P.; Ranville, J. F., Detecting nanoparticulate silver using single-particle inductively coupled plasma-mass spectrometry. *Environ. Toxicol. Chem.* **2012**, *31*, (1), 115-121.
17. Pace, H. E.; Rogers, N. J.; Jarolimek, C.; Coleman, V. A.; Higgins, C. P.; Ranville, J. F., Determining transport efficiency for the purpose of counting and sizing nanoparticles via single particle inductively coupled plasma mass spectrometry. *Anal. Chem. (Washington, DC, U. S.)* **2011**, *83*, (24), 9361-9369.
18. Tuoriniemi, J.; Cornelis, G.; Hasseløev, M., Size discrimination and detection capabilities of single-particle ICPMS for environmental analysis of silver nanoparticles. *Anal. Chem. (Washington, DC, U. S.)* **2012**, *84*, (9), 3965-3972.
19. Mitrano, D. M.; Ranville, J. F.; Bednar, A.; Kazor, K.; Hering, A. S.; Higgins, C. P., Tracking dissolution of silver nanoparticles at environmentally relevant concentrations in laboratory, natural, and processed waters using single particle ICP-MS (spICP-MS). *Environ. Sci.: Nano* **2014**, *1*, (3), 248-259.
20. Gray, E. P.; Coleman, J. G.; Bednar, A. J.; Kennedy, A. J.; Ranville, J. F.; Higgins, C. P., Extraction and analysis of silver and gold nanoparticles from biological tissues using single particle inductively coupled plasma mass spectrometry. *Environ. Sci. Technol.* **2013**, *47*, (24), 14315-14323.
21. Loeschner, K.; Navratilova, J.; Kobler, C.; Molhave, K.; Wagner, S.; von der, K. F.; Larsen, E. H., Detection and characterization of silver nanoparticles in chicken meat by asymmetric flow field flow fractionation with detection by conventional or single particle ICP-MS. *Anal. Bioanal. Chem.* **2013**, *405*, (25), 8185-8195.

22. Peters, R. J. B.; Rivera, Z. H.; van Bommel, G.; Marvin, H. J. P.; Weigel, S.; Bouwmeester, H., Development and validation of single particle ICP-MS for sizing and quantitative determination of nano-silver in chicken meat. *Anal. Bioanal. Chem.* **2014**, *406*, (16), 3875-3885.
23. Loeschner, K.; Brabrand, M. S. J.; Sloth, J. J.; Larsen, E. H., Use of alkaline or enzymatic sample pretreatment prior to characterization of gold nanoparticles in animal tissue by single-particle ICPMS. *Anal. Bioanal. Chem.* **2014**, *406*, (16), 3845-3851.
24. Marshall, A. T.; Haverkamp, R. G.; Davies, C. E.; Parsons, J. G.; Gardea-Torresdey, J. L.; van Agterveld, D., Accumulation of gold nanoparticles in Brassica Juncea. *Int. J. Phytorem.* **2007**, *9*, (3), 197-206.
25. Hineman, A.; Stephan, C., Effect of dwell time on single particle inductively coupled plasma mass spectrometry data acquisition quality. *J. Anal. At. Spectrom.* **2014**, *29*, (7), 1252-1257.
26. Montano, M. D.; Badiei, H. R.; Bazargan, S.; Ranville, J. F., Improvements in the detection and characterization of engineered nanoparticles using spICP-MS with microsecond dwell times. *Environ. Sci.: Nano* **2014**, *1*, (4), 338-346.
27. Montaser, A., *Inductively Coupled Plasma Mass Spectrometry*. Wiley-VCH: 1998.
28. Geisler-Lee, J.; Wang, Q.; Yao, Y.; Zhang, W.; Geisler, M.; Li, K.; Huang, Y.; Chen, Y.; Kolmakov, A.; Ma, X., Phytotoxicity, accumulation and transport of silver nanoparticles by *Arabidopsis thaliana*. *Nanotoxicology* **2013**, *7*, (3), 323-337.
29. Ma, X.; Gurung, A.; Deng, Y., Phytotoxicity and uptake of nanoscale zero-valent iron (nZVI) by two plant species. *Sci. Total Environ.* **2013**, *443*, 844-849.
30. Pace, H. E.; Rogers, N. J.; Jarolimek, C.; Coleman, V. A.; Gray, E. P.; Higgins, C. P.; Ranville, J. F., Single particle inductively coupled plasma-mass spectrometry: a performance evaluation and method comparison in the determination of nanoparticle size. *Environ. Sci. Technol.* **2012**, *46*, (22), 12272-12280.
31. Gottschalk, F.; Sonderer, T.; Scholz, R. W.; Nowack, B., Modeled environmental concentrations of engineered nanomaterials (TiO₂, ZnO, Ag, CNT, Fullerenes) for different regions. *Environ. Sci. Technol.* **2009**, *43*, (24), 9216-9222.
32. Zhai, G.; Walters, K. S.; Peate, D. W.; Alvarez, P. J. J.; Schnoor, J. L., Transport of gold nanoparticles through plasmodesmata and precipitation of gold ions in woody poplar. *Environ. Sci. Technol. Lett.* **2014**, *1*, (2), 146-151.

III. APPLICATION OF SINGLE PARTICLE ICP-MS FOR THE DETERMINATION OF PLANT UPTAKE AND ACCUMULATION OF CeO_2 NANOPARTICLES

Yongbo Dan^{1, 2}, Xingmao Ma^{2,3}, Weilan Zhang³, Kun Liu^{1, 2}, Chady Stephan⁴, Honglan Shi^{1, 2, *}

¹*Department of Chemistry and Environmental Research Center, Missouri University of Science and Technology, Rolla, MO, 65409, USA*

²*Center for Single Nanoparticle, Single Cell, and Single Molecule Monitoring (CS³M), Missouri University of Science and Technology, Rolla, MO, 65409, USA*

³*Zachry Department of Civil Engineering, Texas A&M University, College Station, TX, 77845, USA*

⁴*PerkinElmer, Inc., 501 Rowntree Dairy Rd, Woodbridge, ON, L4L8H1, Canada*

****Corresponding author***

Address: Department of Chemistry
Missouri University of Science and Technology
400 West 11th Street
Rolla, MO 65409
Phone: 573-341-4433
Fax: 573-341-6033
E-mail: honglan@mst.edu

Abstract

As one of the most commonly encountered engineered nanoparticles (ENPs) in industrial applications, cerium oxide nanoparticles (CeO_2NPs) have attracted significant attention on their environmental fate and transport. Plant uptake and accumulation of CeO_2NPs have been investigated as a potential pathway for human exposure to these ENPs. However, the investigation is frequently hampered by the insufficiency of current analytical technologies to determine the quantity and characteristics of cerium (e.g. dissolved Ce vs. particulate Ce) in plant tissues. We herein report an innovative single particle-inductively coupled plasma-mass spectrometry (SP-ICP-MS) technology to simultaneously detect particulate Ce size and size distribution, particle concentration, and dissolved cerium in the shoot of four different plant species, including tomato, cucumber, pumpkin, and soybean. This study demonstrated unequivocally the presence of dissolved cerium in plant seedling shoots exposed to CeO_2NPs hydroponically for the first time. Our results also suggest that CeO_2NPs might be taken up by plant roots both as intact CeO_2NPs and as ionic cerium. Differences on CeO_2NPs uptake and accumulation have been noticed between different plant species, requiring further investigation on the mechanisms.

Key words: single particle-ICP-MS, enzymatic digestion, plant uptake of CeO_2 nanoparticles, nanoparticle biotransformation, food safety, nanoparticle characterization,

1. Introduction

Cerium is the most abundant rare earth element in the earth's crust and it is naturally stabilized in both trivalent (Ce^{3+}) and tetravalent (Ce^{4+}) states [1]. While cerium is primarily in the tetravalent state (Ce^{4+}) in the lattice structure of bulk cerium oxide particles, the concentration of Ce^{3+} increases with the increase of the specific surface area or the reduction of particle size [2]. A recent study indicated that the percentage of Ce^{3+} on the surface of bare cerium oxide nanoparticles (CeO_2NPs) increased from 9.7% to 22.9% when the nanoparticle size was reduced from 64 nm to 9 nm [3]. An increase in Ce^{3+} results in the lattice expansion of CeO_2NPs due to the relatively larger size of Ce^{3+} compared with Ce^{4+} and therefore enhance the reactivity of CeO_2NPs . This unique redox chemistry between $\text{Ce}^{3+}/\text{Ce}^{4+}$ makes CeO_2NPs a popular component in many commercial products such as sun screens, coating materials, fuel additives and nanomedicine [4,5]. The washing off of sun screens, aging of coating materials, and emission of automotive exhaust provide possible routes for them to build up in the environment. Therefore, the broad applications of CeO_2NPs have caused serious concerns about their fate and impact in the ecosystem. Plants are one of the most essential components in the ecosystem and agricultural crops represent a potentially important pathway for human exposure to environmental chemicals. Consequently, there have been a number of investigations on the uptake and accumulation of CeO_2NPs by agricultural crops in the literature. For instance, Zhang *et al.* [6] reported that cucumber (*Cucumis sativus* L.) root could take up CeO_2NPs and transport them to the shoots even though the root-to-shoot translocation was limited and the majority of CeO_2NPs appeared to adsorb on the root surface. The authors also found that plant uptake of CeO_2NPs depends upon the particle size, with

smaller particles more readily taken up by plants. Zhao *et al.* [7] also reported low translocation of CeO₂NPs from root to shoot in corn plants (*Zea mays* L.) after they were exposed to 400 and 800 mg/kg of CeO₂NPs throughout the life cycle of the corn plants. Wang *et al.* [8] exposed tomato (*Solanum lycopersicum* L.) to low concentrations of CeO₂NPs (0.1- 10 mg/L) throughout the life cycle of the plants and found that cerium was detected in all plant tissues, including the edible tissues.

Clearly, the literature suggests that plants are capable of taking up and accumulate Ce when they are exposed to CeO₂NPs. However, it is much less clear about the root uptake mechanisms of CeO₂NPs. Due to the low water solubility of CeO₂NPs, the detection of Ce in plant shoot tissues had been interpreted as evidence that CeO₂NPs are taken up by plants as intact NPs [9]. The interpretation appeared to be supported by the detection of primarily tetravalent oxidation state of cerium in plant shoots. However, a separate study using soft X-ray scanning transmission microscopy (STXM) and near edge X-ray absorption fine structure (XANES) analysis found measurable accumulation of CePO₄ in cucumber roots and cerium carboxylates in the shoots [10]. The detection of biotransformed products in plant tissues and elevated Ce³⁺ around root surface spurred a new theory that CeO₂NPs may release Ce³⁺ on root surface, which are then taken up by plant roots and oxidized to CeO₂NPs [11]. Another unsettled issue associated with the plant and CeO₂NPs interaction is that even though biotransformed products were detected in plant tissues, it is unclear how significant the biotransformation was in plant tissues and whether the biotransformed Ce existed as dissolved Ce³⁺ or combined with other anions to form new particles (e.g. CePO₄). Technologies commonly used for metal

quantification including the inductively coupled plasma-mass spectrometry (ICP-MS) are not sufficient to unravel the above-mentioned convolutions.

Excitingly, a new capability to operate the ICP-MS in single particle mode (SP-ICP-MS) has emerged recently. In the single particle mode, nanoparticle size, size distribution, particle concentration and particle dissolution can be obtained after appropriate sample preparation [12-25]. SP-ICP-MS has been successfully applied for the characterization and quantification of several engineered nanoparticles (ENPs) in complex biological matrices such as chicken meat, animal tissues and earthworms, and plant tissues [18,26,19,21,23]. In SP-ICP-MS, after a dilute suspension of ENPs is introduced into the plasma, the single ENP is ionized individually and generates a packet of ions which will enter into the mass spectrometer and be detected as a pulse signal. The intensity of these pulse signals is proportional to the mass content of the element in a particle and consequently the particle size, and the signal frequency is proportional to the particle concentration [12,27,28,22,23]. By collecting time-resolved data, both the particle concentration and size distribution of the samples can be obtained by appropriate standardization and calibration. If corresponding dissolved metal elements are also present in the sample, they are detected as continuous signal. In this approach, dissolved metal concentration, ENP particle concentration, and particle size distribution can be obtained simultaneously. This unique capability of SP-ICP-MS makes it a potentially powerful tool to study the biotransformation of CeO₂NPs in plant tissues.

For ENPs analysis in plant tissues, the major challenge is the extraction of ENPs from these tissues without compromising their properties. Some research have shown that cellulosic enzymes can effectively digest plant tissues to release ENPs in plant tissues

without dissolving them. For instance, Marshall *et al.* [29] used enzymatic digestion (1- β -endoglucanase) to extract gold NPs (AuNPs) in *Brassic juncea*. Dan *et al.* [23] used Macerozyme R-10 enzyme to extract AuNPs in tomato plant tissues followed by SP-ICP-MS quantification. These advances on SP-ICP-MS and plant tissue digestion provide an excellent opportunity to study the biotransformation of CeO₂NPs in plant tissue. To the best of our knowledge, SP-ICP-MS has not been used to characterize CeO₂NPs in plant tissues and to investigate CeO₂NPs uptake by plants. The objectives of this study were: (1) to develop and optimize the SP-ICP-MS method for the detection of CeO₂NPs and dissolved Ce in plant tissues, and (2) to determine the uptake and accumulation of CeO₂NPs by four agricultural crops using the developed SP-ICP-MS method.

2. Materials and Methods

2.1 Chemicals and Instrumentation

Ultrapure water (18.2 M Ω •cm) was produced by a Simplicity185 Millipore water system. Trace metal grade concentrated nitric acid and 30% hydrogen peroxide were purchased from Fisher Scientific (Pittsburgh, PA). A PowerGen 125 hand-held tissue homogenizer was used to homogenize the plant tissues before enzymatic digestion. The Macerozyme R-10 enzyme (source: *Rhizopus sp.*) purchased from bioWORLD (Dublin, OH, USA) was used to digest the plant tissues for particles extraction. A NexION 300/350D ICP-MS with Syngistix nano application module from PerkinElmer (Shelton, CT, USA) was used for SP-ICP-MS analysis and data processing. Citrate-stabilized 50 nm AuNP standard purchased from Nanocomposix (San Diego, CA, USA) was used for the transport efficiency measurement in plant tissue matrices. The citrate coating prevents

AuNP aggregation/agglomeration to achieve an accurate particle concentration. 2-(N-morpholino) ethanesulfonic acid (MES) was purchased from Sigma-Aldrich (St. Louis, MO, USA). Dissolved Ce standard with a concentration of 1000 mg/L in 2% HNO₃ was purchased from High-Purity Standards (Charleston, SC, USA). Tomato (*Solanum lycopersicum L.*), cucumber (*Cucumis sativus*), pumpkin (*Cucurbita pepo*), and soybean (*Glycine max*) seeds were purchased from Johnny's Selected Seeds (Winslow, ME, USA). CeO₂NPs dispersion (40 wt. %) of 30-50 nm was purchased from US Research Nanomaterials (Houston, TX, USA). Powder CeO₂NPs of 50-100 nm was purchased from Nanosstructured&Amorphous Material (Houston, TX, USA).

2.2 CeO₂NPs SP-ICP-MS method development and validation

2.2.1 SP-ICP-MS method description

The ICP-MS operating conditions and the SP-ICP-MS method parameters are shown in **Table 1**. ¹⁴⁰Ce is the most abundant (88.45%) isotope for cerium and is interference-free in ICP-MS analysis, which makes this isotope the best choice for Ce-bearing NPs analysis. The dwell time is a critical parameter in SP-ICP-MS analysis. Previous research has shown that dwell time shorter than the signal duration of NPs event (typically 0.3-0.5 millisecond) can improve the sizing accuracy and particle concentration dynamic range [30,22,23]. The dwell time was set at 0.1 millisecond and the sampling time was 100 seconds, same with those used in our previous study [23]. Due to the low water solubility of CeO₂NPs, the detection of Ce in plant shoot tissues had been interpreted as evidence that CeO₂NPs are taken up by plants as intact NPs [9]. At the same time some research has also shown plants can biotransform CeO₂NPs to cerium

phosphate and cerium carboxylate, but CeO₂ content still dominates [10]. Therefore, in this study, Ce-bearing particles were assumed as CeO₂NPs. In the developed SP-ICP-MS method, the Ce mass was measured first, and then a mass fraction of 81.39% was used to convert the Ce mass to CeO₂ mass. The CeO₂ mass was then converted into CeO₂ particle size based on the CeO₂ density, with the assumption that the CeO₂ particle within the plant tissues are spherical. Syngistix software, with a Nano application module from PerkinElmer, was used for data collection and processing.

Table 1. ICP-MS conditions for the developed SP-ICP-MS method

Optimized ICP-MS Operating Condition	
Nebulizer Gas Flow, L/min	1.06*
Auxiliary Gas Flow, L/min	1.2
Plasma Gas Flow, L/min	18
ICP RF Power	1600
Analog Stage Voltage	-1675
Pulse Stage Voltage	1250
Cell Entrance Voltage	-2
Cell Exit Voltage	-2
Cell Rod Offset	-15
Sampler Cones	Platinum
Skimmer Cones	Platinum
Sample Introduction System	Cyclonic Spray chamber with Meinhard nebulizer
SP-ICP-MS Method Parameters	
Analyte	Ce
Mass (amu)	140
Dwell Time, ms	0.1
Density, g/cm ³	7.13
Mass Fraction, %	81.39
Ionization Efficiency, %	100

* optimized daily

2.2.2 Size measurement accuracy of the SP-ICP-MS method for CeO₂NPs

Dissolved Ce standard was used to convert raw SP-ICP-MS signal to CeO₂NP size according to published method [31,22]. Two commercial CeO₂NPs as described above were characterized by transmission electron microscope (TEM) to validate the accuracy of the size measurement of the developed SP-ICP-MS method. The CeO₂NPs

with a concentration of 1 $\mu\text{g/L}$ was prepared in both 20 mM MES buffer (pH adjusted to pH5 using 1 M NaOH) and in 100-fold diluted plant tissue digestate for SP-ICP-MS analysis. The details on plant tissue enzymatic digestion is described in our previous study[23] with slight modifications (see section 2.4.). The plant tissue digestate was diluted by 100 times with the 20 mM MES buffer.

2.2.3 Effect of enzyme solution on CeO₂NPs

One hundred $\mu\text{g/L}$ of 50-100 nm CeO₂NPs was prepared in the enzyme solution used for plant tissue digestion and was shaken for 24 hours at 37 °C. After shaking, the samples were diluted 100-fold with 20 mM MES buffer for SP-ICP-MS analysis. Freshly prepared 50-100 nm CeO₂NPs of 1 $\mu\text{g/L}$ in 20 mM MES buffer were also analyzed at the same time to compare with enzyme-treated CeO₂NPs for CeO₂ size distribution.

2.3 Plant growth and CeO₂NPs exposure

A published plant growth protocol was followed with slight modifications [23]. Briefly, plant seeds were surface disinfected with 1.25% sodium hypochlorite solution (m/v) for 10 minutes and then rinsed with deionized water three times. The sterilized seeds were germinated on DI water moistened filter paper in a Petri dish for 5-7 days (depends on different seeds). Healthy young seedlings of similar size were transferred to 50-mL polypropylene centrifuge tubes containing 50 mL quarter strength Hoagland solution, purchased from PhytoTechnology Laboratories (Lenexa, KS). They were then incubated in a growth cart with a 16 hrs-light/8 hrs-dark cycle to allow the seedlings to develop further. The growth cart equipped with four T5 fluorescent tubes provided a light

intensity of approximately $133 \mu\text{mol photons m}^{-2} \text{ s}^{-1}$ at the height of plant leaves except for soybean at later stage of growth that was higher because soybean was taller than the other plants. The plants were grown under room temperature ($\sim 25 \text{ }^\circ\text{C}$) and humidity. The Hoagland solution in the tubes was replenished as needed to keep the roots submerged under the water surface. The incubation time for tomato, pumpkin, soybean, and cucumber were 13, 10, 17 and 17 days, respectively. After the incubation in Hoagland solution, the plants were dosed with 7 mg/L $30\text{-}50 \text{ nm}$ CeO_2NPs for 19 days in quarter strength Hoagland solution before harvested for SP-ICP-MS analysis. Controls without CeO_2NPs dosing were included for each plant species during the treatment. Three replicates of dosed plants and two replicates of controls were analyzed for each type of plants.

2.4 Enzymatic digestion and SP-ICP-MS analysis

After cultivation, the shoots were separated from the roots with caution to avoid contamination. The shoot tissues were weighed and thoroughly washed three times using MilliQ water. The excess water on the shoot surface was removed using Kimwipes, then cut into small pieces using scissors and homogenized by a hand-held tissue homogenizer in 9 mL of 20 mM MES buffer ($\text{pH}5$). After homogenization, 1 mL of 30 mg/ml enzyme solution was added. The buffer and enzyme amount were doubled for soybean and pumpkin due to their larger biomass (about doubled). The samples were digested at $37 \text{ }^\circ\text{C}$ for 24 hours in a water bath shaker with continuous shaking. After digestion, the samples were settled down for approximately 30 min (1 hour for soybean) and 0.1 mL of the supernatant was diluted 100-fold using 20 mM MES buffer for SP-ICP-MS analysis.

Selected sample were also filtered by Millipore 5 kDa Ultrafree[®]-MC centrifugal filter after enzymatic digestion. The filtered samples were analyzed by SP-ICP-MS to confirm the presence of dissolved Ce. The calibration standards (0-5 µg/L dissolved Ce) were prepared in 100-fold diluted control plant digestate to match the sample matrix for each plant. 50 nm AuNPs prepared in each 100-fold diluted control plant digestate was used to measure the transport efficiency.

2.5 Acid digestion of the enzymatic digestate

The supernatant of the enzymatic digestate and the whole enzymatic digestate were acid digested using concentrated nitric acid and hydrogen peroxide [8,10], and analyzed by conventional ICP-MS method, to verify the cerium mass content in plant tissues. Two mL of whole enzymatic digesate or the supernatant of the enzymatic digestate was transferred to a 70-mL digestion vessel. The samples were digested using an electrothermal hotblock digester by heated at 100 °C (open vessel) to evaporate water, then 10 mL of trace metal grade concentrated nitric acid was added for each sample and the samples were digested at 105 °C for three hours. The samples were then cooled down to approximately 50 °C and 3 mL of hydrogen peroxide was added to each vessel and the samples were further digested at 100 °C for another three hours. Eventually the samples were evaporated (open vessel) to ~0.5 mL and 9.5 mL of MilliQ water was added to each vessel to bring the total sample volume to 10 mL. The cerium in acid digested samples was then quantified using conventional ICP-MS method. Reagent blank and known amount of pure CeO₂NPs powder were also digested to make sure the digestion process was complete with satisfied recovery.

2.6 TEM imaging of cucumber shoot

Four shoot specimens (2 mm × 2 mm) were randomly collected from the midrib to the margin of a cucumber leaf kept in the Trump's fixative[32] at 4 °C before embedding. The specimens were then washed with the Trump's buffer and dehydrated with a series of ethanol solution successively. The ethanol concentration was increased from 10% to 100% by 10%. Following dehydration, the specimens were placed in an acetone solution (100%) for 5 min and then submerged into the lower viscosity Quetol 651 modified embedding medium overnight. The medium consists of 61.9 wt. % of nonenyl succinic anhydride (NSA), 17.4 wt. % of Quetol 651, 20.7 wt. % of ERL4221, 1 g DER726/10 g of embedding medium, and 0.25 mL of benzyl dimethylamine (BDMA) /10 g of embedding medium. Afterwards, the specimens were placed in an embedding mold filled with the embedding medium and polymerized overnight at 55 – 60 °C. The polymerized specimens were then sectioned with a diamond knife and stained by uranyl acetate and lead citrate. The processed specimens were observed under a JEOL JEM-2010 transmission electron microscopy (JEOL USA, Inc. Peabody, MA) equipped with an Oxford Instruments ATW type energy dispersive spectroscopy (EDS) detector (Oxford Instruments plc, Abingdon, Oxfordshire, UK).

3. Results and Discussion

3.1 SP-ICP-MS Method Performance

3.1.1 Particle size detection limit

When the particle size detection limit of developed SP-ICP-MS methods was reported, the majority of the publications calculated the average signal intensity of the

blank (usually ultrapure water) and the standard deviation (STD) of the blank deviations. The intensity of (average + 3 * STD) was then converted to particle diameters based on the calibration curve [16,33], and this value was reported as particle size detection limit. The particle size detection limit calculated using this method was suitable for the blank with a continuous background. At 0.1 millisecond dwell time, the background of pH5 20 mM MES buffer blank is not continuous. If calculated this way (average + 3*STD), an unpractical particle size detection limit (~16 nm as CeO₂NP) can be achieved. However, significant amount of signals with an intensity of three counts were always identified in pH5 20 mM MES buffer blank. The enzymatic digestion and SP-ICP-MS analysis were carried out in this buffer, therefore, signal intensity of CeO₂NPs equal to or less than three counts cannot be distinguished. Three counts are equivalent to 23-25 nm particle size of CeO₂NPs based on the dissolved Ce calibration curve in the developed SP-ICP-MS method. Therefore, the particle size detection limit in this study was determined to be 23-25 nm as CeO₂NPs.

3.1.2 Sizing accuracy of the developed SP-ICP-MS method

Figure 1 (a) and (c) shows the measured size distributions of 30-50 nm CeO₂NPs and 50-100 nm CeO₂NPs in pH5 20 mM MES buffer, respectively. The measured size distribution matches the manufacturer-reported size distribution. TEM images were also taken for the purchased CeO₂NPs (**Figure 1** (b) and (d)). The size measured by the developed SP-ICP-MS method is comparable to the size shown in TEM images. The long tailing of **Figure 1** (a) and (c) is likely due to the aggregation of CeO₂NPs in dispersion. TEM images also show that the purchased CeO₂NPs is not perfectly spherical. However,

in SP-ICP-MS, the raw data was processed based on the assumption that particles are spherical CeO_2 NPs. **Figure 2** shows the measured size distribution of spiked 50-100 nm CeO_2 NPs (spiked after tissue enzymatic digestion) in 100-fold diluted different plant digestate matrices. Comparing with **Figure 1(c)** to **Figure 2**, the size distributions of measured CeO_2 NPs are not affected by any of the diluted plant shoot digestate when analyzed by the developed SP-ICP-MS method.

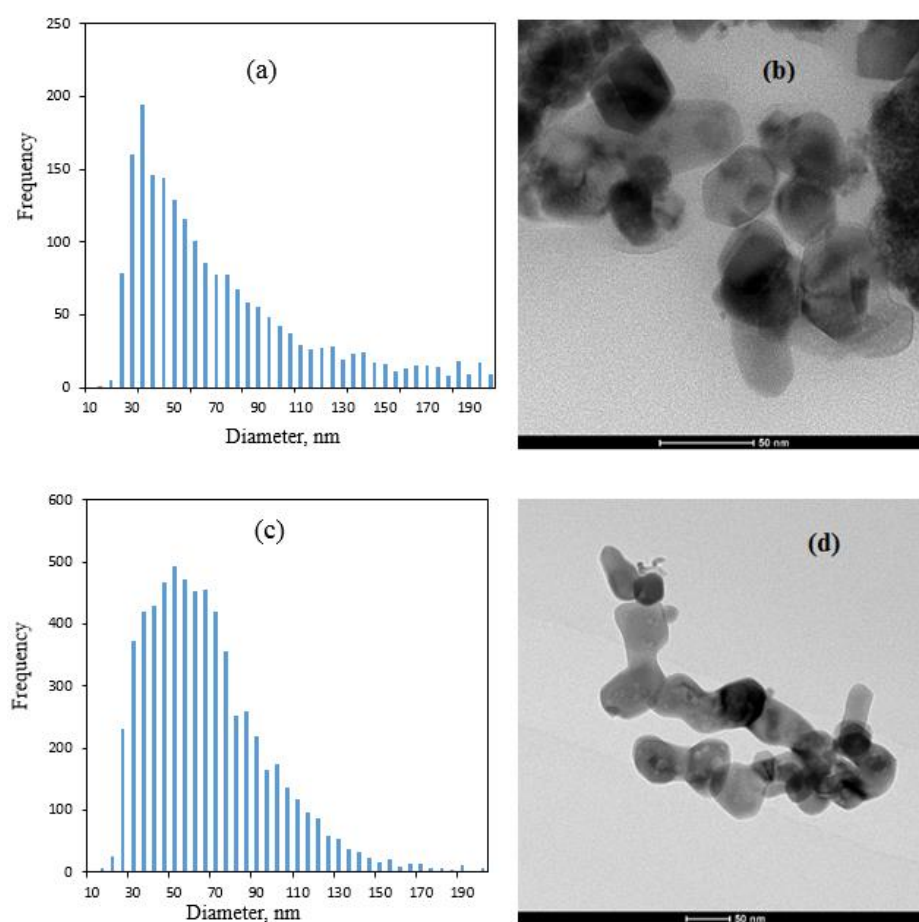


Figure 1. (a) Histogram of 30-50 nm CeO_2 NPs measured by developed SP-ICP-MS method (b) TEM images of purchased 30-50 nm CeO_2 NPs, (c) Histogram of 50-100 nm CeO_2 NPs measured by developed SP-ICP-MS method (d) TEM images of purchased 50-100 nm CeO_2 NPs. (scale bar on both TEM images is 50 nm)

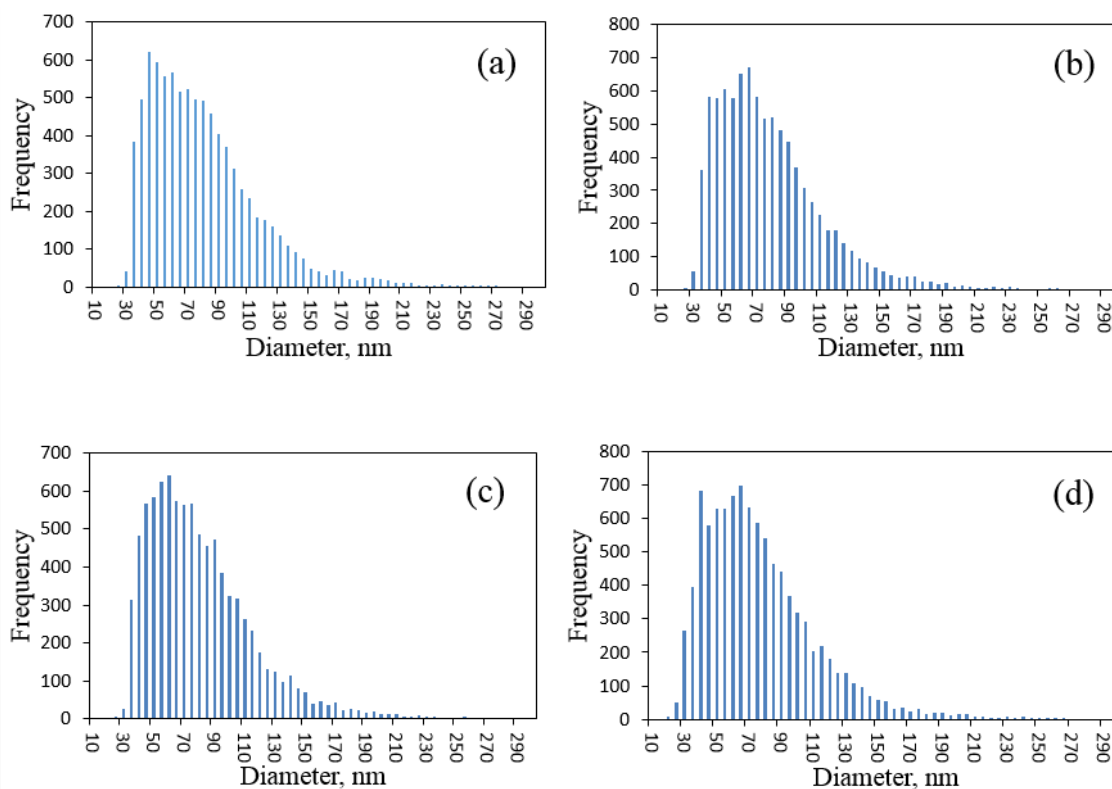


Figure 2. Size distribution of spiked 50-100 nm CeO_2NPs in different plant digestate matrix measured by developed SP-ICP-MS method after 100-fold dilution in 20 mM MES buffer (pH 5): (a) tomato, (b) soybean, (c) cucumber, (d) pumpkin.

3.1.3 Effect of enzymatic digestion on CeO_2NPs

Figure 3 shows the size distributions of 24-h enzyme solution-treated CeO_2NPs (no plant tissue, treated with the same condition of the plant tissue enzymatic digestion) and freshly prepared CeO_2NPs , respectively. Two distributions are comparable to each other and three replicates also demonstrate good reproducibility. The results demonstrated that the Macerozyme R-10 enzyme is feasible for CeO_2NPs extraction from plant tissues without causing dissolution of CeO_2NPs .

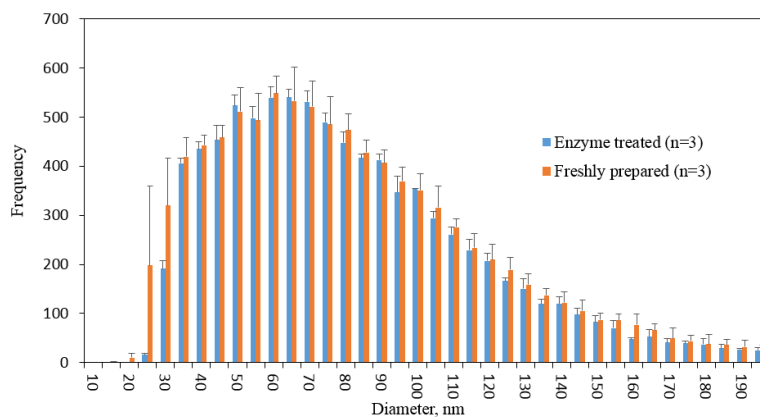


Figure 3. Comparison of the size distribution of 50-100 nm CeO₂NPs after 24 hours digestion in enzyme solution at 37 °C to the size distribution of freshly prepared 50-100 nm CeO₂NPs in enzyme solution.

3.2 CeO₂ NPs Uptake and Biotransformation

Figure 4 shows the raw data of SP-ICP-MS for four types of plants. Figure 4 (a), (c), (e) and (h) show the raw data of control plants for tomato, cucumber, pumpkin and soybean, respectively. Figure 4 (b), (d), (f) and (i) display the raw data for tomato, cucumber, pumpkin and soybean dosed with 7 mg/L of 30-50 nm CeO₂NPs for 19 days, respectively. The quantification data of particle concentrations and dissolved Ce are shown in **Table 2**. It is clear from the SP-ICP-MS outputs and Table 2 that there was uptake of Ce from the dosing solutions. As discussed above, dissolved analyte is detected as a continuous signal and particles are detected as pulse signals in SP-ICP-MS mode. The samples were also tested by 20-fold dilution with 20 mM MES buffer. The intensity of the continuous signals in 20-fold diluted sample was 5 times of the intensity of the continuous signals in 100-fold diluted samples, which means the intensity of the continuous signal decreases proportionally as the dilution factor increases and subsequently suggests that the continuous signals in Figure 4 came from dissolved Ce.

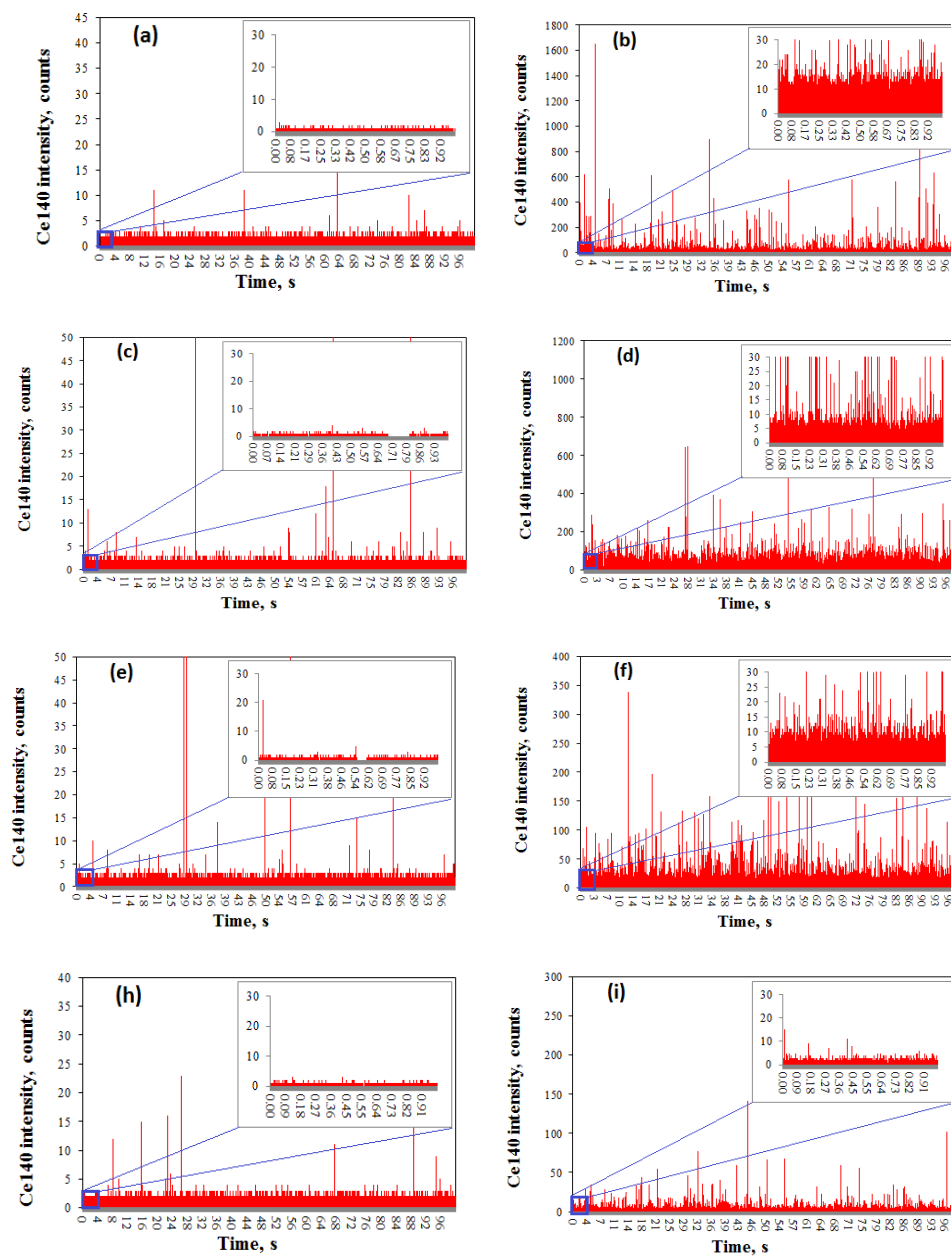


Figure 4. SP-ICP-MS raw data of plant shoots digestates: (a) tomato control without dosing CeO_2NPs , (b) tomato dosed with 7 mg/L 30-50 nm CeO_2NPs for 19 days, (c) cucumber control without dosing CeO_2NPs , (d) cucumber dosed with 7 mg/L 30-50 nm CeO_2NPs for 19 days, (e) pumpkin control without dosing CeO_2NPs , (f) pumpkin dosed with 7 mg/L 30-50 nm CeO_2NPs for 19 days, (g) soybean control without dosing CeO_2NPs , (h) soybean dosed with 7 mg/L 30-50 nm CeO_2NPs for 19 days. The inset shows the data points in the first one second

More convincing data about the presence of dissolved Ce is shown in **Figure 5**, which was the dosed tomato sample filtered by Millipore 5 kDa Ultrafree[®]-MC centrifugal filter (particles cannot pass through this filter) after enzymatic digestion and then analyzed by SP-ICP-MS. Continuous signal was still observed in SP-ICP-MS, which confirmed the presence of dissolved Ce. Cerium is naturally stabilized in both trivalent (Ce^{3+}) and tetravalent (Ce^{4+}) states [1]. However, the further speciation analysis of dissolved Ce detected here is beyond the capability of SP-ICP-MS. Regarding the detailed uptake mechanism study, another technique ion chromatograph-ICP-MS may be evaluated for this purpose. Although a few pulse signals were observed in the control samples, it is not significant comparing with the CeO_2NPs dosed samples.

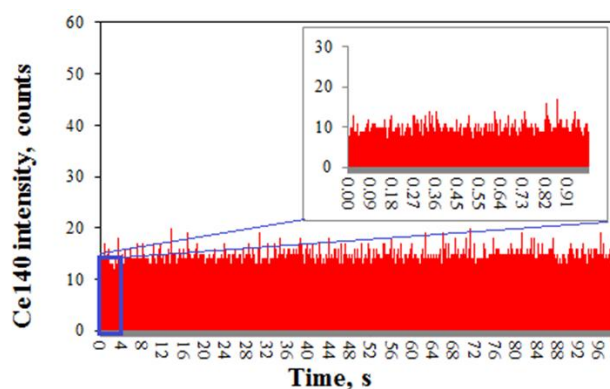


Figure 5. SP-ICP-MS raw data of enzymatic digestate filtered by Millipore 5 kDa Ultrafree[®]-MC centrifugal filter. The inset shows the data points in the first one second.

The presence of both types of signals indicated that both dissolved Ce and particulate Ce were present in plant tissues. However, the exact chemical composition of these particulate Ce was not determined in this study. An interesting finding worth

mentioning is that some pulse signals were also identified in the control digestate spiked with dissolved Ce, and these pulse signals are possibly caused by the adsorption of Ce ions onto the surface of undigested plant tissue colloids. These colloids can act as particulate Ce. So far SP-ICP-MS is not able to differentiate true CeO₂NPs from these colloids with cerium ions adsorbed onto them. Since the presence of dissolved Ce was confirmed in the plants dosed with 7 mg/L CeO₂NPs, the observed pulse signals in SP-ICP-MS shown in Figure 4 may come from true CeO₂NPs or undigested plant tissue colloids with cerium ions adsorbed onto them or both. The size distribution of particulate Ce in plant tissues shown in Figure 6 seems to suggest that some of the particulate Ce was from CeO₂NPs dosed since it agreed well with the primary nanoparticle sizes introduced to the system. However, the interference from the dissolved Ce cannot be ruled out. A previous study also reported that part of the Ce detected in cucumber shoots remained as CeO₂NPs even though cerium carboxylate was also reported in the shoots in that study [34]. Cucumber leaves were selected to perform TEM-EDS examinations. No particulate Ce was detected using EDS. These results might indicate the absence of CeO₂NPs in the selected sample, or CeO₂NPs present but the concentration was too low to be detected by TEM. Other studies have also encountered similar sensitivity problem to find CeO₂NPs in plant shoots using TEM[10]. TEM is a powerful technique to characterize pure synthesized ENPs, however, its applications to the environmental and biological samples are limited by its sensitivity because this technology is difficult to detect the environmentally relevant concentrations of NPs. The discrepancy results of the SP-ICP-MS and TEM was not resolved in this paper and further study by using other

techniques, such as field-flow fractionation (FFF) coupled with ICP-MS, may be useful to confirm the presence or absence of CeO₂NPs in the dosed plant shoots.

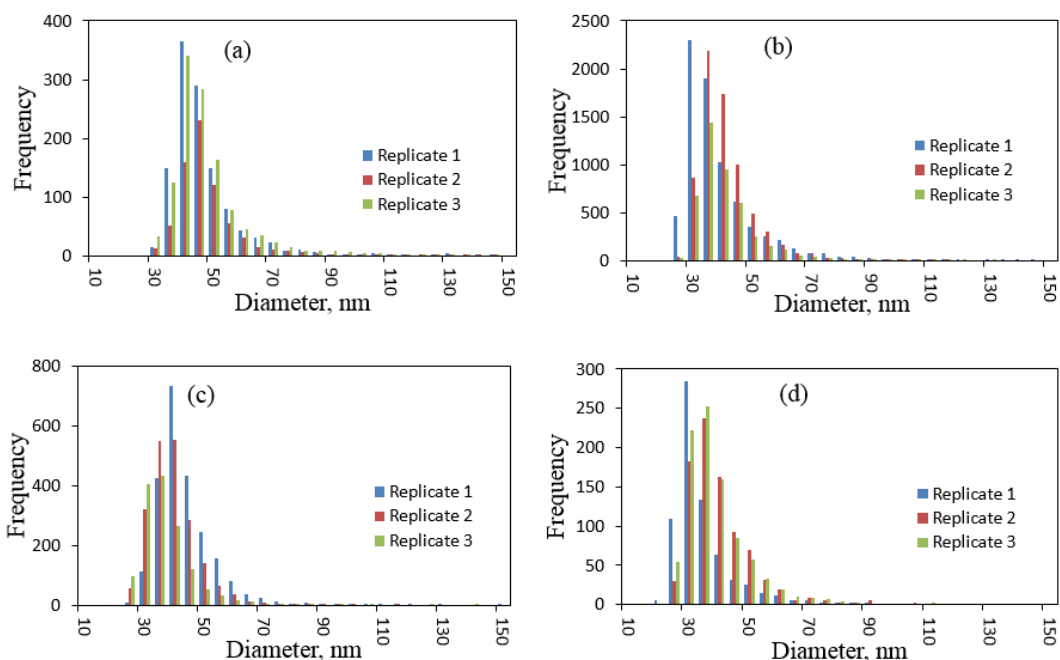


Figure 6. Size distribution of CeO₂NPs in plant shoots dosed with 7 mg/L 30-50 nm CeO₂NPs for 19 days, (a) histogram of tomato shoot, (b) histogram of cucumber shoot, (c) histogram of pumpkin shoot, (d) histogram of soybean shoot

How did plants take up dissolved Ce and/or CeO₂NPs from the growth media?

Were they taken up by plant roots as intact CeO₂NPs as suggested by some previous research [6,34,35] or were they taken up as Ce³⁺ and then oxidized to CeO₂NPs as some recent research proposed [11]? Based on the size and size distribution comparison between the CeO₂NPs in plant shoots and in the dosing media, the results appeared to indicate that part of the CeO₂NPs were taken up by plant roots as intact CeO₂NPs. However, based on some of our preliminary results with cerium ion only, particulate

cerium was also detected in plants exposed solely to ionic cerium (data not published). Therefore, it appears that both mechanisms contribute to the uptake and accumulation of CeO₂NPs in plant shoots. However, the relative significance of the mechanisms is still unclear and deserves further investigation.

CeO₂NP is well recognized for its low solubility in water. Where did the ionic cerium in plant shoots come from? The low solubility and dissolution of CeO₂NPs in water suggested that ionic cerium was not directly taken up from the solution. Figure 7(a) shows there was no dissolved Ce in freshly prepared dosing solution compared to the diluent 20 mM MES shown in Figure 7(b). These results suggest the dissolved Ce observed in plant shoot was due to the biotransformation of CeO₂NPs, not because there was dissolved Ce impurities in the CeO₂NPs dosed. Previous research has shown that Ce in cucumber shoot (leaves and stems) after hydroponically exposed to 2000 mg/L CeO₂NPs contains ~80% CeO₂ and ~20% cerium carboxylate. **Figure 3** indicates that CeO₂NPs did not dissolve during enzymatic digestion. The dissolved Ce observed by SP-ICP-MS here is therefore not due to the dissolution of CeO₂NPs during sample preparation. The fact that we dosed the plants with CeO₂NPs and yet dissolved Ce was observed in plant shoots provides strong evidence that CeO₂ biotransformation has occurred. The same dosing, enzymatic digestion, and SP-ICP-MS analysis of tomato plants were repeated for three times and similar results were observed. Both Ce³⁺ and Ce⁴⁺ can form soluble salts (e.g. Ce(SO₄)₂, Ce₂(SO₄)₃). Therefore, the speciation of dissolved Ce observed here needs to be further verified, may be by ion chromatograph-ICP-MS. According to some previous studies [35], the transformation of CeO₂NPs happened at the root surface, and the physicochemical interaction between CeO₂NPs and

root exudates is the necessary condition for the transformation of CeO₂NPs in hydroponic cucumber. The dissolved Ce on plant root surface might be another source of ionic cerium in plant shoots. Regardless of the mechanisms of ionic cerium, this study is the first to report the widespread presence of dissolved cerium in four different plant species treated with CeO₂NPs hydroponically.

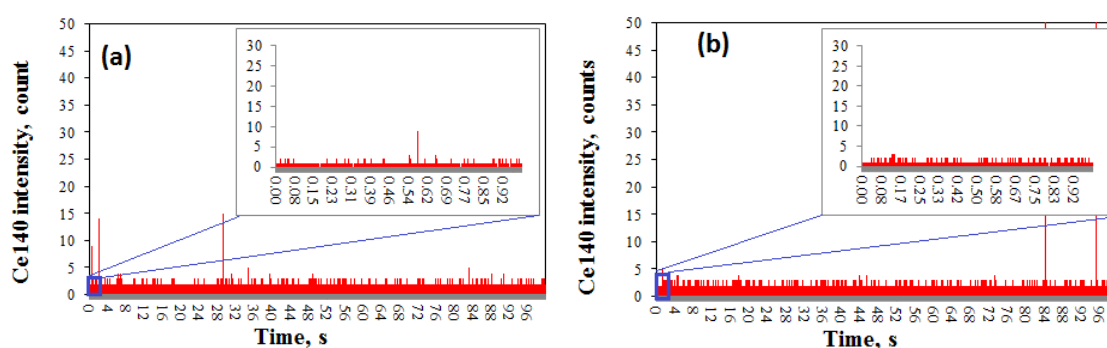


Figure 7. (a) freshly prepared 7 mg/L of CeO₂NPs dosing solution filtered by Millipore 5kDa Ultrafree[®]-MC centrifugal filter, (b) 20 mM MES buffer (Dilution factor:10 for a)

Table 2. Results of fresh shoots obtained by SP-ICP-MS analysis and acid digestion followed by conventional ICP-MS analysis.

Plant	SP-ICP-MS analysis results [n=3, average (%RSD)]		Acid digestion-ICP-MS results [n=2, average (%RSD)]	
	CeO ₂ Particle concentration (particles/g fresh shoot)	Dissolved Ce (SP-ICP-MS data) in fresh shoot (µg/g)	Total Ce in fresh shoot (µg/g)	Ce in the supernatant of enzymatic digestate (µg/g)
Tomato	9886011 (27.22%)	0.19 (8.31%)	0.41 (11.63%)	0.18 (12.73%)
Soybean	13991254 (24.86%)	0.10 (12.79%)	0.2 (11.12%)	0.08 (28.30%)
Cucumber*	142519632 (42.58%)	0.13 (38.68%)	0.5 (1.38%)	0.18 (14.17%)
Pumpkin	26130562 (16.89%)	0.06 (24.53%)	0.15 (21.28%)	0.09 (22.07%)

Note *: For cucumber, one plant varies largely from the other two replicates. SP-ICP-MS analyzed all three replicated plants, but acid digestion selected the more reproducible two plants.

In addition to the general observation of plant uptake and accumulation of CeO₂NPs and dissolved cerium, some differences among the four different plant species have been noticed as shown in Table 2. Cucumber exhibited the highest possibility of accumulation of CeO₂NPs, followed by pumpkin and then soybean and tomato. Another observation which appeared to stand out is the slightly smaller average CeO₂NP size in pumpkin and soybean shoots than in tomato and cucumber shoots. The significance of this difference could not be justified statistically in this study due to the small number of replicates. The underlying mechanisms causing the observed possible differences among different plant species are still elusive, but might be due to the different structures of plant roots or different properties of plant exudates. Further investigation is needed to elucidate the precise mechanisms.

4. Conclusions

In summary, we have successfully developed a SP-ICP-MS protocol to simultaneously detect particle size, size distribution, particle concentration and dissolved analyte of CeO₂NPs in plant tissues. The enzyme extraction method did not alter the properties of CeO₂NPs in plant tissues. Applying this innovative technology, we first reported that CeO₂NPs might be simultaneously taken up by plants both as intact CeO₂NPs and as cerium ions. Once CeO₂NPs are taken up in plant roots, they might be translocated to plant shoots, where CeO₂NPs dissolution could occur. SP-ICP-MS shows great potential to serve as a sensitivity tool to study the uptake mechanism of ENPs by plants, however, more improvements on SP-ICP-MS technique itself are needed, such as the improvement on particle size detection limit. Some other techniques are also needed

to fully characterize the properties of Ce after uptake. For instance, the speciation analysis of dissolved Ce observed in the current study may be further studied using ion chromatograph coupled to ICP-MS to elucidate the dissolution mechanism of CeO₂NPs (e.g. simple dissolution or dissolution involving redox reaction). Even though the sources of dissolved Ce in plant shoots are not clear at this point, it appears that dissolved Ce is commonly present in plant tissues exposed to CeO₂NPs. The extent of plant uptake and accumulation also appear dependent on the plant species, however, future systematic study is needed to confirm it statistically and to probe the underlying mechanism. With these new advancements, several questions remain and future efforts will concentrate on determining the extent of CeO₂NPs dissolution on plant root surface and in plant tissues and understanding why the uptake and accumulation differ among different plant species.

Acknowledgement

The NexION 300/350D ICP-MS was provided by PerkinElmer, Inc. The authors appreciate the support from University of Missouri Research Board, Chemistry Department and Center for Single Nanoparticle, Single Cell, and Single Molecule Monitoring (CS³M) at Missouri University of Science and Technology. Xingmao Ma acknowledges the financial support of the US Department of Agriculture-AFRI (#2011-67006-30181 and USDA-AFRI (#2012-67005-19585).

Conflict of Interest

The authors declare no conflict of interest.

References

1. Perullini M, Bilmes SAA, Jobbagy M (2012) Cerium Oxide Nanoparticles: Structure, Applications, Reactivity, and Eco-Toxicology. In: *Nanomaterial: A Danger or a Promise?* pp 307-333. doi:10.1007/978-1-4471-4213-3_12
2. Deshpande S, Patil S, Kuchibhatla SVNT, Seal S (2005) Size dependency variation in lattice parameter and valency states in nanocrystalline cerium oxide. *Appl Phys Lett* 87 (13):133113/133111-133113/133113. doi:10.1063/1.2061873
3. Schwabe F, Schulin R, Rupper P, Rotzetter A, Stark W, Nowack B (2014) Dissolution and transformation of cerium oxide nanoparticles in plant growth media. *J Nanopart Res* 16 (10):1-11. doi:10.1007/s11051-014-2668-8
4. Collin B, Auffan M, Johnson AC, Kaur I, Keller AA, Lazareva A, Lead JR, Ma X, Merrifield RC, Svendsen C, White JC, Unrine JM (2014) Environmental release, fate and ecotoxicological effects of manufactured ceria nanomaterials. *Environ Sci: Nano* 1 (6):533-548. doi:10.1039/C4EN00149D
5. Cassee FR, van BEC, Singh C, Green D, Muijsers H, Weinstein J, Dreher K (2011) Exposure, health and ecological effects review of engineered nanoscale cerium and cerium oxide associated with its use as a fuel additive. *Crit Rev Toxicol* 41 (3):213-229
6. Zhang Z, He X, Zhang H, Ma Y, Zhang P, Ding Y, Zhao Y (2011) Uptake and distribution of ceria nanoparticles in cucumber plants. *Metallomics* 3 (8):816-822. doi:10.1039/c1mt00049g
7. Zhao L, Sun Y, Hernandez-Viezcas JA, Hong J, Majumdar S, Niu G, Duarte-Gardea M, Peralta-Videa JR, Gardea-Torresdey JL (2015) Monitoring the Environmental Effects of CeO₂ and ZnO Nanoparticles Through the Life Cycle of Corn (*Zea mays*) Plants and in Situ μ -XRF Mapping of Nutrients in Kernels. *Environ Sci Technol* 49 (5):2921-2928. doi:10.1021/es5060226
8. Wang Q, Ma X, Zhang W, Pei H, Chen Y (2012) The impact of cerium oxide nanoparticles on tomato (*Solanum lycopersicum* L.) and its implications for food safety. *Metallomics* 4 (10):1105-1112. doi:10.1039/c2mt20149f
9. Lopez-Moreno ML, de la Rosa G, Hernandez-Viezcas JA, Castillo-Michel H, Botez CE, Peralta-Videa JR, Gardea-Torresdey JL (2010) Evidence of the Differential Biotransformation and Genotoxicity of ZnO and CeO₂ Nanoparticles on Soybean (*Glycine max*) Plants. *Environ Sci Technol* 44 (19):7315-7320. doi:10.1021/es903891g
10. Zhang P, Ma Y, Zhang Z, He X, Zhang J, Guo Z, Tai R, Zhao Y, Chai Z (2012) Biotransformation of Ceria Nanoparticles in Cucumber Plants. *ACS Nano* 6 (11):9943-9950. doi:10.1021/nn303543n

11. Schwabe F, Tanner S, Schulin R, Rotzetter A, Stark W, von Quadt A, Nowack B (2015) Dissolved cerium contributes to uptake of Ce in the presence of differently sized CeO₂-nanoparticles by three crop plants. *Metallomics* 7 (3):466-477. doi:10.1039/C4MT00343H
12. Degueldre C, Favarger PY (2003) Colloid analysis by single particle inductively coupled plasma-mass spectroscopy: a feasibility study. *Colloids Surf, A* 217 (1-3):137-142. doi:10.1016/S0927-7757(02)00568-X
13. Laborda F, Jimenez-Lamana J, Bolea E, Castillo JR (2011) Selective identification, characterization and determination of dissolved silver(I) and silver nanoparticles based on single particle detection by inductively coupled plasma mass spectrometry. *J Anal At Spectrom* 26 (7):1362-1371. doi:10.1039/c0ja00098a
14. Pace HE, Rogers NJ, Jarolimek C, Coleman VA, Higgins CP, Ranville JF (2011) Determining transport efficiency for the purpose of counting and sizing nanoparticles via single particle inductively coupled plasma mass spectrometry. *Anal Chem (Washington, DC, U S)* 83 (24):9361-9369. doi:10.1021/ac201952t
15. Mitrano DM, Leshner EK, Bednar A, Monserud J, Higgins CP, Ranville JF (2012) Detecting nanoparticulate silver using single-particle inductively coupled plasma-mass spectrometry. *Environ Toxicol Chem* 31 (1):115-121. doi:10.1002/etc.719
16. Pace HE, Rogers NJ, Jarolimek C, Coleman VA, Gray EP, Higgins CP, Ranville JF (2012) Single particle inductively coupled plasma-mass spectrometry: a performance evaluation and method comparison in the determination of nanoparticle size. *Environ Sci Technol* 46 (22):12272-12280. doi:10.1021/es301787d
17. Tuoriniemi J, Cornelis G, Hasseloev M (2012) Size Discrimination and Detection Capabilities of Single-Particle ICPMS for Environmental Analysis of Silver Nanoparticles. *Anal Chem* 84 (9):3965-3972. doi:10.1021/ac203005r
18. Gray EP, Coleman JG, Bednar AJ, Kennedy AJ, Ranville JF, Higgins CP (2013) Extraction and Analysis of Silver and Gold Nanoparticles from Biological Tissues Using Single Particle Inductively Coupled Plasma Mass Spectrometry. *Environ Sci Technol* 47 (24):14315-14323. doi:10.1021/es403558c
19. Loeschner K, Brabrand MSJ, Sloth JJ, Larsen EH (2014) Use of alkaline or enzymatic sample pretreatment prior to characterization of gold nanoparticles in animal tissue by single-particle ICPMS. *Anal Bioanal Chem* 406 (16):3845-3851. doi:10.1007/s00216-013-7431-y
20. Mitrano DM, Ranville JF, Bednar A, Kazor K, Hering AS, Higgins CP (2014) Tracking dissolution of silver nanoparticles at environmentally relevant concentrations in laboratory, natural, and processed waters using single particle ICP-MS (spICP-MS). *Environ Sci: Nano* 1 (3):248-259. doi:10.1039/c3en00108c

21. Peters RJB, Rivera ZH, van Bommel G, Marvin HJP, Weigel S, Bouwmeester H (2014) Development and validation of single particle ICP-MS for sizing and quantitative determination of nano-silver in chicken meat. *Anal Bioanal Chem* 406 (16):3875-3885. doi:10.1007/s00216-013-7571-0
22. Dan Y, Shi H, Stephan C, Liang X (2015) Rapid analysis of titanium dioxide nanoparticles in sunscreens using single particle inductively coupled plasma-mass spectrometry. *Microchem J* 122:119-126. doi:10.1016/j.microc.2015.04.018
23. Dan Y, Zhang W, Xue R, Ma X, Stephan C, Shi H (2015) Characterization of Gold Nanoparticle Uptake by Tomato Plants Using Enzymatic Extraction Followed by Single-Particle Inductively Coupled Plasma-Mass Spectrometry Analysis. *Environ Sci Technol* 49 (5):3007-3014. doi:10.1021/es506179e
24. Donovan AR, Adams CD, Ma Y, Stephan C, Eichholz T, Shi H (2016) Single particle ICP-MS characterization of titanium dioxide, silver, and gold nanoparticles during drinking water treatment. *Chemosphere* 144:148-153. doi:10.1016/j.chemosphere.2015.07.081
25. Donovan AR, Adams CD, Ma Y, Stephan C, Eichholz T, Shi H (2016) Detection of zinc oxide and cerium dioxide nanoparticles during drinking water treatment by rapid single particle ICP-MS methods. *Anal Bioanal Chem*:Ahead of Print. doi:10.1007/s00216-016-9432-0
26. Loeschner K, Navratilova J, Kobler C, Molhave K, Wagner S, von der KF, Larsen EH (2013) Detection and characterization of silver nanoparticles in chicken meat by asymmetric flow field flow fractionation with detection by conventional or single particle ICP-MS. *Anal Bioanal Chem* 405 (25):8185-8195. doi:10.1007/s00216-013-7228-z
27. Degueldre C, Favarger PY, Rosse R, Wold S (2006) Uranium colloid analysis by single particle inductively coupled plasma-mass spectrometry. *Talanta* 68 (3):623-628. doi:10.1016/j.talanta.2005.05.006
28. Degueldre C, Favarger PY, Wold S (2006) Gold colloid analysis by inductively coupled plasma-mass spectrometry in a single particle mode. *Anal Chim Acta* 555 (2):263-268. doi:10.1016/j.aca.2005.09.021
29. Marshall AT, Haverkamp RG, Davies CE, Parsons JG, Gardea-Torresdey JL, van Agterveld D (2007) Accumulation of gold nanoparticles in Brassica Juncea. *Int J Phytorem* 9 (3):197-206. doi:10.1080/15226510701376026
30. Hineman A, Stephan C (2014) Effect of dwell time on single particle inductively coupled plasma mass spectrometry data acquisition quality. *J Anal At Spectrom* 29 (7):1252-1257. doi:10.1039/c4ja00097h

31. Pace HE, Rogers NJ, Jarolimek C, Coleman VA, Higgins CP, Ranville JF (2011) Determining Transport Efficiency for the Purpose of Counting and Sizing Nanoparticles via Single Particle Inductively Coupled Plasma Mass Spectrometry. *Anal Chem* 83 (24):9361-9369. doi:10.1021/ac201952t
32. McDowell EM, Trump BF (1976) Histologic fixatives suitable for diagnostic light and electron microscopy. *Arch Pathol Lab Med* 100 (8):405-414
33. Lee S, Bi X, Reed RB, Ranville JF, Herckes P, Westerhoff P (2014) Nanoparticle Size Detection Limits by Single Particle ICP-MS for 40 Elements. *Environ Sci Technol* 48 (17):10291-10300. doi:10.1021/es502422v
34. Ma Y, Zhang P, Zhang Z, He X, Li Y, Zhang J, Zheng L, Chu S, Yang K, Zhao Y, Chai Z (2015) Origin of the different phytotoxicity and biotransformation of cerium and lanthanum oxide nanoparticles in cucumber. *Nanotoxicology* 9 (2):262-270. doi:10.3109/17435390.2014.921344
35. Ma Y, Zhang P, Zhang Z, He X, Zhang J, Ding Y, Zhang J, Zheng L, Guo Z, Zhang L, Chai Z, Zhao Y (2015) Where Does the Transformation of Precipitated Ceria Nanoparticles in Hydroponic Plants Take Place? *Environ Sci Technol* 49 (17):10667-10674. doi:10.1021/acs.est.5b02761

**IV. URINARY METALLOMICS AS A NOVEL BIOMARKER DISCOVERY
PLATFORM: BREAST CANCER AS A CASE STUDY**

Casey Burton¹, Yongbo Dan¹, Ariel Donovan¹, Kun Liu¹, Honglan Shi¹, Yinfa Ma^{1*},
Cynthia P. Bosnak²

¹Department of Chemistry and Center for Single Nanoparticle, Single Cell, and Single
Molecule Monitoring, Missouri University of Science and Technology, Rolla, MO 65409

²PerkinElmer, Inc., 940 Winter Street, Waltham, MA 02451

*** Corresponding Author**

Address: Department of Chemistry

Missouri University of Science and Technology

400 West 11th Street

Rolla, MO 65409

Phone: 573-341-6220

Fax: 573-341-6033

E-mail: yinfa@mst.edu

ABSTRACT

Background: Urinary metallomics is presented here as a new “omics” approach that aims to facilitate personalized cancer screening and prevention by improving our understanding of urinary metals in disease.

Methods: Twenty-two urinary metals were examined with inductively-coupled plasma – mass spectrometry in 138 women newly diagnosed with breast cancer and benign conditions. Urinary metals from spot urine samples were adjusted to renal dilution using urine specific gravity.

Results: Two urinary metals, copper (P -value = 0.036) and lead (P -value = 0.003), were significantly elevated in the urine of breast cancer patients. A multivariate model that comprised copper, lead, and patient age afforded encouraging discriminatory power (AUC: 0.728, P -value < 0.0005), while univariate models of copper (61.7% sensitivity, 50.0% specificity) and lead (76.6% sensitivity, 51.2% specificity) at optimized cutoff thresholds compared favorably with other breast cancer diagnostic modalities such as mammography. Correlations found among various metals suggested potential geographic and dietary influences on the urine metallome that warrant further investigation.

Conclusions: In summary, this proof-of-concept work introduces urinary metallomics as a noninvasive, potentially transformative “omics” approach to early cancer detection. Urinary copper and lead have also been preliminarily identified as potential breast cancer biomarkers.

Keywords: Breast cancer metallomics, urinary metallomics, ICP-MS, urinary lead, urinary copper, noninvasive breast cancer screening

1. Introduction

Metallomics is an emerging field concerned with the comprehensive analysis of metal and metalloid species within a biological system [1, 2]. The extensive and essential roles of metal and metalloids in pathophysiology lend suitability to metallomics as a novel approach to disease detection and monitoring. For example, metalloproteins represent approximately one third of the known proteome and have wide-ranging roles in biologically important processes such as oxygen and electron transport, biosynthesis and biodegradation, and hydrolysis of amides and esters, and others [3]. Metalloprotein dysregulation is frequently associated with pathological status, such as metallothionein overexpression in certain invasive ductal breast cancers [4-6]. Moreover, metal ions are presumed to be highly regulated [7, 8] owing to their critical roles in maintaining cellular redox status and regulating protein expression [9-11]. A comprehensive understanding of metal content, speciation, localization and function under various pathophysiological conditions is therefore becoming increasingly important in understanding disease mechanisms and discovering novel diagnostic, prognostic, and therapeutic targets.

The role of metallomics in understanding breast cancer has led to novel insights into metal functionality in breast cancer carcinogenesis and metastasis. For example, copper hyperaccumulation in cancer cells is required for angiogenesis and tumor growth [12]. Similarly, dysregulated copper transport leads to oxidative stress and perturbed cell signaling pathways via the copper transport protein CTR1 while copper transport protein CTR2 expression has been linked to breast cancer prognosis and cisplatin drug resistance [13]. Intracellular copper additionally stimulates breast cancer metastasis via redox regulation such as inducing reactive oxygen species generation in cellular structures associated with cell motility [14]. Consequently, novel chemotherapy sensitizers that

function as redox modulators via copper(II) chelation have emerged [15]. Similarly, intracellular zinc is physiologically highly regulated in order to maintain cellular redox status [16], but becomes deregulated in breast tumors. Metallothioneins, antioxidant proteins with high binding affinities for essential metals like copper and zinc, are also poorly regulated in invasive ductal carcinomas [17], resulting in increased free cytosolic zinc and copper ions [18]. Zinc importer protein overexpression and zinc hyperaccumulation have similarly been well documented in heterogeneous breast cancers [18-22]. For these reasons, researchers have explored the utility of copper and zinc as diagnostic biomarkers for breast cancer, such as low serum zinc [23] and high serum Zn/Cu serum ratios [24]. Furthermore, divalent transition metals including copper, cobalt, lead, mercury, tin, and chromium have been shown to activate estrogen receptor- α and consequently cell proliferation [25]. Other metals, like lead, have been associated with selenium antagonism, which minimizes the anti-carcinogenic effect of selenium, leading to higher risk for developing breast cancer [26]. Together, these pathophysiological metallomic changes provide a new molecular modality for earlier detection of aggressive breast cancer.

Comprehensive metallomic screening techniques essential to discovering new clinically useful metallomic biomarkers have become popular following advances in advanced analytical techniques that have enabled researchers to study otherwise trace metals in biologically relevant matrices. Inductively-coupled plasma – mass spectrometry (ICP-MS) in particular has emerged as a powerful platform based on its unparalleled sensitivity and throughput. Recent efforts have already used this approach to implicate high lead, uranium [27] in addition to antimony and cadmium [28] in hair samples of

breast cancer patients. Urinary cadmium, another selenium antagonist, has recently been proposed as a noninvasive indicator of breast cancer through multiplicative interactions with selenium [29]. However, application of metallomics to urinalysis remains underdeveloped, despite its distinct advantages that include reduced sample preparation and noninvasive detection modality. While concentration ranges of many urinary metals in healthy populations have been widely reported, other trace elements and concentration ranges in clinically relevant populations, such as women with newly diagnosed breast cancer or with suspected breast cancer, have yet to be described or critically reviewed. This study therefore examined 22 urinary metals using ICP-MS in a proof-of-concept study involving 138 women with newly diagnosed breast cancer and benign conditions in order to quantify the clinical applicability of urinary metals in breast cancer detection and prognosis.

2. Materials and Methods

2.1 Patients and specimens

A total of 138 women 33-84 years of age were recruited to provide urine specimens for this proof-of-concept study and other studies at the Mercy Breast Center - Springfield (Springfield, Missouri) between July 2013 and December 2014. Study protocol was approved by the Mercy Medical Research Institute Institutional Review Board (IRB) and participants were required to provide informed consent. Inclusion criteria for participants included new referrals to the Mercy Breast Center - Springfield following possible indication for breast cancer that required further biopsy and immunohistochemical characterization. Exclusion criteria included individuals with a previous history of cancer and/or any known comorbidities. All women resided in the

Southwest Missouri region which is a predominate lead and zinc mining area. Additional demographic, metal exposure, and patient health information were not collected owing to the retrospective nature of this study. Spot urine specimens comprising first morning and second morning voids were collected for the study and immediately stored at -20°C for 1-6 days at Mercy Breast Center – Springfield followed by shipment to Missouri University of Science and Technology via next-day frozen ground freight for analysis. Urine aliquots were stored at -80°C and underwent 2-4 freeze/thaw cycles prior to analysis which occurred 1-6 months after specimen collection. Urinary metals were shown to be freeze/thaw resistant with minimal metal adsorption on container walls after five freeze/thaw cycles across six months storage at -80°C . Patient diagnoses were independently determined by qualified Mercy Breast Center – Springfield staff using a combination of ultrasound-guided core biopsies and pathological stains. The study was conducted in a double-blind manner. Data and resources including patient urine specimens, pathological reports, and metallomic results were anonymized with numerical identifiers.

2.2 ICP-MS Urinary Metal Assay

Twenty-two urinary metals including vanadium (V), chromium (Cr), manganese (Mn), cobalt (Co), nickel (Ni), copper (Cu), zinc (Zn), gallium (Ga), arsenic (As), selenium (Se), rubidium (Rb), strontium (Sr), molybdenum (Mo), silver (Ag), cadmium (Cd), tin (Sn), antimony (Sb), cesium (Cs), barium (Ba), tellurium (Tl), lead (Pb), and uranium (U) were quantified using a previously described ICP-MS technique with several significant modifications [30]. Briefly, 2 mL urine specimen aliquots were equilibrated to

room temperature and diluted fivefold with 1% Optima grade nitric acid (Fisher Scientific Inc, #A467-1) and internal metal standards ^{45}Sc , ^{89}Y , and ^{159}Tb (PerkinElmer Inc, N9303834) in nitric acid pretreated sample tubes. Two calibration standard mixtures (PerkinElmer Inc, N9300233 and N9301721) comprising the 22 metals were used for instrument calibration. Samples were injected into a NexION 350D ICP-MS (PerkinElmer Inc) using an autosampler and peristaltic pumps. The ICP-MS was operated in kinetic energy discrimination (KED) mode using ultra-high purity helium with a flow rate of 3.9 mL/min for As and Se, and 4.7 mL/min for other metals to minimize polyatomic interferences that may arise in complex urine matrices. Quantitation isotopes included ^{51}V , ^{52}Cr , ^{55}Mn , ^{59}Co , ^{60}Ni , ^{63}Cu , ^{66}Zn , ^{69}Ga , ^{75}As , ^{77}Se , ^{85}Rb , ^{88}Sr , ^{97}Mo , ^{107}Ag , ^{111}Cd , ^{118}Sn , ^{121}Sb , ^{133}Cs , ^{137}Ba , ^{205}Tl , ^{208}Pb , and ^{238}U , while confirmation isotopes included ^{53}Cr , ^{62}Ni , ^{65}Cu , ^{68}Zn , ^{82}Se , ^{86}Sr , ^{95}Mo , ^{110}Cd , ^{117}Sn , ^{123}Sb , ^{135}Ba , ^{203}Tl , ^{206}Pb , and ^{235}U . ICP-MS operational parameters included: RF power, 1600 W; plasma gas flow, 18 L/min; auxiliary gas flow, 1.20 L/min; and nebulizer gas flow: 1.06-1.08 L/min. Urinary metal concentrations were adjusted by internal standard responses and dilution.

Urinary metals were quantified over an element dependent linear range from 0.01 $\mu\text{g/L}$ to 100 $\mu\text{g/L}$ using matrix-matched calibration standards. Matrix-matched calibration standards were prepared using fivefold synthetic urine (CST Technologies Inc, UriSub®) to mimic the high salt content and formation of polyatomic interferences in real urine specimens. A freeze-dried reference urine standard (UTAK Laboratories Inc, Product #12110) with certified metal concentrations was also used as an indicator of trueness. Duplicated samples and spiked recoveries of urine specimens were additionally used to measure reproducibility and accuracy of the technique. Method accuracy ranged from

87% to 127% at biologically relevant concentrations (**Table 1**) while intra- and inter-run reproducibility were calculated as 1-7% and 2-12% relative standard deviation, respectively. Metal concentrations measured below the limit of quantitation (LOQ) were taken as one half the quantitation limit (LOQ/2) for statistical analysis.

Table 1. Method performance parameters for the detection of 22 urinary metals using ICP-MS operating in KED mode.

Analyte	Internal Standard	Quantification Limit ^a (µg/L)	UTAK Certified Value (µg/L)	UTAK Measured Value ^b (µg/L)	Accuracy (%)	Recovery Added Value (µg/L)	Recovery Measured Value ^b (µg/L)	Accuracy (%)
⁵¹ V		0.09	0.08	<LOQ	<LOQ	2.00	1.95 (0.09)	98
⁵² Cr		0.07	1.18	1.33 (0.11)	113	2.00	1.92 (0.10)	96
⁵⁵ Mn		0.32	0.84	1.07 (0.09)	127	2.00	1.97 (0.04)	98
⁵⁹ Co	⁴⁵ Sc	0.01	0.68	0.69 (0.04)	101	2.00	1.94 (0.04)	97
⁶⁰ Ni		0.09	2.29	2.40 (0.13)	105	2.00	1.95 (0.10)	98
⁶³ Cu		0.14	25.2	25.78 (1.20)	102	2.00	1.92 (0.12)	96
⁶⁶ Zn		0.29	517	498.60 (17.58)	96	2.00	2.14 (0.12)	107
⁶⁹ Ga		0.19	N/A	N/A	N/A	1.00	1.05 (0.04)	105
⁷⁵ As		0.11	3.96	5.64 (0.21)	142	1.00	1.53 (0.20)	153
⁷⁷ Se		0.30	55.3	48.01 (4.92)	87	2.00	1.61 (0.24)	80
⁸⁵ Rb		0.04	N/A	N/A	N/A	1.00	1.00 (0.12)	100
⁸⁸ Sr		0.26	N/A	N/A	N/A	2.00	1.89 (0.08)	95
⁹⁷ Mo	⁸⁹ Y	0.35	71.9	67.62 (1.69)	94	1.00	0.99 (0.02)	99
¹⁰⁷ Ag		0.02	N/A	N/A	N/A	2.00	1.77 (0.04)	88
¹¹¹ Cd		0.03	0.04	<LOQ	<LOQ	2.00	2.04 (0.07)	102
¹¹⁸ Sn		0.02	N/A	N/A	N/A	1.00	1.03 (0.03)	103
¹²¹ Sb		0.03	N/A	N/A	N/A	1.00	1.03 (0.05)	103
¹³³ Cs		0.01	N/A	N/A	N/A	1.00	1.00 (0.04)	100
¹³⁷ Ba		0.34	N/A	N/A	N/A	2.00	2.04 (0.04)	102
²⁰⁵ Tl	¹⁵⁹ Tb	0.002	N/A	N/A	N/A	2.00	1.95 (0.02)	98
²⁰⁸ Pb		0.01	0.29	0.30 (0.04)	103	2.00	2.00 (0.02)	100
²³⁸ U		0.002	N/A	N/A	N/A	1.00	0.98 (0.02)	98

^a Quantification limits were calculated as 10×STD of seven replicates and not adjusted for dilution.

^b Measured values are expressed as mean (SD) for triplicate samples.

2.3 Urine specific gravity assay

Urinary metals were adjusted for patient hydration-dilution status using urine specific gravity (USG). Conventional creatinine normalizations were excluded since urinary creatinine varies with age [31], diet [32], physical activity [33], and presence of breast cancer [34]. USG was measured using a temperature-corrected Reichert TS 400

clinical refractometer. Bulk urine specimens were allowed to equilibrate to room temperature followed by analysis of a 200 μ L aliquot. Ultra-pure water (USG = 1.000) and synthetic urine (USG = 1.022) of known specific gravity were used as reference standards. USG was measured with inter- and intra-assay RSDs of 0.12% and 0.04%, respectively. Biomarker concentrations were adjusted to USG using the Levine-Fahy equation and a reference USG of 1.020:

$$C_{corrected} = C_{raw} \times \frac{USG_{reference} - 1}{USG_{experimental} - 1}$$

where $C_{corrected}$ is the adjusted analyte concentration, C_{raw} is the uncorrected analyte concentration, $USG_{reference}$ is a reference USG for a given population, and $USG_{experimental}$ is the measured USG.

2.4 Statistical analyses

Anderson-Darling normality tests indicated non-normal distributions for all 22 urinary metals (Anderson-Darling > 3.5, $P < 0.005$), while \log_{10} transformation failed to approximate the normal curve (Anderson-Darling > 3.0, $P < 0.005$). For this reason, nonparametric analyses were performed on untransformed USG-adjusted metal concentrations and the covariates USG and patient age. Mann-Whitney U analyses were used to compare women newly diagnosed with breast cancer and benign conditions. Kruskal-Wallis and Dunn's multiple comparisons tests were used to compare urinary metal concentrations across individual carcinoma types and grades. Correlations among different urinary metals and clinicopathological factors were measured with Pearson

correlations. Logistic regression analyses were used to generate classification models, compute odds-ratios, and construct receiver-operating characteristic (ROC) curves for metals that were found to be associated with breast cancer. Odds-ratios were computed using interquartile range (IQR) increments for each covariate. The ROC curves evaluated the potential of each classification model to distinguish invasive breast cancer across all thresholds and were constructed by plotting sensitivity vs. 1-specificity. Statistical uncertainty was quantified with 95% confidence intervals where appropriate. A *P*-value below 0.05 was considered statistically significant.

3. Results

3.1 Patient Population

One hundred thirty-eight urine specimens were collected among which seven were excluded for being overly dilute or concentrated, defined as having a USG value below 1.003 or above 1.030, respectively. These cutoff thresholds were selected based on the diminished ability of USG to accurately model patient hydration-dilution status beyond these points [35]. The remaining 131 eligible patients were classified as 79 (60%) women diagnosed with benign fibroadenomas, fibrocystic changes, benign papillomas, and stromal fibrosis, and 52 (40%) women with newly diagnosed breast carcinomas. Carcinomas were further characterized as comprising 12 ductal carcinomas in situ (DCIS), 38 invasive ductal carcinomas (IDC), and 2 invasive lobular carcinomas (ILC) (**Fig. 1**). Low-grade DCIS cases ($n = 5$) were considered pre-invasive, indolent disease [36], which resulted in their classification as a benign condition. The retrospective nature of this study, whereby samples were originally collected for a different purpose, precluded the inclusion of healthy, age-matched controls. As a proof-of-concept study,

the benign cases, which lacked known comorbidities, previous history of cancer, and had pathologically confirmed absence of breast cancer were used as approximate controls. However, future studies should include healthy control populations since urinary metals may associate with benign conditions of the breast.

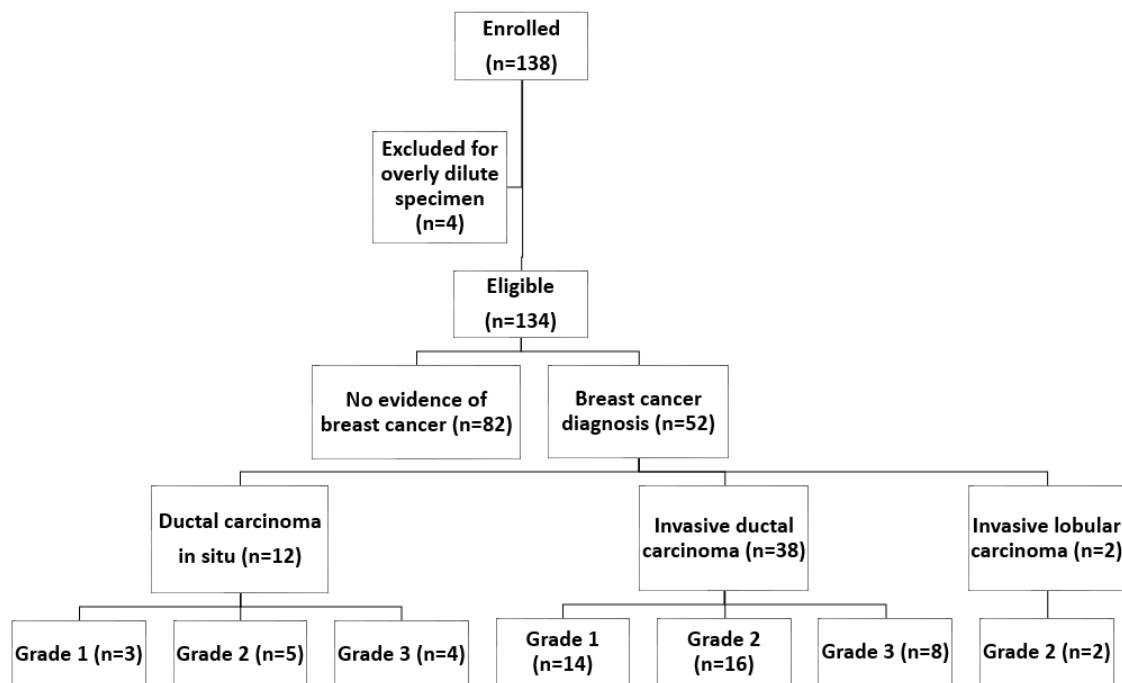


Figure 1. Patient enrollment flowchart including excluded specimens.

3.2 Association of Urinary Metals with Breast Cancer

Urinary metal concentrations encountered in the two patient groups were summarized in **Table 2**. All 22 urinary metals were reliably detected by the ICP-MS analysis with the exceptions of V, Mn, Ag, and U. Trace levels of Cr and Ga were also unquantifiable (signal-to-noise < 10) in a majority of samples. Notably, the heavy metals Cu (P -value = 0.036) and Pb (P -value = 0.003) were significantly elevated in the women

with newly diagnosed breast cancer. Weak associations from Cd (P -value = 0.163) in addition to non-significant increases in Zn, Ba, and Rb were also observed. Patient age was additionally considered a disease correlate ($P < 0.0005$) with means (SD) of 64.7 (10.9) years in the breast cancer group and 56.7 (11.8) years in the benign group. Patient age was not found to correlate with any of the urinary metals, which indicated that patient age was not a confounding factor for the observed relationships between metals and breast cancer. USG was not associated with presence of breast cancer and had a pooled mean (SD) of 1.013 (0.001).

Table 2 Comparison of USG-adjusted urinary metal levels in women with benign conditions (n=84) and breast cancer (n=47). All data are expressed as median (IQR).

<i>Metal</i>	LOQ^a ($\mu\text{g/L}$)	Breast Cancer Patients ($\mu\text{g/L}$)	Benign Conditions ($\mu\text{g/L}$)	<i>P</i>-value^b
⁵¹ V	0.45	<LOQ	<LOQ	N/A
⁵² Cr	0.35	0.175 (0.175-0.580) ^c	0.175 (0.175-0.424) ^c	0.541
⁵⁵ Mn	1.60	<LOQ	<LOQ	N/A
⁵⁹ Co	0.05	0.316 (0.235-0.439)	0.254 (0.191-0.431)	0.405
⁶⁰ Ni	0.45	1.28 (0.99-2.75)	1.54 (0.99-2.39)	0.730
⁶³ Cu	0.70	9.35 (7.43-13.61)	8.47 (6.92-10.46)	0.036
⁶⁶ Zn	1.45	447 (286-757)	386 (263-664)	0.272
⁶⁹ Ga	0.95	0.475 (0.475-1.152) ^c	0.475 (0.475-1.047) ^c	0.310
⁷⁵ As	0.55	4.15 (2.94-6.34)	4.28 (2.74-6.44)	0.981
⁷⁷ Se	1.50	36.66 (29.07-53.26)	38.92 (29.64-49.10)	0.726
⁸⁵ Rb	0.20	1318 (1104-1747)	1239 (958-1819)	0.330
⁸⁸ Sr	1.30	123.43 (84.27-162.41)	123.00 (80.45-167.46)	0.814
⁹⁷ Mo	1.75	38.43 (26.43-56.69)	42.33 (29.85-70.92)	0.420
¹⁰⁷ Ag	0.10	<LOQ	<LOQ	N/A
¹¹¹ Cd	0.15	0.669 (0.440-1.262)	0.611 (0.472 – 0.885)	0.163
¹¹⁸ Sn	0.10	0.482 (0.191-1.475)	0.469 (0.137-1.005)	0.467
¹²¹ Sb	0.15	0.163 (0.075-0.234)	0.075 (0.075-0.210)	0.348
¹³³ Cs	0.05	6.01 (5.25-8.57)	6.58 (4.56-9.00)	0.950
¹³⁷ Ba	1.70	2.82 (0.85-4.71)	2.19 (0.85-3.38)	0.205
²⁰⁵ Tl	0.01	0.165 (0.131-0.223)	0.175 (0.129-0.256)	0.781
²⁰⁸ Pb	0.05	0.578 (0.395-0.876)	0.388 (0.260-0.597)	0.003
²³⁸ U	0.01	<LOQ	<LOQ	N/A

^a Quantification limits and urinary concentrations have been adjusted by a dilution factor of five.

^b P -values represent group comparisons between women newly diagnosed with breast cancer and benign conditions using nonparametric Mann-Whitney U analyses.

^c Unquantifiable levels of Cr, Ga, Sb, and Ba in some samples were taken as LOQ/2 and semi-quantitatively measured.

Logistic regression models were used to evaluate the clinical performance of various classification models in distinguishing invasive breast cancer. Univariate models were independently developed for Cu (odds-ratio increment = 4.48 $\mu\text{g/L}$) and Pb (odds-ratio increment = 0.368 $\mu\text{g/L}$) owing to their significant elevation in breast cancer patients. Both Cu (odds-ratio: 1.77, 95% CI: 1.15-2.72, P -value = 0.008) and Pb (odds-ratio: 1.65, 95% CI: 1.14-2.40, P -value = 0.005) were found to be significant factors for having breast cancer. A multivariate model that comprised Cu, Pb, and patient age (odds-ratio increment = 19 years) was additionally constructed where Cu (odds-ratio: 1.52, 95% CI: 0.95-2.43, P -value = 0.079) and Pb (odds-ratio: 1.46, 95% CI: 0.97 – 2.18, P -value = 0.064) did not significantly contribute to the regression line which was dominated by patient age (odds-ratio: 2.77, 95% CI: 1.44-5.32, P -value < 0.0005). ROC analysis suggested clinical performance of individual models was ordered as follows: Cu < Pb < Patient Age < Multivariate Model (**Fig. 2**). Specifically, Cu poorly distinguished invasive breast carcinomas across all thresholds (AUC: 0.611, 95% CI: 0.510-0.712, P -value = 0.035) while Pb demonstrated slightly improved discriminatory power (AUC: 0.659, 95% CI: 0.562-0.756, P -value = 0.003). Although patient age possessed marginally better discriminatory power (AUC: 0.685, 95% CI: 0.593 – 0.778, P -value < 0.0005), the combined multivariate model provided optimal results (AUC: 0.728, 95% CI: 0.641-0.816, P -value < 0.0005). The univariate Cu and Pb models both had 19.2% sensitivity (95% CI: 9.2%-33.3%) and 91.2% specificity (95% CI: 83.6%-96.6%) while the multivariate model afforded 36.2% sensitivity (95% CI: 22.7%-51.5%) and 88.1% specificity (95% CI: 79.2%-94.1%). While characteristic performance permits objective classification model ranking, clinical applicability is better assessed at optimal cutoff

thresholds. To this end, Cu had 61.7% sensitivity (95% CI: 46.4%-75.5%) and 50.0% specificity (95% CI: 38.9%-61.1%) using a cutoff of 8.50 $\mu\text{g/L}$, while Pb had 76.6% sensitivity (95% CI: 62.0%-87.7%) and 51.2% specificity (95% CI: 40.0%-62.3%) using an optimal threshold of 0.400 $\mu\text{g/L}$.

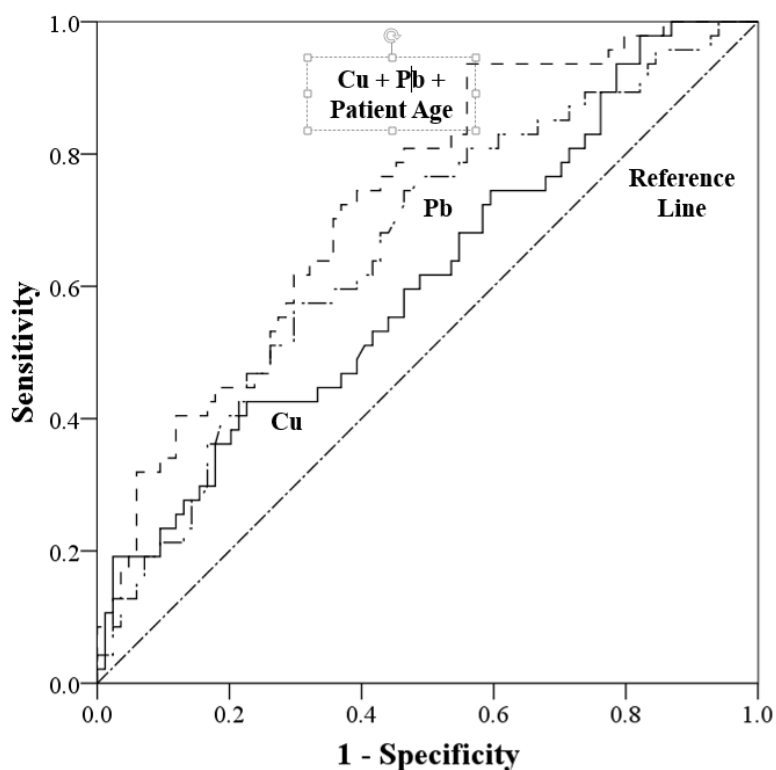


Figure 2 ROC data comparing incremental increases in diagnostic performance for the univariate models of Cu and Pb and the multivariate model comprising Cu, Pb, and patient age in women newly diagnosed with breast cancer (n=47) and benign conditions (n=84).

3.3 Correlations among urinary metals and clinicopathological factors

It was also of interest to identify potential correlations among different urinary metals to better understand exposure routes and possible pathophysiological mechanisms.

Significant correlations ($|\text{Pearson } r| > 0.3$, $P\text{-value} < 0.05$) among different urinary metals were summarized in **Table 3**. Notably, twice as many correlations were noted in breast cancer patients compared with women with benign conditions, although this finding may result from the limited sample size of the breast cancer group. Among the benign condition group, interactions among Ba, Sr, and Ga were the strongest. Moderate correlations included those between Cu with Ni, Zn, and Cs in addition to those among trace essential metal Se with Zn and Cu, and heavy metal Sn with Co and Zn. The correlations from the breast cancer subgroup were markedly different from those observed in the benign condition group, although strong interactions among Ba, Sr, and Ga were similarly observed. Urinary Cd was correlated with several heavy metals including As, Zn, Sb, Tl, Rb, and Cu. The heavy metal Cr was also found to be correlated with Sn, Ni, Se, and Sb. Urinary Pb was correlated with Se, Ni, and Zn. Correlations among USG, patient age, Cu, and Pb also suggested Pb was weakly correlated with both USG ($r = 0.201$, $P\text{-value} = 0.021$) and age ($r = 0.178$, $P\text{-value} = 0.042$).

Prognostic immunohistochemical factors including progesterone receptor status, estrogen receptor status, Her-2/neu, and Ki67 cell proliferation marker for the 45 invasive breast cancers were compared with the 22 urinary metals to identify possible prognostic capabilities. Urinary As was found to have a weak inverse relationship with progesterone receptor status ($r = -0.294$, $P\text{-value} = 0.023$) and Her-2/neu ($r = 0.362$, $P\text{-value} = 0.028$). Other correlations included Sr and estrogen receptor status ($r = 0.340$, $P\text{-value} = 0.037$), Mo and Her-2/neu ($r = -0.350$, $P\text{-value} = 0.034$), and Cd and estrogen receptor status ($r = -0.334$, $P\text{-value} = 0.04$). Urinary Pb correlated moderately with estrogen receptor status ($r =$

= -0.441, P -value = 0.006), progesterone receptor status (r = -0.315, P -value = 0.044), and Ki67 (r = 0.385, P -value = 0.017).

Table 3 Significant correlations among USG-adjusted urinary metals.

Benign Conditions			Breast Cancer		
Correlation	Pearson Correlation, r	P -value	Correlation	Pearson Correlation, r	P -value
Sn-Zn	0.305	0.005	Zn-Cu	0.304	0.038
Sn-Co	0.307	0.004	Cd-As	0.318	0.029
Mo-Se	0.307	0.005	Zn-Ni	0.323	0.027
Cs-Sr	0.307	0.004	Cd-Zn	0.325	0.026
Cs-Rb	0.333	0.002	Pb-Se	0.327	0.025
Se-Cu	0.347	0.001	Sn-Cr	0.337	0.020
Se-Zn	0.365	0.001	Sb-Cu	0.357	0.014
Sb-Mo	0.381	<0.0005	Cs-Rb	0.359	0.014
Cu-Ni	0.427	<0.0005	Sn-Cu	0.360	0.013
Tl-Sr	0.433	<0.0005	Ni-Cr	0.371	0.010
Cs-Cu	0.470	<0.0005	Mo-Sr	0.384	0.008
Zn-Cu	0.506	<0.0005	Mo-Se	0.391	0.007
Sr-Ga	0.543	<0.0005	Ba-Se	0.394	0.006
Ba-Sr	0.666	<0.0005	Ni-Cu	0.415	0.004
Ba-Ga	0.874	<0.0005	Pb-Ni	0.415	0.004
			Sr-Ga	0.419	0.03
			Se-Cr	0.422	0.003
			Sb-Cd	0.431	0.002
			Cs-Co	0.433	0.002
			Pb-Zn	0.443	0.002
			Sb-Ni	0.457	0.001
			Tl-Cd	0.462	0.001
			Sn-Ni	0.510	<0.0005
			Sb-Cr	0.528	<0.0005
			Se-Zn	0.551	<0.0005
			Cd-Rb	0.581	<0.0005
			Ba-Sr	0.652	<0.0005
			Cd-Cu	0.656	<0.0005
			Ba-Ga	0.838	<0.0005

Finally, the correlation between Pb and Cu with cancer progression was explored using Kruskal-Wallis analyses and Dunn's multiple comparisons tests. The highly limited sample size of the DCIS subgroups warrant cautious interpretation of their results.

Urinary Pb levels were arranged in the following order: Benign Condition < Grade 3

DCIS < Grade 1 DCIS < Grade 2 DCIS < Grade 1 IDC \leq Grade 2 IDC < Grade 3 IDC.

The difference between Grade 3 IDC and benign conditions was most significant (Dunn's multiple comparisons P -value = 0.0006). Similarly, urinary Pb was weakly correlated with cancer grade using cancer grade as a continuous variable ($r = 0.265$, P -value = 0.002). No significant differences among cancer grades were noted for urinary Cu, which was ranked in the following order: Benign conditions < Grade 2 DCIS < Grade 1 DCIS < Grade 1 IDC < Grade 3 DCIS < Grade 2 IDC < Grade 3 IDC. Weak correlations between urinary Cu and continuous variable cancer grade ($r = 0.254$, P -value = 0.003) were similarly noted.

4. Discussion

We investigated 22 urinary metals in women newly diagnosed with breast cancer and benign conditions in a proof-of-concept study to determine whether urinary metallomics may serve as a useful platform for biomarker discovery. In this study, two metals, copper and lead, were encountered at significantly elevated levels in the urine of breast cancer patients. This finding is consistent with a growing body of literature concerned with *in vivo* metallomics of breast cancer tissue. For example, copper hyperaccumulation occurs in breast carcinomas [12] through dysregulated copper transport proteins [13]. Importantly, the association of urinary copper with high-grade breast cancers in particular appeared to reflect copper-based mechanisms related to

cancer motility in metastatic breast carcinomas [15]. Elevated urinary lead concentrations were similarly more pronounced in high-grade breast carcinomas. Environmental lead exposure, a salient consideration for our study population, is associated with risk for developing breast cancer while recent work has suggested that lead functions as a selenium antagonist that competitively binds selenium [26]. The significant indirect correlation between lead and selenium in breast cancer patients observed in this study appears to support this proposed mechanism. While urinary cadmium weakly associated with breast cancer, no multiplicative interactions with selenium were observed ($r = -0.02$, P -value = 0.82) as previously cited, presumably due to substantial differences in environmental cadmium exposure between our study population and that of Wei [29]. Although univariate classification models for copper and lead demonstrated limitations in breast cancer diagnostics, the multivariate model that included patient age performed remarkably well. The clinical performance of copper and particularly lead at optimized cutoff thresholds compared favorably with other breast cancer diagnostic modalities such as clinical breast examinations and mammography [37]. This diagnostic performance appears promising given the inexpensive and noninvasive character of urinary metal screening. However, the authors acknowledge the limited sample size of this study and point out that larger clinical studies are required to validate these preliminary findings.

Moreover, our results suggest that diagnostic performance may be further improved through enhanced understanding of metal and metalloid exposure routes. For example, numerous correlations among various metals in this study provided pertinent information regarding common exposure routes that include dietary intake, residential exposure, occupational exposure, and more broadly, environmental exposure. For

instance, barium, strontium, and gallium, which together represented the strongest metal-metal correlations, are typically co-present in ore-bearing rock. The interaction between nickel and copper among other interactions may be similarly attributed to shared geochemical distribution [38]. Although this study was not designed to evaluate the influence of local mineralogy on urinary metal epidemiology, we feel it necessary to mention that geochemical distributions likely represent a major determinant of biometal concentrations. Supporting this claim is a comparison of previously reported urinary metal concentrations in baseline populations and those reported from our southwest Missouri cohort which demonstrates that while many essential metals obtained primarily from dietary exposure were in good agreement [39, 40], trace and toxic metals like cadmium varied considerably [29]. Differences arising from unique local geochemistry will additionally be influenced by environmental regulations. For example, the similar urinary lead values reported in our study population compared with other reported industrialized country populations likely reflects lead removal from drinking water. Further investigations into local geochemical distributions and metallomic correlations will be needed to qualify these considerations. Finally some correlations, such as those between copper, zinc, and nickel, may additionally reflect dietary supplement use and other dietary fortifications. Hence, characterization of the exposure routes to urinary metals of interest is critical to advancing urinary metal molecular pathological epidemiology.

Finally, the correlations between urinary metals and clinicopathological factors provided new insights into disease mechanisms and clinical applicability of urinary metals in breast cancer patients. Notably, both copper and lead correlated weakly with

cancer progression and peaked in high-grade IDC patients. This observation suggests copper and lead may have applicability in the detection of early stage breast cancer, an observation that merits further investigation. The ability to detect early stage breast cancer is especially critical given the potential to reduce tumor upstaging and improve patient mortality. Finally, several metals and particularly lead were shown to have potential use in prognostics. Because prognostic capability was not directly quantified, future studies should aim to quantitatively assess urinary metals for their ability to predict breast cancer outcome. Such a finding would render urinary metals a valuable supplementary technique for current immunohistochemical techniques.

5. Conclusions

In conclusion, this proof-of-concept study introduces urinary metallomics as a noninvasive platform for biomarker discovery and clinical translational research. This work provides new insights into the epidemiology of urinary metals in suspected breast cancer cases. Specifically, this work highlights the potential of urinary copper and lead as noninvasive diagnostic breast cancer biomarkers in addition to an array of urinary metals with prognostic capabilities. Future studies should aim to improve understanding of the relationship between urinary metals and source exposure, to measure the prognostic capability of individual metals in prospective clinical studies, and to evaluate copper and lead applicability to early stage breast cancer detection.

Acknowledgements

Special thanks are given to the Mercy Breast Center – Springfield staff including V. Roger Holden, Adrianna Moore, and Pearlena Hamlet for their appreciated assistance

in participant recruitment. The authors also thank Millipore Inc and the Center for Single Cell, Single Nanoparticle, and Single Molecule Monitoring at Missouri University of Science and Technology for their valuable instrumentation support. C. Burton received financial support through a National Science Foundation Graduate Research Fellowship (#DGE-1011744).

References

- [1] Haraguchi H. Metallomics as integrated biometal science. *Journal of Analytical Atomic Spectrometry* 2004; 19:5-14.
- [2] Szpunar J. Metallomics: a new frontier in analytical chemistry. *Analytical and bioanalytical chemistry* 2004; 378:54-56.
- [3] Tainer JA, Roberts VA, Getzoff ED. Metal-binding sites in proteins. *Current opinion in biotechnology* 1991; 2:582-591.
- [4] Jin R, Bay B, Chow V, Tan P, Lin V. Metallothionein 1E mRNA is highly expressed in oestrogen receptor-negative human invasive ductal breast cancer. *British journal of cancer* 2000; 83:319.
- [5] Goulding H, Jasani B, Pereira H, et al. Metallothionein expression in human breast cancer. *British journal of cancer* 1995; 72:968.
- [6] Krześlak A, Forma E, Józwiak P, et al. Metallothionein 2A genetic polymorphisms and risk of ductal breast cancer. *Clinical and experimental medicine* 2014; 14:107-113.
- [7] Finney LA, O'Halloran TV. Transition metal speciation in the cell: insights from the chemistry of metal ion receptors. *Science* 2003; 300:931-936.
- [8] Outten CE, O'Halloran TV. Femtomolar sensitivity of metalloregulatory proteins controlling zinc homeostasis. *Science* 2001; 292:2488-2492.
- [9] Furukawa K, Ramesh A, Zhou Z, et al. Bacterial Riboswitches Cooperatively Bind Ni²⁺ or Co²⁺ Ions and Control Expression of Heavy Metal Transporters. *Molecular Cell* 2015; 57:1088-1098.
- [10] Dambach M, Sandoval M, Updegrove TB, et al. The Ubiquitous yybP-ykoY Riboswitch Is a Manganese-Responsive Regulatory Element. *Molecular Cell* 2015; 57:1099-1109.
- [11] Andrews GK. Regulation of metallothionein gene expression by oxidative stress and metal ions. *Biochemical pharmacology* 2000; 59:95-104.
- [12] Daniel KG, Chen D, Orlu S, Cui QC, Miller FR, Dou QP. Clioquinol and pyrrolidine dithiocarbamate complex with copper to form proteasome inhibitors and apoptosis inducers in human breast cancer cells. *Breast Cancer Res* 2005; 7:R897-R908.
- [13] Wee NK, Weinstein DC, Fraser ST, Assinder SJ. The mammalian copper transporters CTR1 and CTR2 and their roles in development and disease. *The international journal of biochemistry & cell biology* 2013; 45:960-963.

- [14] MacDonald G, Nalvarte I, Smirnova T, et al. Memo is a copper-dependent redox protein with an essential role in migration and metastasis. *Science signaling* 2014; 7:ra56-ra56.
- [15] Fernandes AS, Flório A, Saraiva N, et al. Role of the copper (II) complex Cu(15)pyN5 in intracellular ROS and breast cancer cell motility and invasion. *Chemical biology & drug design* 2015.
- [16] Maret W. Zinc coordination environments in proteins as redox sensors and signal transducers. *Antioxidants & redox signaling* 2006; 8:1419-1441.
- [17] Bier B, Douglas-Jones A, Tötsch M, et al. Immunohistochemical demonstration of metallothionein in normal human breast tissue and benign and malignant breast lesions. *Breast cancer research and treatment* 1994; 30:213-221.
- [18] Alam S, Kelleher SL. Cellular mechanisms of zinc dysregulation: a perspective on zinc homeostasis as an etiological factor in the development and progression of breast cancer. *Nutrients* 2012; 4:875-903.
- [19] Lopez V, Foolad F, Kelleher SL. ZnT2-overexpression represses the cytotoxic effects of zinc hyper-accumulation in malignant metallothionein-null T47D breast tumor cells. *Cancer letters* 2011; 304:41-51.
- [20] Chowanadisai W, Lönnerdal B, Kelleher SL. Identification of a mutation in SLC30A2 (ZnT-2) in women with low milk zinc concentration that results in transient neonatal zinc deficiency. *Journal of Biological Chemistry* 2006; 281:39699-39707.
- [21] Kelleher SL, Lönnerdal B. Zn transporter levels and localization change throughout lactation in rat mammary gland and are regulated by Zn in mammary cells. *The Journal of nutrition* 2003; 133:3378-3385.
- [22] Margalioth EJ, Schenker JG, Chevion M. Copper and zinc levels in normal and malignant tissues. *Cancer* 1983; 52:868-872.
- [23] Pires LV, Pimentel JC, do Nascimento-Nogueira N, do Nascimento-Marreiro D. Analysis of plasma and erythrocyte zinc levels in premenopausal women with breast cancer. *Nutr Hosp* 2011; 26:293-297.
- [24] Yücel I, Arpacı F, Özet A, et al. Serum copper and zinc levels and copper/zinc ratio in patients with breast cancer. *Biological trace element research* 1994; 40:31-38.
- [25] Martin MB, Reiter R, Pham T, et al. Estrogen-like activity of metals in MCF-7 breast cancer cells. *Endocrinology* 2003; 144:2425-2436.
- [26] Alatisé OI, Schrauzer GN. Lead exposure: a contributing cause of the current breast cancer epidemic in Nigerian women. *Biological trace element research* 2010; 136:127-139.

- [27] Blaurock-Busch E, Busch YM, Friedle A, Buerner H, Parkash C, Kaur A. Comparing the metal concentration in the hair of cancer patients and healthy people living in the Malwa region of Punjab, India. *Clinical Medicine Insights Oncology* 2014; 8:1.
- [28] Cihan YB, Sözen S, Yıldırım SÖ. Trace elements and heavy metals in hair of stage III breast cancer patients. *Biological trace element research* 2011; 144:360-379.
- [29] Wei X-L, He J-R, Cen Y-L, et al. Modified effect of urinary cadmium on breast cancer risk by selenium. *Clinica Chimica Acta* 2015; 438:80-85.
- [30] Bass D, Jones D, Determination of Trace Metals in Human Urine Using the NexION 300/350 ICP-MS. PerkinElmer, Inc: Application Note, 2010: 1-5.
- [31] James GD, Sealey JE, Alderman M, et al. A longitudinal study of urinary creatinine and creatinine clearance in normal subjects race, sex, and age differences. *American journal of hypertension* 1988; 1:124-131.
- [32] Walser M. Creatinine excretion as a measure of protein nutrition in adults of varying age. *Journal of Parenteral and Enteral Nutrition* 1987; 11:73S-78S.
- [33] Heymsfield SB, Arteaga C, McManus C, Smith J, Moffitt S. Measurement of muscle mass in humans: validity of the 24-hour urinary creatinine method. *The American Journal of Clinical Nutrition* 1983; 37:478-494.
- [34] Pan H, Xia K, Zhou W, et al. Low serum creatine kinase levels in breast cancer patients: a case-control study. *PloS one* 2013; 8:e62112.
- [35] Cook JD, Caplan YH, LoDico CP, Bush DM. The characterization of human urine for specimen validity determination in workplace drug testing: a review. *Journal of analytical toxicology* 2000; 24:579-588.
- [36] Ozanne EM, Shieh Y, Barnes J, Bouzan C, Hwang ES, Esserman LJ. Characterizing the impact of 25 years of DCIS treatment. *Breast cancer research and treatment* 2011; 129:165-173.
- [37] Berg WA, Gutierrez L, NessAiver MS, et al. Diagnostic Accuracy of Mammography, Clinical Examination, US, and MR Imaging in Preoperative Assessment of Breast Cancer1. *Radiology* 2004; 233:830-849.
- [38] Woodruff L, Cannon WF, Smith DB, Solano F. The distribution of selected elements and minerals in soil of the conterminous United States. *Journal of Geochemical Exploration* 2015.
- [39] Heitland P, Köster HD. Biomonitoring of 30 trace elements in urine of children and adults by ICP-MS. *Clinica chimica acta* 2006; 365:310-318.

[40] Goullé J-P, Mahieu L, Castermant J, et al. Metal and metalloid multi-elementary ICP-MS validation in whole blood, plasma, urine and hair: Reference values. *Forensic Science International* 2005; 153:39-44.

SECTION

2. CONCLUSIONS

SP-ICP-MS shows great potential to become a high throughput nanometrology technique. It was successfully applied to characterize TiO₂ NPs in sunscreens and to study the interactions between ENPs and various plants in the presented study. The biotransformation of CeO₂ NPs into soluble Ce was discovered by SP-ICP-MS, which is a critical finding in the field of studying the interactions between ENPs and plants. Its superior sensitivity (particle concentration wise) makes it a perfect technique to characterize samples with low particle concentrations, especially useful for environmental and biological samples. Also due to its super sensitivity, large dilution factors can be applied to the samples and subsequently significantly decreases the matrix effect during analysis. In SP-ICP-MS analysis, the data processing was a significant part of the whole analysis and also was a time-consuming process. The high throughput analysis is made possible by the commercialization of dedicated software for SP-ICP-MS (e.g. PerkinElmer Syngistix Nano Application module).

However, some disadvantages also come along with SP-ICP-MS. SP-ICP-MS only detects one isotope in a single particle rather than the whole chemical analysis of the particles. For example, it detects Ti and then converts Ti to TiO₂ by assuming that particle is TiO₂ particle. Owing to the complexity of environmental and biological samples, this disadvantage significantly limits its applications in various ways. As mentioned in the introduction of this dissertation, multi-element/isotope capability is urgently needed to push current application boundaries of SP-ICP-MS further. Despite

the powerful capability of SP-ICP-MS, another caveat is there is no single technique can fully characterize ENPs including SP-ICP-MS. Complementary technique and instrumentation is always necessary and beneficial.

BIBLIOGRAPHY

- [1] Lead, J.; Emma, S., Environmental and human health impacts of nanotechnology. *Environ. Chem.* 2010, 7, (1), 132.
- [2] Ma, Y. In *In vitro models for nanotoxicity testing*, 2009; John Wiley & Sons Ltd.: 2009; pp 349-377.
- [3] Lewicka, S. A.; Colvin, V. L., Photoactivity tests of TiO₂ and ZnO sunscreen ingredients. *MRS Online Proc. Libr.* 2011, 1413, No pp. given.
- [4] Lewicka, Z. A.; Yu, W. W.; Oliva, B. L.; Contreras, E. Q.; Colvin, V. L., Photochemical behavior of nanoscale TiO₂ and ZnO sunscreen ingredients. *J. Photochem. Photobiol., A* 2013, 263, 24-33.
- [5] Weir, A.; Westerhoff, P.; Fabricius, L.; Hristovski, K.; von Goetz, N., Titanium dioxide nanoparticles in food and personal care products. *Environ. Sci. Technol.* 2012, 46, (4), 2242-2250.
- [6] Wiechers, S.; Biehl, P.; Luven, C.; Maier, M.; Meyer, J.; Muenzenberg, J.; Schulze-Isfort, C.; Albers, P., Titanium dioxide particle size vs. sun protection performance. *Cosmet. Toiletries* 2013, 128, (5), 332, 334, 336, 338-339.
- [7] Collin, B.; Auffan, M.; Johnson, A. C.; Kaur, I.; Keller, A. A.; Lazareva, A.; Lead, J. R.; Ma, X.; Merrifield, R. C.; Svendsen, C.; White, J. C.; Unrine, J. M., Environmental release, fate and ecotoxicological effects of manufactured ceria nanomaterials. *Environ. Sci.: Nano* 2014, 1, (6), 533-548.
- [8] Keller, A. A.; Lazareva, A., Predicted Releases of Engineered Nanomaterials: From Global to Regional to Local. *Environ. Sci. Technol. Lett.* 2014, 1, (1), 65-70.
- [9] Mudalige, T. K.; Qu, H.; Sanchez-Pomales, G.; Sisco, P. N.; Linder, S. W., Simple Functionalization Strategies for Enhancing Nanoparticle Separation and Recovery with Asymmetric Flow Field Flow Fractionation. *Anal. Chem.* (Washington, DC, U. S.) 2015, 87, (3), 1764-1772.
- [10] Wagner, S.; Legros, S.; Loeschner, K.; Liu, J.; Navratilova, J.; Grombe, R.; Linsinger, T. P. J.; Larsen, E. H.; von der Kammer, F.; Hofmann, T., First steps towards a generic sample preparation scheme for inorganic engineered nanoparticles in a complex matrix for detection, characterization, and quantification by asymmetric flow-field flow fractionation coupled to multi-angle light scattering and ICP-MS. *J. Anal. At. Spectrom.* 2015, 30, (6), 1286-1296.

- [11] Loeschner, K.; Navratilova, J.; Grombe, R.; Linsinger, T. P. J.; Koebler, C.; Moelhave, K.; Larsen, E. H., In-house validation of a method for determination of silver nanoparticles in chicken meat based on asymmetric flow field-flow fractionation and inductively coupled plasma mass spectrometric detection. *Food Chem.* 2015, 181, 78-84.
- [12] Giddings, J. C., Field-flow fractionation: analysis of macromolecular, colloidal, and particulate materials. *Science (Washington, D. C., 1883-)* 1993, 260, (5113), 1456-65.
- [13] Leshner, E. K.; Ranville, J. F.; Honeyman, B. D., Analysis of pH Dependent Uranium(VI) Sorption to Nanoparticulate Hematite by Flow Field-Flow Fractionation - Inductively Coupled Plasma Mass Spectrometry. *Environ. Sci. Technol.* 2009, 43, (14), 5403-5409.
- [14] Bouby, M.; Geckeis, H.; Luetzenkirchen, J.; Mihai, S.; Schaefer, T., Interaction of bentonite colloids with Cs, Eu, Th and U in presence of humic acid: A flow field-flow fractionation study. *Geochim. Cosmochim. Acta* 2011, 75, (13), 3866-3880.
- [15] Hartland, A.; Fairchild, I. J.; Lead, J. R.; Zhang, H.; Baalousha, M., Size, speciation and lability of NOM-metal complexes in hyperalkaline cave dripwater. *Geochim. Cosmochim. Acta* 2011, 75, (23), 7533-7551.
- [16] Hagendorfer, H.; Kaegi, R.; Traber, J.; Mertens, S. F. L.; Scherrers, R.; Ludwig, C.; Ulrich, A., Application of an asymmetric flow field flow fractionation multi-detector approach for metallic engineered nanoparticle characterization - Prospects and limitations demonstrated on Au nanoparticles. *Anal. Chim. Acta* 2011, 706, (2), 367-378.
- [17] Ulrich, A.; Losert, S.; Bendixen, N.; Al-Kattan, A.; Hagendorfer, H.; Nowack, B.; Adlhart, C.; Ebert, J.; Lattuada, M.; Hungerbuehler, K., Critical aspects of sample handling for direct nanoparticle analysis and analytical challenges using asymmetric field flow fractionation in a multi-detector approach. *J. Anal. At. Spectrom.* 2012, 27, (7), 1120-1130.
- [18] Degueldre, C.; Favarger, P. Y., Colloid analysis by single particle inductively coupled plasma-mass spectroscopy: a feasibility study. *Colloids Surf., A* 2003, 217, (1-3), 137-142.
- [19] Degueldre, C.; Favarger, P. Y., Thorium colloid analysis by single particle inductively coupled plasma-mass spectrometry. *Talanta* 2004, 62, (5), 1051-1054.
- [20] Degueldre, C.; Favarger, P. Y.; Bitea, C., Zirconia colloid analysis by single particle inductively coupled plasma-mass spectrometry. *Anal. Chim. Acta* 2004, 518, (1-2), 137-142.

- [21] Degueldre, C.; Favarger, P. Y.; Rosse, R.; Wold, S., Uranium colloid analysis by single particle inductively coupled plasma-mass spectrometry. *Talanta* 2006, 68, (3), 623-628.
- [22] Degueldre, C.; Favarger, P. Y.; Wold, S., Gold colloid analysis by inductively coupled plasma-mass spectrometry in a single particle mode. *Anal. Chim. Acta* 2006, 555, (2), 263-268.
- [23] Dan, Y.; Shi, H.; Stephan, C.; Liang, X., Rapid analysis of titanium dioxide nanoparticles in sunscreens using single particle inductively coupled plasma-mass spectrometry. *Microchem. J.* 2015, 122, 119-126.
- [24] Dan, Y.; Zhang, W.; Xue, R.; Ma, X.; Stephan, C.; Shi, H., Characterization of Gold Nanoparticle Uptake by Tomato Plants Using Enzymatic Extraction Followed by Single-Particle Inductively Coupled Plasma-Mass Spectrometry Analysis. *Environ. Sci. Technol.* 2015, 49, (5), 3007-3014.
- [25] Laborda, F.; Jimenez-Lamana, J.; Bolea, E.; Castillo, J. R., Selective identification, characterization and determination of dissolved silver(I) and silver nanoparticles based on single particle detection by inductively coupled plasma mass spectrometry. *J. Anal. At. Spectrom.* 2011, 26, (7), 1362-1371.
- [26] Mitrano, D. M.; Leshner, E. K.; Bednar, A.; Monserud, J.; Higgins, C. P.; Ranville, J. F., Detecting nanoparticulate silver using single-particle inductively coupled plasma-mass spectrometry. *Environ. Toxicol. Chem.* 2012, 31, (1), 115-121.
- [27] Pace, H. E.; Rogers, N. J.; Jarolimek, C.; Coleman, V. A.; Higgins, C. P.; Ranville, J. F., Determining Transport Efficiency for the Purpose of Counting and Sizing Nanoparticles via Single Particle Inductively Coupled Plasma Mass Spectrometry. *Anal. Chem.* 2011, 83, (24), 9361-9369.
- [28] Hineman, A.; Stephan, C., Effect of dwell time on single particle inductively coupled plasma mass spectrometry data acquisition quality. *J. Anal. At. Spectrom.* 2014, 29, (7), 1252-1257.
- [29] Montano, M. D.; Badiei, H. R.; Bazargan, S.; Ranville, J. F., Improvements in the detection and characterization of engineered nanoparticles using spICP-MS with microsecond dwell times. *Environ. Sci.: Nano* 2014, 1, (4), 338-346.
- [30] Hadioui, M.; Merdzan, V.; Wilkinson, K. J., Detection and Characterization of ZnO Nanoparticles in Surface and Waste Waters Using Single Particle ICPMS. *Environ. Sci. Technol.* 2015, 49, (10), 6141-6148.
- [31] Hadioui, M.; Peyrot, C.; Wilkinson, K. J., Improvements to Single Particle ICPMS by the Online Coupling of Ion Exchange Resins. *Anal. Chem.* (Washington, DC, U. S.) 2014, 86, (10), 4668-4674.

- [32] Tuoriniemi, J.; Cornelis, G.; Hasseløev, M., Size Discrimination and Detection Capabilities of Single-Particle ICPMS for Environmental Analysis of Silver Nanoparticles. *Anal. Chem.* 2012, 84, (9), 3965-3972.
- [33] Mitrano, D. M.; Ranville, J. F.; Bednar, A.; Kazor, K.; Hering, A. S.; Higgins, C. P., Tracking dissolution of silver nanoparticles at environmentally relevant concentrations in laboratory, natural, and processed waters using single particle ICP-MS (spICP-MS). *Environ. Sci.: Nano* 2014, 1, (3), 248-259.
- [34] Gray, E. P.; Coleman, J. G.; Bednar, A. J.; Kennedy, A. J.; Ranville, J. F.; Higgins, C. P., Extraction and Analysis of Silver and Gold Nanoparticles from Biological Tissues Using Single Particle Inductively Coupled Plasma Mass Spectrometry. *Environ. Sci. Technol.* 2013, 47, (24), 14315-14323.
- [35] Loeschner, K.; Navratilova, J.; Kobler, C.; Molhave, K.; Wagner, S.; von der, K. F.; Larsen, E. H., Detection and characterization of silver nanoparticles in chicken meat by asymmetric flow field flow fractionation with detection by conventional or single particle ICP-MS. *Anal. Bioanal. Chem.* 2013, 405, (25), 8185-8195.
- [36] Peters, R. J. B.; Rivera, Z. H.; van Bommel, G.; Marvin, H. J. P.; Weigel, S.; Bouwmeester, H., Development and validation of single particle ICP-MS for sizing and quantitative determination of nano-silver in chicken meat. *Anal. Bioanal. Chem.* 2014, 406, (16), 3875-3885.
- [37] Loeschner, K.; Brabrand, M. S. J.; Sloth, J. J.; Larsen, E. H., Use of alkaline or enzymatic sample pretreatment prior to characterization of gold nanoparticles in animal tissue by single-particle ICPMS. *Anal. Bioanal. Chem.* 2014, 406, (16), 3845-3851.
- [38] Marshall, A. T.; Haverkamp, R. G.; Davies, C. E.; Parsons, J. G.; Gardea-Torresdey, J. L.; van Agterveld, D., Accumulation of gold nanoparticles in Brassica Juncea. *Int. J. Phytorem.* 2007, 9, (3), 197-206.
- [39] Schwabe, F.; Tanner, S.; Schulin, R.; Rotzetter, A.; Stark, W.; von Quadt, A.; Nowack, B., Dissolved cerium contributes to uptake of Ce in the presence of differently sized CeO₂-nanoparticles by three crop plants. *Metallomics* 2015, 7, (3), 466-477.
- [40] Zhang, P.; Ma, Y.; Zhang, Z.; He, X.; Zhang, J.; Guo, Z.; Tai, R.; Zhao, Y.; Chai, Z., Biotransformation of Ceria Nanoparticles in Cucumber Plants. *ACS Nano* 2012, 6, (11), 9943-9950.

VITA

Yongbo Dan was born on August 27, 1987 in Zaoyang, Hubei Province, China. In 2010, he received his Bachelor of Science in Pharmaceutical Science from Tianjin University in Tianjin, China. In 2011, he started his Master of Science in Chemistry at Missouri University of Science and Technology and finished in May 2013. After receiving his master degree, he continued to his Ph.D in Chemistry and finished in May, 2016 at Missouri University of Science and Technology.